

3D Digital Analysis of Mammographic Composition

Von der Fakultät Informatik, Elektrotechnik und Informationstechnik der
Universität Stuttgart zur Erlangung der Würde eines
Doktors der Naturwissenschaften (Dr. rer. nat.)
genehmigte Abhandlung

Vorgelegt von
Constanza Lampasona
aus San Miguel de Tucumán, Argentinien

Hauptberichter: Prof. Dr. Dieter Roller
Mitberichter: Prof. Dr. Thomas Ertl

Tag der mündlicher Prüfung: 29.08.2008

Institut für Rechnergeschützte Ingenieursysteme
2009

TABLE OF CONTENTS

List of Figures	5
List of Tables.....	9
List of Abbreviations.....	11
Abstract	13
Zusammenfassung	15
1 Introduction	17
2 Related Technologies.....	21
2.1 Breast Density Measurement.....	21
2.2 Segmentation	23
2.3 Registration.....	29
2.4 Visualization.....	32
3 Medical Background	39
3.1 Breast Imaging.....	40
3.2 Breast Density as a Breast Cancer Risk Factor	41
3.3 Breast Cancer Screening.....	42
4 Physical Background.....	45
4.1 Exponential Law of Attenuation.....	46
4.2 Attenuation Coefficients.....	47
5 DICOM File Format.....	49
5.1 DICOM File Meta Information	51
5.2 Data Set	51
5.3 Data Elements.....	51
5.4 Data Elements Fields	51
5.5 Explicit Value Representation	52
5.6 Implicit Value Representation	54
5.7 Byte Ordering	54
5.8 Pixel Data Encoding	55
5.9 Transfer Syntax	55
6 Mammography	57
6.1 Conventional and Digital Mammography	57
6.2 Digital Mammography Systems	58
6.3 Mammograms used for Tests	60
7 Computational Methods for the Analysis of Digital Mammograms.....	63
7.1 Breast Segmentation.....	65

7.2	Pectoral Muscle Segmentation	66
7.3	Determination of Breast Composition.....	69
7.4	Breast Border Detection	76
7.5	Detection of Calcifications	76
7.6	Data Visualization	77
7.7	Digital Mammogram Standardization.....	79
7.8	Registration and Comparison of Mammograms	81
8	Software Architecture.....	89
8.1	System View	89
8.2	Requirements.....	90
8.3	Conceptual Modular View	91
8.4	Structural Design.....	93
8.5	Behavioral Design	96
8.6	User Interface	101
9	Results	105
10	Conclusions	115
	References	119

LIST OF FIGURES

Figure 2.1: Some examples of transformations (Maintz and Viergever 1998).....	31
Figure 2.2: A quadratic Bézier curve and a Bézier curve of 4th degree.	34
Figure 2.3: A bicubic Bézier surface. Adapted from Orlamünder and Mascolus (2004)..	34
Figure 2.4: Sixteen cases of vertex labeling with contours (Angel 2003).	36
Figure 2.5: Code for creating a contour plot (Angel 2003).....	36
Figure 2.6: Code for assigning the cell to one of the four canonical cases (Angel 2003).	37
Figure 3.1: Age standardized disease frequency in women in the European Union 1998. Diseases per 100000 (Bertz et al. 2004).....	39
Figure 3.2: Cranial-caudal and mediolateral-oblique views (Imaginis Corporation 2006).	41
Figure 3.3: Two examples of images showing the mediolateral-oblique (left) and cranial- caudal (right) views.	41
Figure 4.1: Linear attenuation coefficients of the different breast tissues and their variation with respect to photon energy (Aichinger et al. 2004).	45
Figure 5.1: DICOM file set and file format. A SOP (Service-Object Pair) is a concrete instantiation of a class with attributes and methods (NEMA 2004d).....	50
Figure 5.2: Data element structure (NEMA 2004b).	51
Figure 5.3: Two examples of bit organization with values of bits allocated of 16, bits stored 12, and high bit equal to 11 and 15 respectively.	55
Figure 6.1: Mammographic image technique. Overview of components. Adapted from Heywang-Köbrunner (2001).....	58
Figure 6.2: Giotto Mammography System developed and commercialized by Internazionale Medico Scientifica S.r.l. (2006).....	60
Figure 7.1: A mammogram and its histogram with thresholds: red means pure glandular tissue, green purely fatty tissue, and yellow separates the breast from the background pixels.....	64
Figure 7.2: The methods developed and their interaction.....	65
Figure 7.3: For the segmentation of the pectoral muscle, the seeds are automatically selected in the image left edge, where the muscle is situated.....	67
Figure 7.4: The pectoral boundary (in yellow) is detected by a change of high intensity into low intensity. Note that later the seeds will not grow inside the breast. ..	67

Figure 7.5: The seeds situated on the left side of the image grow independently from left to right until the muscle edge in the image is met.....	68
Figure 7.6: If one of these horizontal regions grows extremely, its edge is determined by interpolating between the upper and bottom adjacent regions.	69
Figure 7.7: For each limit found the region is merged with upper regions, to include intermediate regions that did not grow enough.....	69
Figure 7.8: Density error as a function of the difference of the linear attenuation coefficients. In diagram (a) $\Delta\mu_1 = -0.005$ and in diagram (b) $\Delta\mu_1 = 0.005$. The value of term $\ln(X/I_{fat})$ is -0.75, -0.33 and -0.1 for the black, dashed and gray curves, respectively.	74
Figure 7.9: Density error as a function of the difference of the linear attenuation coefficients. In diagram (a) $\Delta\mu_2 = -0.005$ and in diagram (b) $\Delta\mu_2 = 0.005$. The value of the term $\ln(X/I_{fat})$ is -0.75, -0.33 and -0.1 for the black, dashed and gray curves, respectively.	75
Figure 7.10: Algorithm for the transformation between “real pixels” and “display pixels”.	77
Figure 7.11: Effect of changes of window center and window width (Rorden 2006).....	78
Figure 7.12: A schematic view of the mammogram visualization as surface.	79
Figure 7.13: The color scale used to show the standardized mammograms.....	80
Figure 7.14: Mapping of the amount of glandular tissue in millimeters into a color in the color scale.....	81
Figure 7.15: The color scale and the correspondence of color and pixel value.....	81
Figure 7.16: The magnitude of breast compression may change between examinations (Wirth 2000).....	82
Figure 7.17: (a) When the breast is properly positioned, it should be symmetrically distributed among the nipple. (b) Inappropriate positioning may cause the breast to roll (Wirth 2000).....	83
Figure 7.18: Translational and rotational changes occur due to differences in positioning (Wirth 2000).....	83
Figure 7.19: The process of maximizing mutual information.	87
Figure 8.1: Structure of a digital mammography environment.	89
Figure 8.2: The DICOM Reader loads the mammograms and gives them to be evaluated to the Image Analyzer and to be shown to the 2D Viewer. The Image Analyzer performs the main operations and delivers the results to the 2D and 3D Viewers.....	91

Figure 8.3: Class hierarchy and relationships.	95
Figure 8.4: Sequence to read photon energy.	97
Figure 8.5: Sequence to read the linear attenuation coefficients.	98
Figure 8.6: Sequence to treat one image by opening it, loading the DICOM data elements, segmenting the breast region, calculating the volumetric breast density, showing the image and setting it into the standard format.	98
Figure 8.7: Sequence to load the DICOM header and data elements.	99
Figure 8.8: Sequence to display the image.	100
Figure 8.9: Sequence to create the difference image.	100
Figure 8.10: Main program window.	101
Figure 8.11: Open Window.	102
Figure 8.12: Viewer Window.	102
Figure 8.13: Brightness/Contrast Window.	103
Figure 8.14: 3D Viewer Window.	104
Figure 9.1: Volumes of glandular tissue [cm ³]. Comparison of the CC/MLO pairs, with pectoral muscle segmentation.	106
Figure 9.2: Volumes of glandular tissue [cm ³]. Comparison of the CC/MLO pairs, without pectoral muscle segmentation.	106
Figure 9.3: Volumes of glandular tissue [cm ³]. Comparison of the CC-Left/CC-Right pairs.	107
Figure 9.4: Volumes of glandular tissue [cm ³]. Comparison of the MLO-Left/MLO-Right pairs.	107
Figure 9.5: Examples for the pectoral muscle segmentation for four patients showing the original mammogram and the mammogram obtained after the pectoral muscle subtraction.	108
Figure 9.6: An example showing undersegmentation. This is caused due to weak differences of intensity between the pectoral muscle and the breast tissue...	109
Figure 9.7: Image segmentation and histogram for a fraction of dense tissue of 54%. ...	109
Figure 9.8: Image segmentation and histogram for a fraction of dense tissue of 40%. ...	110
Figure 9.9: Image segmentation and histogram for a fraction of dense tissue of 18%. ...	110
Figure 9.10: Segmentation of the mammogram according to percentages of glandular tissue: 70% (magenta), 50% (yellow), 25% (green) and 0% (blue).	110
Figure 9.11: Two mammograms (left, center) and the result of their registration (right)..	111

Figure 9.12: Two standardized mammograms (left, center) and the standardized result of their registration (right).	111
Figure 9.13: View as height fields.	112
Figure 9.14: View as contours.	112
Figure 9.15: View as NURBS surface.	113
Figure 9.16: View as Bézier surface.	113

LIST OF TABLES

Table 2.1: A comparison of methods for mammogram registration.....	32
Table 4.1: The components of fat and glandular tissues.....	48
Table 5.1: Schematic representation of a DICOM file. The pixel data is actually also a data element with tag (07FE0, 0010), value length and value field.....	50
Table 5.2: Some tags and their meanings.	52
Table 5.3: Data element with explicit value representation of OB, OW, OF, SQ, UN or UT (NEMA 2004b).....	53
Table 5.4: Data element with explicit value representation other than shown in table 3.3 (NEMA 2004b).....	53
Table 5.5: Data element with implicit value representation (NEMA 2004b).....	54
Table 7.1: Examples of the thresholds used to show the tissues combinations.....	78
Table 8.1: Summary of UML notation for class diagrams.	93
Table 8.2: Summary of UML notation for sequence diagrams.	96

LIST OF ABBREVIATIONS

ACR	American College of Radiology
BI-RADS	Breast Imaging Reporting and Data System
B-Rep	Boundary Representaion
B-Spline	Basis Spline
CAD/CAM	Computer-Aided Design/Computer-Aided Manufacturing
CC	Craneo-caudal
cm	Centimeters
cm ²	Square Centimeters
CSG	Constructive Solid Modeling
DICOM	Digital Imaging and Communication in Medicine
FFDM	Full-field digital mammography / Full-field digital mammogram
g	Gramms
kVp	Peak Kilovoltage
MI	Mutual Information
MLO	Mediolateral-Oblique
mm	Milimeters
NEMA	National Electrical Manufacturers Association
NURBS	Non Uniform Rational Basis Spline
OB	Other Byte String
OF	Other Float String
OW	Other Word String
PACS	Picture Archiving and Communication Systems
RGB	Red-Green-Blue
SQ	Sequence of Items
UN	Unknown
UT	Unlimited Text
VL	Value Lenght
VR	Value Representation

ABSTRACT

Breast cancer represents the most frequent cancer within women. Besides clinical examination and self-examination, breast imaging plays a very important role in detecting breast cancer before tumors turn clinically visible. The mammography, a radiograph of the breast, is the most widespread test for the early detection of breast cancer.

The images obtained through mammography are known as mammograms and they visualize the breast structure. The woman breast consists of fibroglandular and fatty tissue. Increased mammographic breast density, an increase of fibroglandular tissue, is a factor that influences the risk of becoming affected with breast cancer. Computer-based image analysis could help to find such abnormal changes in the breast tissues from digital mammograms.

Full-field digital mammograms are acquired using an electronic detector and they are stored using the DICOM standard file format. In this thesis we first describe the image acquisition process, the DICOM file format as well as the conventional and digital mammography, together with its advantages for computer-based image processing.

Former image processing methods and their application into mammograms were also studied. These methods include the measurement of area and volumetric mammographic breast density, the segmentation and the registration of mammograms and methods that could be applied to visualize the breast density. Based on the knowledge on the acquisition process, the DICOM file format and the former methods, computer-based image analysis methods were developed during this research project. All the methods were implemented in a software prototype to test them. The software architecture of the prototype is also shown in this thesis.

The main contribution of this work is a new method for the measurement of volumetric breast density. This measurement of volumetric breast density consists in the interpretation of pixels gray levels from full-field digital mammograms to determine which combinations of tissues they represent. In order to be able to compare many images, after performing the measurements, the images are standardized and registered. From the breast composition and its changes, a conclusion could be reached in relation to a suspected cancer or an elevated breast cancer risk.

Additionally, some image processing methods were developed to prepare the images for the analysis. These methods segment the mammogram into background, pectoral muscle and breast tissue. The information obtained from the analysis of the mammograms could also be used for the detection of microcalcifications and the skin line or breast border. The mammograms are then graphically shown using different two and three-dimensional views.

The last chapters show the results of the computer-based image analysis of the full-filed digital mammograms using the software prototype, conclusions and future work.

ZUSAMMENFASSUNG

Brustkrebs ist die häufigste Krebsart bei Frauen. Neben klinischer Untersuchung und Selbstuntersuchung, stellen bildgebende Untersuchungen der Brust eine sehr wichtige Rolle zur Erkennung von Brustkrebs dar, noch bevor Tumoren klinisch sichtbar werden. Dabei ist die Mammographie, eine Röntgenuntersuchung der Brust, der bedeutendste Test zur Früherkennung von Brustkrebs.

Das Bild, das durch eine Mammographie gewonnen wird, wird Mammogramm genannt und stellt die Bruststruktur dar. Die weibliche Brust besteht aus Drüsen- und Fettgewebe. Eine erhöhte mammographische Brustdichte, welche eine Zunahme des Drüsengewebes bedeutet, ist ein Faktor, der die Brustkrebsgefahr beeinflusst. Computer-gestützte Bildanalyse könnte helfen, solche abnormale Veränderungen im Brustgewebe anhand von digitalen Mammogrammen zu finden.

Digitale Vollfeld-Mammogramme werden mit einem elektronischen Detektor erzeugt und üblicherweise im DICOM Standard Dateiformat gespeichert. In der vorliegenden Dissertation beschreiben wir zunächst das Bildaufnahmeverfahren, das DICOM Dateiformat sowie die herkömmliche und digitale Mammographie, zusammen mit den Vorteilen für die computer-gestützte Bildbearbeitung.

Frühere Bildbearbeitungsmethoden und ihre Anwendung in Mammogrammen wurden ebenfalls erforscht. Diese Methoden schließen die Messung der mammographischen Brustdichte sowohl als Fläche als auch als Volumen, sowie die Segmentierung und die Registrierung der Mammogramme ein. Es wurden auch Methoden untersucht, die zur graphischen Brustdichtedarstellung angewendet werden könnten. Basierend auf dem Wissen über das Bildaufnahmeverfahren, das DICOM Dateiformat und die bereits existierenden Methoden, wurden in diesem Forschungsprojekt computer-gestützte Bildanalysemethoden entwickelt. Alle Methoden wurden in einem Softwareprototyp realisiert, um sie zu testen. Die Softwarearchitektur des Prototyps wird in dieser Dissertation ebenfalls dargestellt.

Der zentrale Beitrag dieser Arbeit ist die Entwicklung einer neuen Methode zur Messung der volumetrischen Brustdichte. Die Messung der volumetrischen Brustdichte besteht in der Interpretation der Pixelgraustufen von digitalen Vollfeld-Mammogrammen, um festzustellen, welche Gewebeszusammensetzung ihnen zugrunde liegt. Um mehrere Bilder miteinander vergleichen zu können, werden sie standardisiert und registriert. Aus der Brustzusammensetzung und deren Veränderungen könnte eine Aussage bezüglich des Brustkrebsrisikos getroffen werden.

Zusätzlich wurden Bildbearbeitungsverfahren entwickelt, um die Bilder für die Analyse vorzubereiten. Diese Methoden segmentieren das Mammogramm in Hintergrund, Brustmuskel und Brustgewebe. Die Informationen, die man aus der Analyse der

Mammogramme ziehen kann, könnten für die Lokalisation von Mikrokalzifikationen und des Brustrand es verwendet werden. Die Mammogramme werden dann graphisch mit unterschiedlichen zwei- und dreidimensionalen Ansichten dargestellt.

Die letzten Kapitel zeigen die Ergebnisse der computer-gestützten Bildanalyse der digitalen Vollfeld-Mammogramme nach Verwendung des Softwareprototyps, die Zusammenfassung und die Perspektiven.

1 INTRODUCTION

Automatic pattern recognition aims to classify data by the extraction of meaningful information from the input data. When digital images are used as input, it is then called image analysis. Computer-based image analysis can solve a wide range of problems. Its applications range from cell counting in microscopy to star counting in astronomy, to quality control in manufacturing, or handwritten character recognition. When the images to be processed show parts of the human body, it is called medical image analysis.

Digital image processing techniques include an almost unlimited number of topics: image acquisition, image formation, image reconstruction, image enhancement, image compression and storage, image analysis, image-based visualization, image segmentation, image registration, motion tracking and change detection, measurement of structures and so forth.

In this work, we present computer-based image analysis methods and their application in digital mammograms, together with a software prototype that implements them to probe their practical use. These methods are related to the topics of classification, standardization, image segmentation, image registration, and change detection from image sequences.

Classification consists in assigning objects to a certain class. This means studying the relation between object features and object classes, and of course selecting appropriate features that best characterize the objects and classes. The process can be summarized in four steps: first, the definition of the classes and attributes; second, the definition of the feature space; third, the setting of a decision algorithm that partitions the feature space and assign labels to each region; and last, the measurement of the performance. For our application, we use classification as segmentation, pixel and object based, to identify the regions (classes) in the image (background, muscle and breast). Afterwards, to sub-classify the most interesting class (breast) into subclasses describing a qualitative third dimension that is defined as the amount of fibroglandular tissue represented by each gray level. This was the most difficult problem to solve, because it consists actually in deriving a combination of tissue that only exists in the real world from a gray level in an image.

Standardization means for us the definition of the classes. Because for different images different classes are generated, this step consists in making these classes compatible and comparable, by annulling acquisition parameters.

Once the images are comparable, the next step is to align them. The process of finding the geometrical transformation that best aligns the images is called registration.

In the application, these techniques are applied to digital mammograms to find abnormal changes in the breast tissues. Increased mammographic breast density is such a change and

a factor that influences the risk of becoming affected with breast cancer. Unlike other risk factors, it can be quantified. The estimation of breast density could then help to find high-risk populations and to take preventive decisions.

Breast density is a feature that can be understood as area breast density or volumetric breast density. The first estimates the breast density as the ratio of the projected area of dense tissue to the projected area of the whole breast. Area breast density considers each pixel as either fibroglandular tissue or fatty tissue. Volumetric breast density assumes that each pixel represents a combination of these tissues. Volumetric breast density can be considered as the volume of fibroglandular tissue in the breast.

In addition to the question of measuring breast density, other issues should be solved in order to make the measurements valuable. These consist in making measurements from different equipment comparable, in aligning the images to make a better comparison, and in presenting the results in an appropriate manner.

We present algorithms and a system that integrates all these features, including:

- A method for the measurement of volumetric breast density from full-field digital mammograms (FFDM), adding a qualitative third dimension to the images;
- A standardization of images based on the breast density measurements;
- A comparison of images as mutual information based registration.

Besides these main solutions, we present methods that are needed to prepare the images for the evaluation. We also propose some approaches to show the results and the application of the evaluation algorithm to other problems related to the analysis of mammograms.

These methods are:

- The segmentation of the image into background and breast;
- The segmentation of the pectoral muscle when present;
- The detection of the breast border;
- The detection of calcification;
- The visual presentation of the results.

Some parts of this dissertation were previously published (Lampasona 2006, Roller and Lampasona 2006, Lampasona 2007, Lampasona and Roller 2008).

This document is organized in ten chapters. In Chapter 2 former image processing methods and their application into mammograms are presented. These methods include the measurement of area and volumetric mammographic breast density, the segmentation and the registration of mammograms and methods that could be applied to visualize the breast density. Chapter 3 and 4 shortly present the medical and physical background. In Chapter 5 the medical imaging standard DICOM is introduced and the file format is presented in

detail. Conventional and digital mammography, together with its advantages for computer-based image processing are shown in Chapter 6. The computational methods developed during this research project for the analysis of digital mammograms are extensively described in Chapter 7. Chapter 8 contains the documentation of the software architecture. The results of the application of the methods developed are summarized in Chapter 9. Conclusions and proposed future work are presented in Chapter 10.

2 RELATED TECHNOLOGIES

This project is centered in four topics from the wide scope of image analysis: classification, image segmentation, image registration, and change detection from image sequences.

The segmentation of structures began to be investigated in the early 1980s with the use of growing regions, the detection of contrast edges, contour search and deformable boundary search. These techniques have been improved and extended until now with, for example, three-dimensional segmentation and texture-based segmentation.

The need for image registration appeared also in the 1980s. Registration was first used in angiography for the subtraction of images taken with and without a contrast medium. It was also used for the quantification of cardiac motion and for three-dimensional multimodality registration.

In the 1990s, medical image analysis began to be researched for the use in surgery and it is now broadly applied in minimally invasive surgical procedures, preoperative planning and training (Duncan and Ayache 2000).

Nowadays, many methods are included as a common software package as a part of commercial medical equipment and workstations.

In this chapter, the state of the art of medical image analysis and visualization of medical images in relation to mammography is presented. The methods are grouped in four categories: 1) breast density measurement, 2) segmentation, 3) registration, and 4) visualization.

2.1 Breast Density Measurement

The main objective of this thesis is to explore the possibilities of analyzing digital mammograms to measure breast density in a quantitative and reproducible way.

In their survey, Harvey and Bovbjerg (2004) found no standard method to quantify breast density, but they believe that digital mammography could offer possibilities for objective quantification.

Many different approaches have been used throughout time to measure breast density. They could be classified in area and volume-based methods. The first estimates the breast density as the ratio of the projected area of dense tissue to the projected area of the whole breast. Volumetric breast density assumes that behind each pixel there is a combination of these tissues and can be considered as the volume of fibroglandular tissue in the breast.

Area-based Estimation of Breast Density

The most widespread approach is visual estimation, which only uses the expertise of the radiologist. It consists in classifying the mammograms according to some category system. The number of categories can vary from five to twenty. Boyd *et al.* (1995) proposed the most frequently used method having six categories.

The American College of Radiology developed BI-RADS (Breast Imaging Reporting and Data System) in 1993 to standardize mammography reporting terminology and the classification categories. BI-RADS considers four categories: 1) almost entirely fat; 2) scattered fibroglandular densities; 3) heterogeneously dense, may lower the sensitivity of mammography; and 4) extremely dense, which could obscure a lesion on mammography. This classification system is based on quantitative assessment, although the categories are not defined by the percentage of density. The advantage of the BI-RADS classification is its wide use in USA, allowing the analysis of large study populations. The last version of BI-RADS appeared in 2003 (American College of Radiology 2003).

The first methods that used computer assistance were based in planimetry. In 1987, Wolfe *et al.* (1987) used computer-assisted planimetry: an acetate overlay was placed over the mammogram and a wax pencil was used to outline the breast and the glandular tissue. To obtain the total area of the breast and the total area of glandular tissue a computerized planimeter was used (Wolfe *et al.* 1987, Saftlas *et al.* 1991, Kato *et al.* 1995). The percentage of density is then given by the ratio between the area of glandular tissue and the total area of the breast.

With the digitization of mammograms, glandular tissue and the total area of the breast were outlined by using a mouse (Ursin *et al.* 2001) or through interactive thresholding segmentation of the mammogram (Byng *et al.* 1998, Freedman *et al.* 2001).

Automated calculation of the percentage of density using segmentation was investigated by many authors. Karssemeijer (1998) developed a technique that uses a distance transform to obtain regions whose distance to the skin line is approximately equal. Sivaramakrishna *et al.* (2001) applied Kittler's optimal threshold to estimate breast density. Zhou *et al.* (2001) used rule-based classification to classify the mammograms into different categories of density.

Volume-based Estimation of Breast Density

Some authors investigated the use of magnetic resonance imaging (Lee *et al.* 1997, Graham *et al.* 1996) and ultrasonography (Blend *et al.* 1995), but these methods may not result as useful for widespread use as the density information obtained from mammograms.

The volume-based estimation of breast density from mammograms has been investigated more intensively in the last years.

Highnam and Brady (1999) developed the so-called h_{int} calculation: normal fibrous tissue and tumorous tissue cannot reasonably be distinguished at a local scale based on pixel brightness. For this reason fat (clinically uninteresting), and fibrous tissue/tumor (interesting) are differentiated. From an analysis of the image degrading effects, the percentage of interesting tissue is determined from digitized mammograms. This approach has been improved and is now known as SMF (standard mammogram form) (Highnam *et al.* 2007).

Shepherd *et al.* investigated the use of dual (Shepherd *et al.* 2002) and single (Shepherd *et al.* 2005) x-ray absorptiometry for measuring breast density. They presented an automated method called “Breast Compositional Density measured using x-ray absorptiometry techniques” or BD(SXA). It measures breast compositional density by comparing the opacity on the mammogram to two reference standards imaged with each breast.

Van Engeland *et al.* (2006) developed a method for FFDM, which uses a physical model of image acquisition.

2.2 Segmentation

Segmentation methods are used in the analysis of digital mammograms to separate the different regions of interest in the image: i.e. breast tissue, fatty tissue, breast border, pectoral muscle and background. They are also needed for segmenting microcalcifications, cysts and tumors.

Segmentation consists in partitioning an image into non-overlapping constituent regions that are homogeneous with respect to some characteristic such as intensity or texture (Haralick and Shapiro 1985, Gonzalez and Woods 1992, Pal and Pal 1993).

If Ω is the domain of the image, the segmentation consists in finding the sets $S_k \subseteq \Omega$, whose union is the entire image Ω (Pham *et al.* 2000). Thus, the sets that conform a segmentation of an image must satisfy:

$$\Omega = \bigcup_{k=1}^K S_k \quad (\text{Equation 2.1})$$

with the following properties:

- a) $S_k \cap S_j = \emptyset$ for $k \neq j$;
- b) Each S_k is a connected region for $k = 1, 2, 3, \dots, K$;
- c) $P(S_k) = \text{TRUE}$ for $k = 1, 2, 3, \dots, K$;
- d) $P(S_k \cup S_j) = \text{FALSE}$ for $k \neq j$.

$P(S_k)$ is a logical predicate defined over the points in set S_k , and \emptyset is the null set.

If the regions are not connected, then determining the sets S_k is called pixel classification, and the sets themselves are called classes. The process of assigning a meaningful designation to each region or class is called labeling.

The amount of interaction in segmentation methods can vary from the manual delineation of the structure to the selection of a seed point for a region growing method. Different interactions require different amounts of time and effort, and more interaction requires more training of the operators (Davenport *et al.* 1988).

Experiments for validation are used to quantify the performance of segmentation. The most used validation strategy consists in comparing the automated segmentation with manual segmentations. Alternative methods to validate segmentation are software simulations, anthropomorphic phantoms and cadaver studies (Suetens 2002).

Partial-volume effects are common in medical images and occur where different tissues contribute to a single pixel, resulting in a clouded portion of intensity across boundaries. The most common approach to addressing partial-volume effects is to produce segmentations that allow regions or classes to overlap, called soft segmentations. This soft segmentation is different to the normal hard segmentation that enforces a binary decision on whether a pixel is inside or outside the object (Pham *et al.* 2000).

Soft segmentations can be defined by the generalization of a characteristic function. A characteristic function can be defined by denoting whether a pixel is inside or outside a set. For a location $j \in \Omega$, where Ω is the entire image, the characteristic function $X_k(j)$ of set S_k is defined as

$$\begin{aligned} X_k(j) &= 1 & \text{if } j \in S_k \\ X_k(j) &= 0 & \text{otherwise} \end{aligned} \tag{Equation 2.2}$$

A characteristic function can be generalized to a membership function $m_k(j)$ satisfying the following constraints (Zadeh 1965):

$$\begin{aligned} 0 \leq m_k(j) \leq 1 & \quad \text{for all } j, k \\ \sum_{k=1}^K m_k(j) = 1 & \quad \text{for all } j \end{aligned} \tag{Equation 2.3}$$

Membership functions can be probability functions or they can be computed as estimates of partial-volume fractions. Soft segmentations can be converted to hard segmentations by assigning a pixel to the class with the highest membership value.

Intensity inhomogeneities cause a shading effect to appear over the image and can degrade the performance of methods that assume that the intensity value of a tissue class is constant over the image. There are two prevailing approaches for modeling inhomogeneities. The first one assumes that the main intensity for each tissue class is spatially varied and that these main intensities are independent of one another (Rajapakse 1997). The second one

models the inhomogeneities as a multiplicative gain field (Pham and Prince 1999) or additive bias field of the image logarithm (Wells *et al.* 1996).

In the next paragraphs, important image segmentation methods are described. These methods are commonly used in combination to solve different segmentation problems.

Thresholding Methods

Thresholding methods are based on histogram analysis and are a common first step in a sequence of image analysis operations.

The histogram h_{Ω} of an image Ω is a probability distribution on a set of possible gray levels (or colors). The probability $P(r_k)$ of a gray value r_k is given by its relative frequency in the image:

$$P(r_k) = \frac{n_k}{n} \quad (\text{Equation 2.4})$$

$r_k = k^{\text{th}}$ gray level;

n_k = number of pixels in image Ω with that gray level;

n = total number of pixels in the image Ω ;

$k = 0, 1, 2, \dots, K$;

K = total number of gray levels in the image Ω .

During the thresholding procedure, an intensity value (the threshold) is identified that separates the desired classes. The segmentation is done by grouping in a class all pixels with intensities greater than the threshold and the other pixels into another class. The determination of more than one threshold value is a process called multithresholding (Sahoo 1988).

Histogram based techniques are widely used in digital mammography to separate the breast region from the background under the assumption that the background has a homogeneous gray level. This can be problematic because a homogeneous background is not always the case, so the threshold should be carefully selected. This technique has been used based on simple thresholding by Hoyer and Spiesberg (1979); Lau and Bischoff (1991) and; Byng and Boyd (1996). Bick and Giger (1995) used a combination of thresholding, region growing and morphological filtering. Masek and Attikiouzel (2000) proposed a local thresholding method.

Edge Detection

Edge detection is commonly used to find meaningful discontinuities in gray level that represent edges of objects in the image.

The most used edge detection techniques include convolution-matrix based operators and Hough transforms. Common post-processing techniques used to refine the results are edge image thresholding, edge relaxation and border tracing.

Convolution matrices are matrices used to calculate the gradient in different directions over the image. Convolution operators are often defined as 2×2 , 3×3 , and 5×5 matrices that convolved with the image produce a number of filtered images, which are combined together to obtain an edge (Pham *et al.* 2000). The simplest of these filters is the Robert operator. Other widely used filters are the Prewitt operator, the Sobel operator and the Laplacian gradient operator. The difference between them is whether they use the first derivative or the second for the calculation. The Laplacian gradient operator uses the second derivative of the image and the first derivative is used by the Sobel operator and by the Prewitt operator.

The Hough transform is based in the parameterization of the regular curves in the image space. The curve commonly used is a straight line that can be parameterized as

$$y_i = m x_i + c \quad \text{(Equation 2.5)}$$

for some m and c and for all points (x_i, y_i) on the line.

There is an infinite number of lines that pass through (x_i, y_i) , but not all satisfy equation 2.5 for varying values of m and c (Pham *et al.* 2000).

The process begins by calculating for every pair of edge points from the image the m and c , which correspond to a line between them. If a line is present, many points will map to the same m and c . The parameter space is represented as a grid, a counter indicates each time a given value for m and c results from a pair of edge points, which allows finding the largest value. Once a value is identified corresponding to m and c , the definitive line is approached. The problem of finding a line in the image has been changed to finding local maxima in the parameter space.

A possible problem that may arise when using these parameters is that, for a vertical line, slope and intercept approach infinity. For this reason sometimes it is better to work with other parameters.

The disadvantage of this method is the beforehand knowledge of which kind of curve is being looked for.

Through edge relaxation, a probability is calculated on how likely an edge detected is actually an edge. The probability is calculated taking into account factors like the proximity or the direction of adjacent edge pixels, as well as the strength and length of the edge. If a weak edge between two strong ones is considered, it should be taken like part of the edge. However, an isolated edge, even a strong one, is likely to be false (Pham *et al.* 2000). The procedure is done iteratively. During each iteration a label it is given of *yes*, *no* or *maybe* for an edge pixel, until there are no *maybes* left.

Border tracing can be implemented by using different methods. One method is based on detecting either the inner or outer boundary perimeters. Another approach calculates the extended boundary and stores the pixels defining the edge into a string. Once the boundary of a region has been defined, it is easy to label the region for segmentation purposes.

Edge detection techniques have been used since the early work of Semmlow and Shadagopappan (1980), who used spatial filters and a Sobel operator to obtain the breast boundary. Méndez and Tahoces (1996) used a combination of two-level thresholding with gradient calculation to detect the breast border. Karssemeijer and te Brake (1998) used global thresholding to find a preliminary region, which was then processed using a Sobel operator. They extracted the pectoral muscle using a Hough transform. Abdel-Mottaleb and Carman (1996) detected the breast border via a gradient calculation in two images and their union. Zhou *et al.* (2001) also used gradient calculation to estimate the position of the breast border.

Region Growing Methods

Region growing partitions an image into regions by grouping adjacent pixels based on some predefined criteria as color, gray level, texture, or any other criterion. Region growing requires one or more seed points and extracts all pixels connected to it/them, based on the predefined similarity property (Pham *et al.* 2000).

The breast segmentation presented by Raba *et al.* (2005) uses an adaptive histogram approach to separate the breast from the background and a region-growing algorithm to obtain the pectoral muscle suppression. Guliato *et al.* (1998) presented a method based on fuzzy region growing for the segmentation of tumor regions in mammograms.

Classifiers

Classifiers intent to partition a feature space obtained from the image using data with known levels (Pham *et al.* 2000). A feature space is a range of some function of the image, like the image intensities. Classifiers need training data and they are called supervised methods. These methods require partitions to be found to have a distinctive quantifiable feature.

Saha and Udupa (2001), Rickard *et al.*(2003) and Wirth *et al.* (2004) used classifiers-based techniques to segment the breast part of the image from the background.

Clustering

Clustering methods work in the same way as classifiers, but they do not use training data. For this reason, they are known as unsupervised methods. Instead of using training data, they iteratively check the results by alternation of segmentation and characterization of each class (Pham *et al.* 2000).

Markov Random Field Models

A Markov random field model itself is not a segmentation method but is incorporated into clustering segmentation algorithms. It is based on interaction between neighboring or nearby pixels. Under the assumption that most pixels belong to the same class as their neighbors, classes with a very small amount of pixels have a lower probability of occurrence. The segmentation maximizes the probability of a partition to appear. This maximization can be achieved using iteration of conditional modes (Pham *et al.* 2000).

Li *et al.* (1995) proposed a technique for the detection of tumors in mammograms. They used adaptive thresholding to extract regions of interest and achieved a further segmentation by a modified Markov random field. McGarry and Deriche (2000) presented an approach to mammographic image segmentation based on tissue mixtures using Markov random fields.

Artificial Neural Networks

Artificial neural networks are parallel networks of processing elements that simulate biological learning. Each node in the network performs elementary computations. Learning is achieved through the adaptation of weights assigned to the connections between nodes (Clark 1991). Artificial neural networks can be used as a classifier, in which the weights are determined by using training data and the artificial neural network is then used to segment new data. They can also be used as a clustering method or for deformable models. Although artificial neural networks are inherently parallel, their processing is usually simulated on a standard serial computer, thus reducing the potential computational advantage.

Hassanien and Ali (2004) developed an algorithm for segmenting masses in mammograms based on neural networks and fuzzy set theory. Eckert *et al.* (2003) used a radial-basis-function neural network to segment mammograms into tissue and non-tissue regions. Suckling *et al.* (1995) developed an algorithm that uses neural networks for the segmentation of the mammogram into background, pectoral muscle, glandular tissue and adipose tissue. Zheng *et al.* (1996) proposed a mixed-feature-based neural network for the detection of microcalcifications clusters.

Deformable Models

Deformable models delineate region boundaries by using closed parametric curves or surfaces that deform under the influence of internal and external forces (Suetens 2002). A closed curve or surface must first be placed near the desired boundary and then allowed to undergo an iterative relaxation process. Internal forces are computed from within the curve or surface to keep it smooth throughout the deformation. External forces are usually derived from the image to drive the curve or surface toward the desired feature of interest. Ma *et al.* (2005) presented a method for pectoral muscle segmentation based on an

adaptive deformable contour model. Valverde *et al.* (2004) used a deformable model for the segmentation of vessels from mammograms.

Atlas-Guided Approaches

Atlas-guided approaches are based on a standard atlas or template. The atlas is generated by compiling information on the anatomy that requires segmenting and used as a reference frame for segmenting new images. Atlas-guided approaches are similar to classifiers but they are implemented in the spatial domain of the image rather than in a feature space.

Model Fitting

Model fitting consists in fitting a geometric shape to the locations of extracted image features in an image. Model fitting can be easily implemented and it provides good results when the model is appropriate. However, it is specialized to the structure being segmented. The main disadvantage of model fitting is that it requires the image features to be extracted before the fitting (Pham *et al.* 2000).

Stamatakis and Cairns (1994) used a threshold and a cubic B-Spline to extract the breast border. Chandrasekhar and Attikiouzel (1996) presented a polynomial model that uses an initial threshold to approximate the breast region. A polynomial fitting model was also proposed by Goodsitt and Chan (1998).

Watershed Algorithms

Watershed algorithms combine edge detection and mathematical morphology to partition images into homogeneous regions. The method can produce over-segmentation, an unnecessarily large number of regions. In medical image analysis, it is usually followed by a post-processing step to merge separate regions that belong to the same structure (Pham *et al.* 2000).

Sheshadri and Kandaswamy (2005a, 2005b) presented different methods based on the watershed transform for the identification of abnormal growth of tissues and tumors in mammograms. Toledo Santos *et al.* (2002) described a segmentation technique that uses the watershed transformation to provide mass detection in digitized images of dense breasts.

2.3 Registration

Radiologists inspect mammograms to find signs of a potential cancer. They compare the views of left and right breasts, looking for asymmetries, and mammograms from current and previous examinations. These comparisons help the radiologist in finding abnormalities. Performing such comparisons is complicated because many factors cause changes in the images, such as acquisition parameters, positioning and compression of the

breast. An image normalization method that suppresses these technical variations is registration.

Registration methods try to align images, shifted on time or from different modalities, in such a way that corresponding features can be compared and integrated. In other words, registration is concerned with determining a transform, which optimally matches the two images (Lehmann *et al.* 2002). During registration, a target image is mapped onto an original image, also called reference image. Usually, the reference image remains invariable, while the target image is moved.

Registration methods in general can be classified according to different criteria (Lehmann *et al.* 2002, Maintz and Viergever 1998):

- Dimensionality: Depending on the spatial dimensions of the images to be registered, the algorithms are classified according to the dimensions of original and target images in 2D/2D, 2D/3D, or 3D/3D. Considering time adds a new dimension.
- Basis: If the registration method is based on markers introduced in the image, it is called extrinsic registration. If the registration is based only on the image information, it is called intrinsic. A non-image based registration is performed on the calibration of the coordinate systems of the scanners used.
- Transformation: The transformation performed can be rigid (translation, rotation), affine (mapping parallel lines onto parallel lines), projective (mapping lines onto lines), or elastic (mapping lines onto curves). Elastic transformations are also known as curved transformations (figure 2.1).
- Domain of Transformation: The transformation is global if it is applied to the entire image and local if it is applied to a section of the image (figure 2.1).
- Interaction: The registration is automatic, if the algorithm only uses the image or information on the image acquisition. If the user interacts rejecting or accepting the registration, it is called semi-automatic. Finally, if the user does the registration itself assisted with software, it is called interactive.
- Optimization Procedure: The process of registration is sometimes reduced to the maximization or minimization of some function or parameter. These parameters can be found iteratively, in brute force methods, or using some heuristics.
- Modalities Involved: According to this criterion, the images to be registered could be acquired using different imaging methods or modalities. Therefore, the registration can be monomodal, multimodal, modality to model (atlas), or patient to modality (image compared to the patient itself).
- Subject: When the images to be registered were derived from the same patient, it is an intrasubject registration. If the images belong to different patients, it is an intersubject

registration. The atlas/patient registration occurs when comparing the image of a patient with an image constructed based on data from several patients.

- Object: Based on the body part to be compared, e.g. brain, thorax, spine, heart, breast, abdomen, liver, pelvis, and tissue.

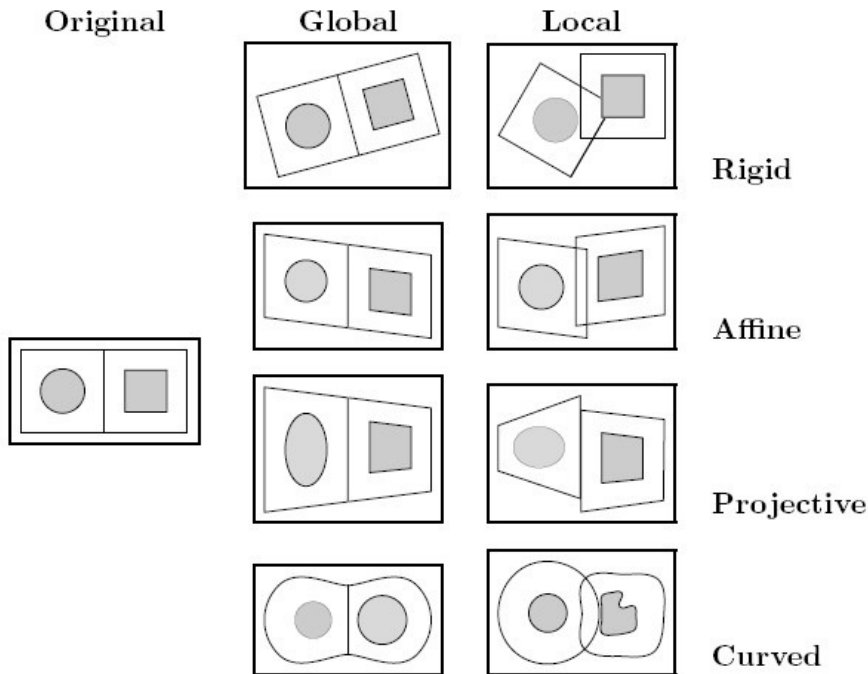


Figure 2.1: Some examples of transformations (Maintz and Viergever 1998).

Table 2.1 shows a comparison of methods for mammogram registration. These approaches use a combination of three criteria:

- Anatomical characteristics to be mapped: The methods based on this criterion use alignment procedures based on the location of the breast border, the nipple, the breast tissue or the chest wall. Once the anatomical characteristic is detected in the different views, they are positioned at the same location.
- Deformation criteria: Based on this criterion, the methods perform rigid or elastic transforms. In the last years, approaches performing elastic transforms usually used the maximization of mutual information (MI), which is computed from the joint probability distribution of the images' intensities. The warping approach uses control points located on the breast contour and the pectoral muscle. The control points are mapped onto each other and the warped images are obtained by interpolating between the control points.
- Type of comparison: While in temporal registration, two images, which were taken at different times, are registered, bilateral registration aligns projections of left and right

breast, which were taken at the same time. The appearance of breast tissue in previous and current mammograms of a patient can considerably differ due to differences in breast compression, positioning, in imaging techniques and in the breast itself.

Table 2.1: A comparison of methods for mammogram registration.

	Breast border	Nipple	Glandular	Chest wall	Rigid	Elastic	Temporal	Bilateral
Brzakovic <i>et al.</i> (1994a, 1994b)							X	
Giger <i>et al.</i> (1994)	X	X			X		X	X
Hadjiiski <i>et al.</i> (2001)							X	
Karssemeijer and te Brake (1998)	X							
Kok-Wiles <i>et al.</i> (1998)			X					
Kostelec <i>et al.</i> (1998)						X		X
Lau and Bischoff (1991)		X		X	X			X
Marti <i>et al.</i> (2001)			X					
Méndez <i>et al.</i> (1996, 1998)	X	X			X			X
Nishikawa <i>et al.</i> (1993)	X	X			X			X
Richard and Cohen (2003)						X		
Richard <i>et al.</i> (2002)					X			
Sallam <i>et al.</i> (1992)	X		X			X	X	
Sallam and Bowyer (1994, 1996)	X		X			X	X	
Sallam (1997)	x		X			X	X	
Semmlow and Shadagopappan (1980)	X	X			X			X
Sivaramakrishna and Gordon(1995, 1998)						X	X	
Sivaramakrishna (1998)						X	X	
Stamatakis and Cairns (1994)	X				X		X	X
Vujovic <i>et al.</i> (1996)							X	
Wirth <i>et al.</i> (2002)						X		
Yin <i>et al.</i> (1991, 1993, 1994)	X	X			X			X
Zouras <i>et al.</i> (1996)	X				X		X	

2.4 Visualization

Scientific visualization aims to represent data graphically. It is the mapping of data or information into images in order to gain a better understanding and insight into the data. It transforms numerical data into a geometric representation and allows observing simulated or measured data. It is very important because it allows compressing many data into one image, making possible to observe correlations between different quantities in space and time.

Visualization techniques can be classified according to the dimension of the domain of the quantity that is visualized. Digital mammography provides two-dimensional images. The aim of this project is to add a third abstract qualitative dimension to these images. For this reason, different options for the three-dimensional modeling are presented here.

There are three main approaches to three-dimensional modeling: wire frame, surface and volume modeling (Roller 1995).

Wire Frame Model

A wire frame model presents an object through its edges and vertices using straight lines or curves. Wire frame models do not describe an object's surface, but its underlying design structure. They are relatively simple and fast to calculate.

Surface Modeling

A surface model describes an object through its surface. The most used methods for surface modeling are polygonal modeling and parametric surfaces.

A polygonal model presents an object's geometry using polygons such as triangles and parallelograms. The use of a greater amount of surfaces for modeling results in a very detailed model, but it also needs more computing time.

Surface modeling with parametric surfaces was developed in the 1970s for the design and manufacture of complex shapes in automobile bodies (Orlamünder and Mascolus 2004, Abramowski and Müller 1991). Typical parametric representations are Bézier and NURBS (Non Uniform Rational Basis Spline) curves and surfaces. Parametric means that the curve or surface is a sequence of connected segments that use parameters to calculate points along the curve or surface.

NURBS modeling is the most frequently used modeling technology. The NURBS consists of a control net tangent to the curve or surface. This control net is compound by points, weights and parameter values. In a NURBS surface, the control net is a rectangular grid of connected straight-line elements that describe the tangency of the surface at positions along the control net. The points that describe the control net are not on the surface. The weights in the NURBS determine the amount of surface deflection toward or away from its control point.

The formal description of the Bézier surfaces is based on Bézier curves. The Bézier curve of degree n , given controls points P_0, P_1, \dots, P_n is described by:

$$B(t) = \sum_{i=0}^n P_i b_{i,n}(t) \quad t \in [0,1] \quad \text{(Equation 2.6)}$$

where the polynomials

$$b_{i,n}(t) = \binom{n}{i} t^i (1-t)^{n-i} \quad i = 0, \dots, n \quad \text{(Equation 2.7)}$$

are the Bernstein polynomials of degree n .

Figure 2.2 shows some examples of Bézier curves.

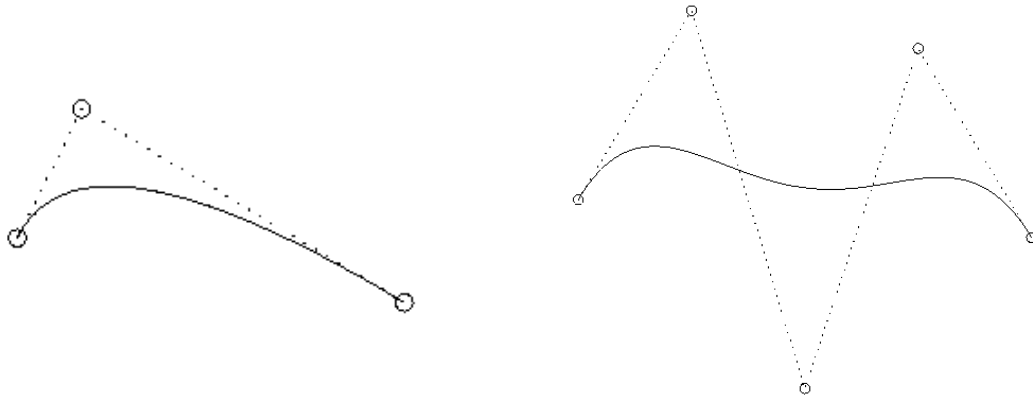


Figure 2.2: A quadratic Bézier curve and a Bézier curve of 4th degree.

A Bézier surface of order (n, m) , given control points $P_{i,j}$ for $i = 0 \dots n$ and $j = 0 \dots m$, and parameters (u, v) is given by:

$$B(u, v) = \sum_{i=0}^n \sum_{j=0}^m b_{i,n}(u) b_{j,m}(v) P_{i,j} \quad (u, v) \in [0,1]^2 \quad \text{(Equation 2.8)}$$

where $b_{i,n}(u)$ and $b_{j,m}(v)$ are Bernstein polynomials.

An example of a bicubic Bézier surface is shown in figure 2.3.

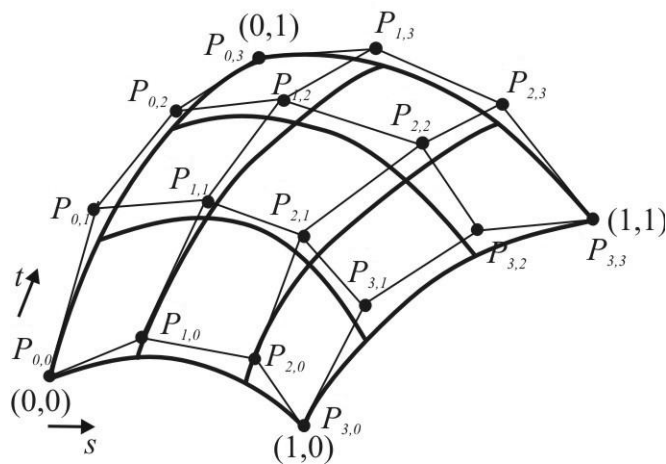


Figure 2.3: A bicubic Bézier surface. Adapted from Orlamünder and Mascolus (2004).

A NURBS curve is formally described as:

$$P(t) = \sum_{i=0}^n R_{i,k}(t) P_i \quad (\text{Equation 2.9})$$

with

$$R_{i,k}(t) = \frac{w_i B_{i,k}(t)}{\sum_{i=0}^n w_i B_{i,k}(t)} \quad (\text{Equation 2.10})$$

The B-Spline basic functions $B_{i,k}(t)$ are recursively defined as:

$$B_{i,1}(t) = \begin{cases} 1 & \text{for } t_i \leq t \leq t_{i+1} \\ 0 & \text{otherwise} \end{cases} \quad (\text{Equation 2.11})$$

$$B_{i,k}(t) = \frac{t - t_i}{t_{i+k-1} - t_i} B_{i,k-1}(t) + \frac{t_{i+k} - t}{t_{i+k} - t_{i+1}} B_{i+1,k-1}(t) \quad (\text{Equation 2.12})$$

with $k > 1, 0 \leq i \leq n$

NURBS curves properties can be translated into NURBS surfaces. A NURBS surface is defined by:

$$Q(s, t) = \frac{\sum_{i=0}^n \sum_{j=0}^m w_{i,j} B_{i,k}(t) B_{j,l}(s) P_{i,j}}{\sum_{i=0}^n \sum_{j=0}^m w_{i,j} B_{i,k}(t) B_{j,l}(s)} \quad (\text{Equation 2.13})$$

The functions $B_{i,k}(t)$ and $B_{j,l}(s)$ are B-Spline basic functions and $w_{i,j}$ the weights of the control points $P_{i,j}$.

Another option to show a qualitative third dimension in a two-dimensional image is contouring.

Contouring: The marching squares algorithm

Contouring consists in finding isolines. Isolines are curves that connect all points with the same value (isovalue). The marching squares algorithm is the simplest cell-based algorithm.

The first step consists in assigning to each cell one of the cases, in which an isoline may cross a cell (figure 2.4).

The isovalue is assigned to the variable *threshold*. The vertices of a cell are named *a*, *b*, *c* and *d*, where *a* is assigned to the bottom-left vertex and *b*, *c* and *d* are given to the other vertices in a counterclockwise direction. The points in white in figure 2.4 are assigned to

vertices, whose values are greater than the isovalue, and they belong to an isoline. To find the corresponding case for each cell the code in figure 2.5 is used.

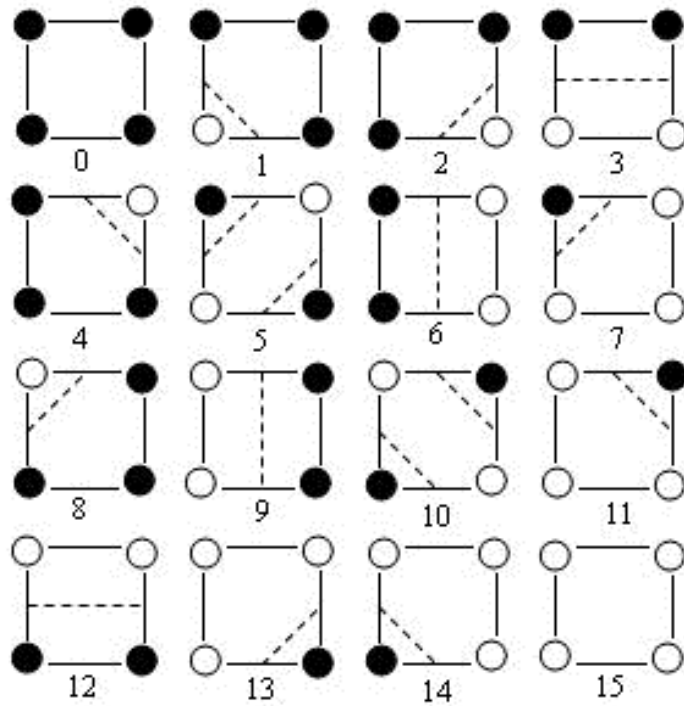


Figure 2.4: Sixteen cases of vertex labeling with contours (Angel 2003).

```
int cell(double a, double b, double c, double d){
    int n=0;
    if(a>THRESHOLD) n+=1;
    if(b>THRESHOLD) n+=8;
    if(c>THRESHOLD) n+=4;
    if(d>THRESHOLD) n+=2;
    return n;
}
```

Figure 2.5: Code for creating a contour plot (Angel 2003).

If symmetries are considered, only four cases are left:

- In the first case, only one point of the cell is cut by the isoline;
- In the second case, the isoline cuts the cell from one edge to the edge on the opposite side;
- For the third case, there exist two possibilities: the solutions 5 and 10. For this situation, a solution can be randomly chosen or the cells can be subdivided until a unique solution is found;

- In the fourth case, the isoline does not cut the cell.

Immediately after finding the cases, the points belonging to the same isoline are connected using the methods *draw_one()*, *draw_adjacent()* and *draw_opposite()*, as shown in figure 2.6.

```
switch(n){
  case 1: case 2: case 4: case 7: case 8: case 11: case 13: case 14:
    draw_one(n,i,j,a,b,c,d); // contour cuts off one vertex
    break;
  case 3: case 6: case 9: case 12:
    draw_adjacent(n,i,j,a,b,c,d); // contour crosses cell
    break;
  case 5: case 10:
    draw_opposite(n,i,j,a,b,c,d); // ambiguous cases
    break;
  case 0: case 15: break; // no contour in cell
}
```

Figure 2.6: Code for assigning the cell to one of the four canonical cases (Angel 2003).

Volume Modeling

There are several visualization methods used in medical applications and research. Two approaches to three-dimensional display of medical data will be discussed, namely geometrical modeling and volume rendering.

Constructive solid geometry (CSG) modeling is a well-known technology, which was developed for the use in computer-aided design and manufacturing (CAD/CAM). CSG combines geometric shapes, the so-called primitive solids, using regularized Boolean set operations (union, intersection, difference). A CSG model is represented as a tree, where the leaves represent primitive solids or transformation data and the nodes are set operations or transformed objects. These solids can be also represented as a set of vertices, edges and faces, using boundary representation (B-Rep) models (Roller 1995, Encarnaç o et al. 1990). Most medical CAD/CAM work has focused on hip, knee and cranial implants (Viceconti 2001, Eufinger and Saylor 2001, Dean and Min 2003).

Volume rendering is typically used to display two-dimensional projections of a three-dimensional discretely sampled data set. Such three-dimensional data set is a group of two-dimensional slice images. The volume can be displayed using surfaces made-up of polygonal meshes or by rendering the volume as a block of data. The most widespread technique for volume rendering in medical applications is based on ray-casting algorithms (Robb 2000). In this approach, a ray is generated for each desired image pixel to define the geometry of the rays cast through the scene.

In medicine, the visualization of the human body is not only used for diagnosis, but also for therapy and training. Many cases in which visualization is applied in medical solutions are shown in the brochure of the INI-GraphicsNet foundation (Encarnaç o 2006), like virtual reality simulators used in the training of surgeons, virtual reality systems for the

diagnosis and therapy of centrifuge traumas, a system for the design of dental prostheses, and clinical navigation systems for computer-assisted surgery.

3 MEDICAL BACKGROUND

The statistics of 2004 show that more than 47500 women get breast cancer annually in Germany, 19300 of them at an age under 60 years. Breast cancer represents the most frequent cancer within women. This disease is responsible for 24.4% of all new cases of cancer within women and more than one third (34%) of the new diseases within women under 60 years. The average disease age was in 2002 with 63 years, scarcely 4 years under the average disease age of cancer in general (Bertz *et al.* 2004). The statistics of 2006 show an increase of women suffering of breast cancer (55150), with an average disease age of 62 years. During 2004, 17592 women died of breast cancer in Germany (Bertz *et al.* 2006).

Breast cancer rates for Germany lie, in comparison with the European, in the middle third (figure 3.1). In Denmark, Belgium, Sweden and the Netherlands the probability of disease is higher, and clearly lower in South European countries such as Spain, Greece and Portugal (Bertz *et al.* 2004).

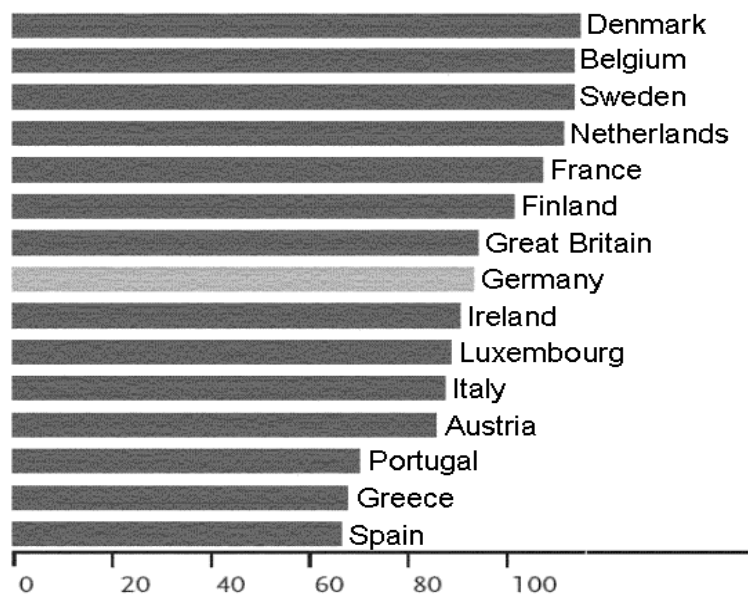


Figure 3.1: Age standardized disease frequency in women in the European Union 1998. Diseases per 100000 (Bertz *et al.* 2004).

The German mortality rate due to breast cancer is already declining since beginning of the 1990s (Bertz *et al.* 2004). Meanwhile, one of 10 women will develop cancer in her live. The probability of having this disease increases with aging (~1/5 under an age of 50, 2/5 between 50 and 70, 2/5 over 70) (von Minckwitz and Loibl 2001).

Fortunately, with an early diagnosis the healing probability is very high. In the early phase of the disease, it often does not have symptoms perceivable by the woman.

The most widespread procedure to detect breast cancer includes clinical examination by a trained professional, self-examination, and breast imaging.

3.1 Breast Imaging

Besides clinical examination and self-examination, breast imaging plays a very important role in detecting breast cancer before tumors turn clinically visible.

There are two kinds of breast imaging tests (Reem Diagnostic 2006): 1) screening, which is performed in patients with no symptoms to detect cancer when it is still too small to be felt by a woman or her physician; and 2) diagnostic, which is performed in women who either have a breast complaint or have had an abnormality found during screening.

The most used technologies for breast imaging are mammography, ultrasonography, and magnetic resonance imaging. Mammography is the most widespread test for the early detection of breast cancer and the chosen method for screening (Kolb *et al.* 2002).

The mammography is an x-ray examination, with which in many cases lumps can be recognized in a stage, in which they are not yet palpable. The terms mammography and mammogram are used to designate the test and the image produced using this examination. With the mammography, small details of the breast can be perceived, so that already microcalcifications starting from 0.1 mm in diameter, and small tumors starting from 5 mm diameter are detectable (Kolb *et al.* 2002).

The woman breast consists of fibroglandular and fatty tissue. The musculature behind the glandular tissue protects the ribs. Malignant tumors proceed generally from glandular tissue. A mammogram can show calcifications¹, masses² or other rare conditions.

During the breast examination with the mammography system, the breast is carefully held and compressed by the system's compression plate. Breast compression is necessary to flatten the breast so that the maximum amount of tissue can be imaged and examined. During a routine mammography examination, each breast is imaged separately: once from above (cranial-caudal view, CC) and once from an oblique view (mediolateral-oblique, MLO) (figures 3.2 and 3.3).

¹ Calcifications: Small mineral deposits in the breast tissue. They can be macrocalcifications or microcalcifications (less than 1/50 of an inch) (Imaginis Corporation 2006).

² Masses: These can be cysts, benign breast conditions or breast cancer. A cyst is formed by fluid in the breast. Benign breast conditions shall be monitored with periodic mammography and they may require biopsy. Breast cancer may be lobular carcinoma in situ, ductal carcinoma in situ or invasive carcinoma (Heywang-Köbrunner *et al.* 2001).

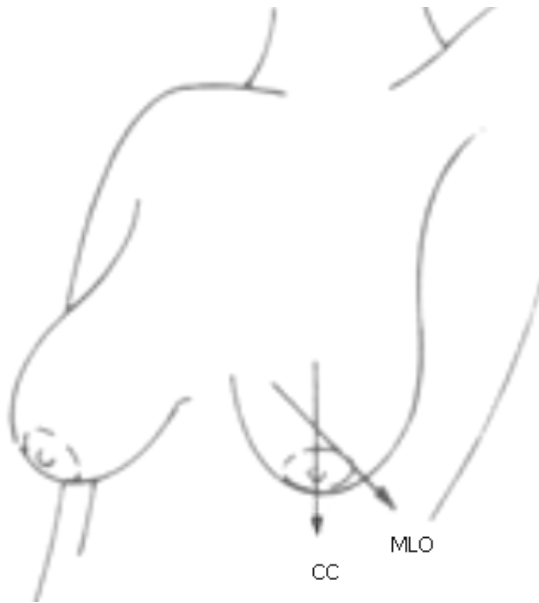


Figure 3.2: Cranial-caudal and mediolateral-oblique views (Imaginis Corporation 2006).

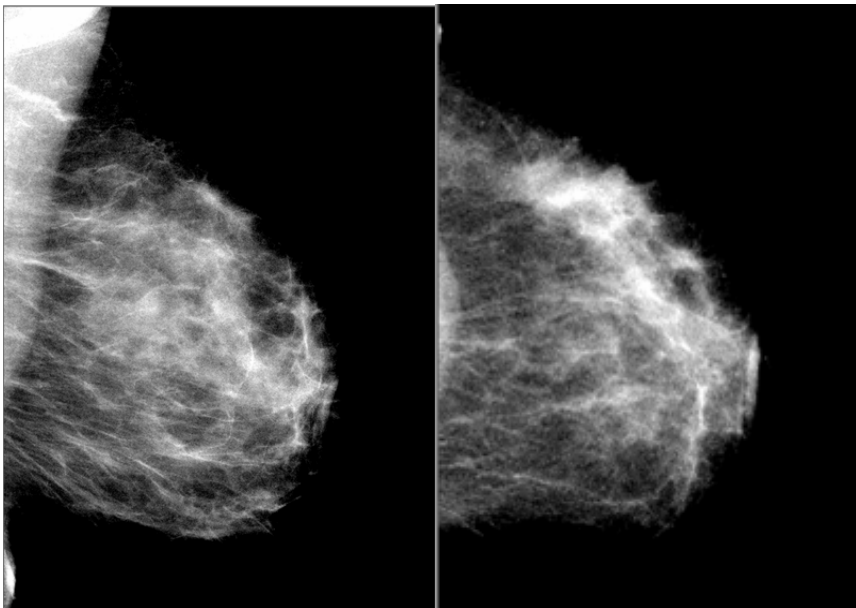


Figure 3.3: Two examples of images showing the mediolateral-oblique (left) and cranial-caudal (right) views.

3.2 Breast Density as a Breast Cancer Risk Factor

The more influencing breast cancer risk factors are being a woman, being 50 years of age or older, familiar history of breast cancer, having suffered of other malign diseases, early menarche, late pregnancy, childlessness, short lactation and overweight (von Minckwitz and Loibl 2001).

A breast cancer risk factor that could be quantified from mammograms is the breast density. Wolfe (1976) was the first to refer to the connection between the density of mammograms and an increased breast cancer risk. Increased mammographic densities are the consequence of a proliferation of the fibroglandular tissue. Harvey and Bovbjerg (2004) correlated mammographic breast density with relative breast cancer risk and the causes, which lead to a density increase. Breast cancer risk for women with increased breast density is in many studies four to six times higher than that for women with less dense tissue.

3.3 Breast Cancer Screening

The fact, that breast cancer can be detected at an early phase and that it is a common significant disease, makes it a screening disease. Other screening criteria are that it should have high sensitivity¹, high specificity² and low morbidity³. It should be reproducible, have low costs and produce more benefits than harm (Jong 2005).

In her surveillance, Roberta Jong (2005) discusses screening test criteria, options, pros and contras of the performance of different imaging modalities for screening. She concluded that mammography is the best method for screening of breast cancer.

The conduction of mammography-screening in Germany started in 2005 after many years of preparation, including the implementation of model projects, to test the use of the “European Guidelines for the Quality Assurance of Mammography-Screenings” under the conditions of the German health system. This screening follows a resolution of the Federal Ministry of Health of 1 January 2004 (Deutsche Bundestag 2006).

The objective of this mammography screening is to reduce the mortality caused by breast cancer. A requirement for this screening is the participation of at least 70% of the corresponding population group, i.e. all women between 50 and 69 years old.

The quality requirements are, among others, that two radiologists evaluate each mammogram, that each radiologist evaluates annually at least 5000 women, and that findings are clarified within the program.

The Central Offices, at a federal state level, invite the women between 50 and 69 years of age to participate in the program every two years, based on civil registration data.

¹ Sensitivity: Probability that if the person has the disease, the test will be positive (National Cancer Institute 2006).

² Specificity: The probability that if the person does not have the disease, the test will be negative (National Cancer Institute 2006).

³ Morbidity: Adverse effects caused by the test (National Cancer Institute 2006).

In general, a mortality reduction of 20% to 30% is expected, which means a significant benefit for the women participating in the screening (Hoeschen 2006).

4 PHYSICAL BACKGROUND

In the process of producing the x-ray images, photons penetrate the patient and are absorbed, transmitted or scattered. The image is produced by the primary photons leaving the patient and spoiled by secondary scattered photons. As a result, the image appears as a two-dimensional projection of the three-dimensional volume of the patient's breast depending upon the attenuation by the tissues (Aichinger *et al.* 2004). The absorption of x-rays depends on the density and atomic weight of the absorbing substance. At less atomic weight, there is more transparency to x-rays.

The various tissues composing the human body attenuate x-rays differently. Therefore, the images show several gray tones. The patient's body varies the velocity of the radiation. This modulation depends on the linear attenuation coefficients. The linear attenuation coefficient incorporates the contributions of all the photon interactions and depends on the material density. The thickness of the tissue structures and the selected exposure parameters affect also the radiation modulation. In mammography, it is difficult to visualize important image details due to the very similar tissue compositions. Figure 4.1 shows how the linear attenuation coefficients of the different breast tissues decrease with increasing energy in the energy range of x-rays used in mammography.

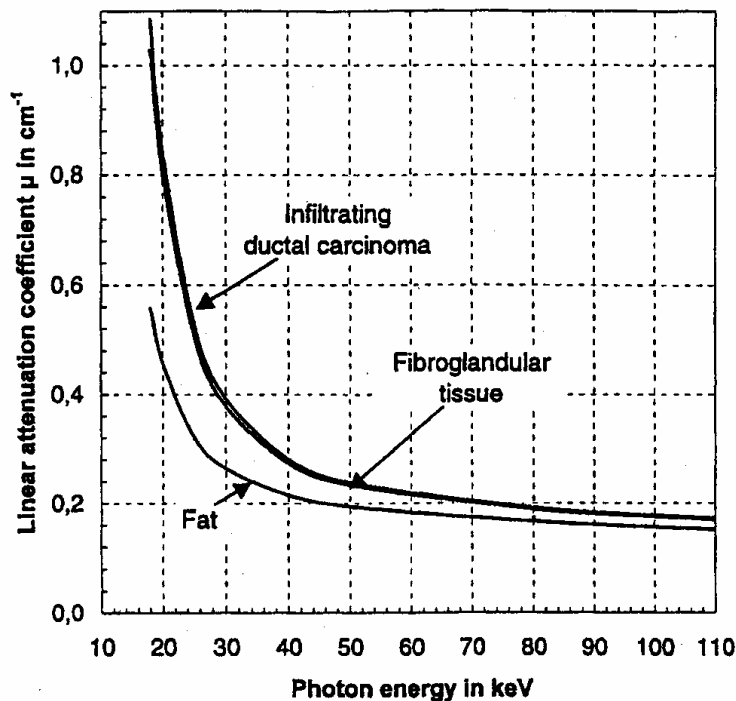


Figure 4.1: Linear attenuation coefficients of the different breast tissues and their variation with respect to photon energy (Aichinger *et al.* 2004).

4.1 Exponential Law of Attenuation

The exponential attenuation of a photon beam follows from the different ways in which photons interact with the material they cross. The exponential law of attenuation states the following:

“When a parallel beam of a number n_0 of mono-energetic photons passes a flat plate of material of thickness x , the number n of photons transmitted is given by:

$$n = n_0 e^{-\mu x} \quad \text{(Equation 4.1)}$$

where μ is the linear attenuation coefficient and depends upon the density of the material” (Aichinger *et al.* 2004).

The next paragraphs describe how this law is derived (Garbett 2004, Dössel 2000).

On a first step a thin slice of material, whose thickness (Δx) tends to zero, is considered. The assumption is made that if a molecule of material is in the way of an incoming photon, then the photon will be absorbed by the molecule. It is further assumed that the photons are spread out in space randomly in the y - z plane (parallel to the face of the slice) and that the photons travel only in the positive x direction. The number of photons absorbed by such a slice depends on the number of molecules in the slice. It also depends on the time interval, so the number of photons absorbed per second is considered as the dependent variable. The number of incoming photons is n , and it changes by Δn (so if photons are absorbed, Δn is negative). It can be said that the number of absorbed photons of a beam as the beam travels through such a thin slice is proportional to the thickness Δx of that thin slice, which is thought as made by placing very thin slices behind each other. That is, Δn is proportional to Δx .

Moreover, if the number of incoming photons per second is doubled, then twice as many photons are expected to be removed (since twice as many absorptions take place per second). This tells that also Δn is proportional to n .

If a quantity is proportional to two different quantities independently, then it is also proportional to the product of those two quantities. Therefore, Δn is proportional to $n \Delta x$.

A constant of proportion, m , is introduced and an equality is obtained. Since Δn was negative, it is written as $\Delta n = -m n \Delta x$ or $\Delta n/\Delta x = -m n$, where $m > 0$.

Now the limit as the thickness of the slice tends to zero is taken: $\lim_{(\Delta x \rightarrow 0)} \Delta n/\Delta x = dn/dx$ so, $\lim_{(\Delta x \rightarrow 0)} \Delta n/\Delta x = dn/dx = -m n$.

The relationship $dn/dx = -m n$ is the differential form of the attenuation law for light transmission. Its particular form is that of the general equation form: $dy/dx = c y$. This general form states that the value of the rate of change of a quantity (y), with respect to a certain independent variable (x), is proportional to the quantity itself. This property leads to

a process obeying an exponential law. The sign of the constant of proportion, c , will determine whether the process is one of growth or of decay. Both sides of the equation above are divided by y and integrated with respect to x on both sides:

$$\int \frac{1}{y} \frac{dy}{dx} dx = \int c dx$$

$$\int \frac{1}{y} dy = \int c dx$$

$$\ln y = c x + k$$

$$y = e^{cx+k} = e^{cx} e^k = A e^{cx}$$

The solution to the attenuation law of light photons can then be written as $n = A e^{-mx}$ where the negative sign attached to m has been carried into the solution.

When the beam is at the surface of the material, no photons will have been absorbed. Thus, n is the value of photons per second measured at $x = 0$. Call this value n_0 . Inserting $x = 0$ into the equation above gives $n_0 = A e^{-m \cdot 0} = A$ and so the equation becomes $n = n_0 e^{-mx}$.

This last formula is the exponential law of attenuation. It is also called the Lambert Law of Absorption, in honor of the Swiss-German physicist Johann Heinrich Lambert. The quantity m is called a coefficient, and is known specifically in radiation physics as the linear attenuation coefficient μ .

4.2 Attenuation Coefficients

The linear attenuation coefficient μ changes in proportion to the density of the material. To have a factor that does not change, μ is frequently normalized by the density ρ , making it a constant ($\mu/\rho = \text{constant}$).

The relation μ/ρ is known as mass attenuation coefficient and has units of cm^2/g . The value normally found tabulated is μ/ρ . In order to convert it to the linear attenuation coefficient, the variable in the exponential law of attenuation, μ/ρ is multiplied by the density of the material: $\mu = \rho \mu/\rho$.

The measurements of μ/ρ are compiled for elements (Hubbell and Seltzer 2004). Values of the mass attenuation coefficient, μ/ρ , for the different tissues in the breast are obtained according to simple additivity: $\mu/\rho = \sum [w_i (\mu/\rho)_i]$, where w_i is the fraction by weight of the i^{th} atomic constituent. Table 4.1 shows the components of fat (adipose) and glandular tissues.

Table 4.1: The components of fat and glandular tissues.

Tissue	Density	i	Component
Adipose	0.92	1	H (hydrogen)
		2	C (carbon)
		3	N (nitrogen)
		4	O (oxygen)
		5	Na (sodium)
		6	S (sulphur)
		7	Cl (chlorine)
Glandular	1.02	1	H (hydrogen)
		2	C (carbon)
		3	N (nitrogen)
		4	O (oxygen)
		5	Na (sodium)
		6	P (phosphorus)
		7	S (sulphur)
		8	Cl (chlorine)

5 DICOM FILE FORMAT

Medical image analysis usually requires a network environment involving multiple computers that communicate with each other. Typically, the images are transferred to a medical archive. In a modern hospital, a so-called “Picture Archiving and Communication System” connects all the digital imaging modalities via a communication network. The images are stored in the standard format DICOM in a central archive from where they can be retrieved for display and analysis on any suitable workstation.

DICOM stands for “Digital Imaging and Communications in Medicine” and it was developed by the American College of Radiology (ACR) and companies that manufacture medical equipment, members of the National Electrical Manufacturers Association (NEMA 2004a).

DICOM appeared as response to the need of a standard method for transferring images and related information between devices from different companies.

A commission to develop a standard was created in 1983 by the American College of Radiology and the National Electrical Manufacturers Association. As a result, two versions of a standard arose. The first one appeared in 1985, followed by two revisions. A second version in 1988 integrated version 1.0 and the former revisions. These publications gave specifications for hardware interface, software commands, and data formats (NEMA 2004a). The DICOM standard as known now was published in 1993 as DICOM 3.0 and since then improvements have been constantly made.

The main purposes of the standard are (NEMA 2004a):

- To support communication of digital image information, independently from device manufacturer;
- To ease the expansion and development of PACS (Picture Archiving and Communication Systems) being able of interfacing with other hospital information systems;
- To allow the creation of diagnostic information databases that could be accessed by a variety of geographically distributed devices.

The DICOM standard indicates (NEMA 2004a):

- A set of protocols for network communications;
- The syntax and semantics of commands and related information that can be exchanged using these protocols;
- A set of media storage services for media communication;

- A file format and a medical directory structure to ease access to the images and associated information stored on interchange media;
- Information that must be provided with an implementation for which conformance to the standard is stated.

The DICOM standard is structured as a combination of sixteen related but independent documents. As the standard is in constant evolution, the development level and approval status of the different documents may differ and additional parts may be added.

The data describing a digital mammogram is stored in a file using the DICOM file format. The DICOM data set is found in the file after the DICOM file meta information (figure 5.1). Each single image is associated to one file. Table 5.1 shows a schematic representation of the DICOM file.

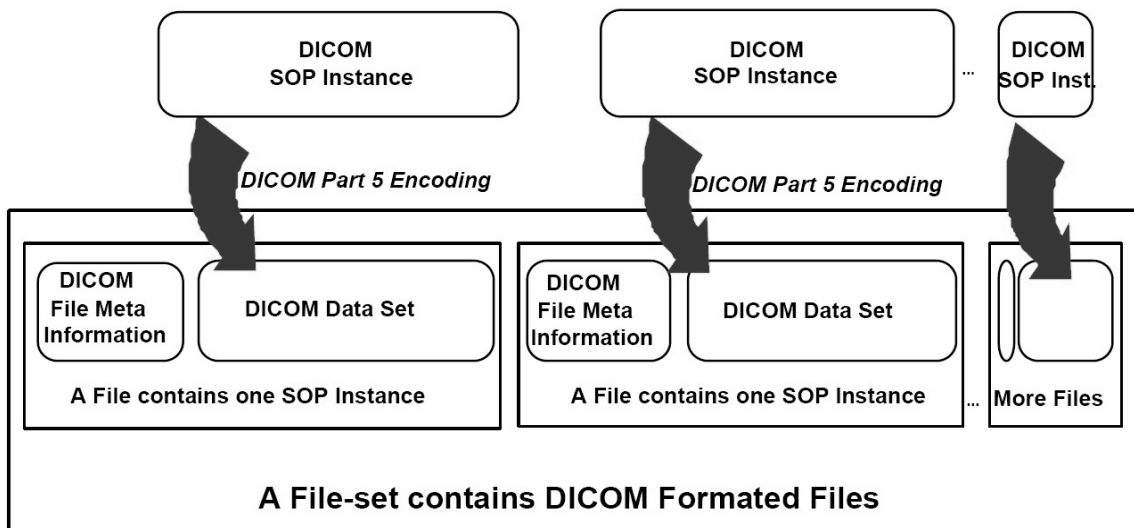


Figure 5.1: DICOM file set and file format. A SOP (Service-Object Pair) is a concrete instantiation of a class with attributes and methods (NEMA 2004d).

Table 5.1: Schematic representation of a DICOM file. The pixel data is actually also a data element with tag (07FE0, 0010), value length and value field.

Preamble: 128 bytes
Prefix: "DICM"
Data Set consisting of:
Data Elements [Tag, VR, VL, Value]
...
Pixel Data

5.1 DICOM File Meta Information

The file meta information consists of a header that includes a 128-byte preamble, a 4-byte DICOM prefix and file meta elements. All the information related to the image, patient, study, etc. is stored in the header. The first 128 bytes can be used by specific implementations. If the file preamble is not used, all 128 bytes are set to 00H. The DICOM prefix consists of the sequence “DICM”. The data set of DICOM data elements comes after preamble and prefix.

5.2 Data Set

Each file contains one data set related to a single mammogram. A data set is made up of data elements that have encoded values of attributes corresponding to the image.

5.3 Data Elements

The data elements in a data set are presented in ascending order and each one appears only once to avoid ambiguities. A data element can have one of three configurations: 1) with implicit value representation; 2) with explicit value representation and defined value length; and 3) with explicit value representation and undefined value length. The transfer syntax specifies which of these configurations is used in the data set.

5.4 Data Elements Fields

A data element consists of fields. Every data element contains the fields “data element tag”, “value length”, and “value”. Data elements with explicit value representation have also a “value representation” field. Figure 5.2 shows a schema of the data elements.

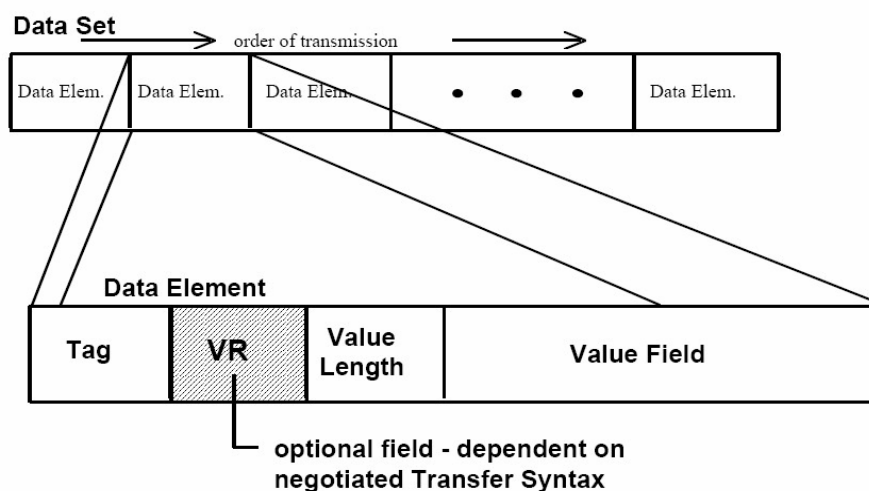


Figure 5.2: Data element structure (NEMA 2004b).

The different fields are defined as follows:

- Data Element Tag (Tag): Consists of “group number” and “element number”, it is 16-bit long and is a unique identifier for each image information. The group number describes some general characteristic and the element number refines this information. Table 5.2 shows some examples of tags and their meanings.
- Value Representation (VR): Describes the data type of the information stored in the value field. It is a two-byte character string.
- Value Length: Indicates the length of the value, it is either:
 - o A 16 or 32-bit (dependent on value representation) field containing the number of bytes of the value or,
 - o A 32-bit field set to undefined length (FFFFFFFFH) used to describe values with value representations equal to SQ (Sequence of Items), UN (Unknown), OW (Other Word String) and OB (Other Byte String).
- Value Field: It contains the actual value of the element and has an even number of bytes. For values of undefined length delimitation elements are used.

Table 5.2: Some tags and their meanings.

Tag	Meaning
0008,0068	Presentation intent type
0018,0060	KVP [Peak KV]
0018,11A0	Body part thickness
0028,0004	Photometric interpretation
0028,1040	Pixel intensity relationship
0028,1041	Pixel intensity relationship sign
7FE0,0010	Pixel data

5.5 Explicit Value Representation

Data elements with explicit value representation consist of four fields: Tag, Value Representation, Value Length, and Value. Depending on the value representation, the data element is structured in one of these ways:

- For value representations of OB (Other Byte String), OW (Other Word String), OF (Other Float String), SQ (Sequence of Items), and UN (Unknown), the 16 bits following the two-character value representation field are reserved for use by later versions of the standard. These bytes are set to 0000H. The value length field is a 32-bit unsigned integer that either contains a value equal to the length of the value field or has an undefined length and a sequence delimitation item marks the end of the value field.

- For a value representation of UT (Unlimited Text), the 16 bits following the two-character value representation field are reserved for use by later versions of the standard and are set to 0000H. The value length field is a 32-bit unsigned integer and describes the length of the value stored in the value field.
- For all other value representations, the value length field is a 16-bit unsigned integer following the two-character value representation field. The value of the value length field must be equal to the length of the value field. The different data element structures with explicit value representation are illustrated in tables 5.3 and 5.4.

Table 5.3: Data element with explicit value representation of OB, OW, OF, SQ, UN or UT (NEMA 2004b).

Tag		Value Representation		Value Length	Value
Group Number (16-bit unsigned integer)	Element Number (16-bit unsigned integer)	VR (2-byte character string) of "OB", "OW", "OF", "SQ", "UT" or "UN"	Reserved 2 bytes set to 0000H	32-bit unsigned integer	Even number of bytes containing the data elements value(s) encoded according to the VR and negotiated Transfer Syntax. Delimited with sequence delimitation item if of undefined length.
2 bytes	2 bytes	2 bytes	2 bytes	4 bytes	Value Length bytes

Table 5.4: Data element with explicit value representation other than shown in table 3.3 (NEMA 2004b).

Tag		Value Representation		Value Length	Value
Group Number (16-bit unsigned integer)	Element Number (16-bit unsigned integer)	VR (2-byte character string)	Reserved 2 bytes set to 0000H	16-bit unsigned integer	Even number of bytes containing the data elements value(s) encoded according to the VR and negotiated Transfer Syntax.
2 bytes	2 bytes	2 bytes	2 bytes	2 bytes	Value Length bytes

5.6 Implicit Value Representation

Data elements with implicit value representation consist of three fields: Tag, Value Length, and Value. If the value field has an explicit length then the value length field shall contain a value equal to the length (in bytes) of the value field. Otherwise, the value field has an undefined length and a sequence delimitation item marks the end of the value field. The data elements structures with implicit value representation are illustrated in table 5.5.

Table 5.5: Data element with implicit value representation (NEMA 2004b).

Tag		Value Length	Value
Group Number (16-bit unsigned integer)	Element Number (16-bit unsigned integer)	32-bit unsigned integer	Even number of bytes containing the data elements value(s) encoded according to the VR specified in (NEMA 2004c) and negotiated Transfer Syntax. Delimited with sequence delimitation item, if of undefined length.
2 bytes	2 bytes	4 bytes	Value Length bytes or undefined length

5.7 Byte Ordering

The byte ordering used to encode the data set is a very important component and should be known by applications when communicating with each other. It can be either little endian or big endian (NEMA 2004b).

Little endian byte ordering is specified as:

- In a binary number consisting of multiple bytes the least significant byte shall be encoded first; with the remaining bytes encoded in increasing order of significance.
- In a character string consisting of multiple 8-bit single byte codes, the characters will be encoded in the order of occurrence in the string (left to right).

Big endian byte ordering is defined as follows:

- In a binary number consisting of multiple bytes, the most significant byte shall be encoded first; with the remaining bytes encoded in decreasing order of significance.
- In a character string consisting of multiple 8-bit single byte codes, the characters will be encoded in the order of occurrence in the string (left to right).

Byte ordering depends upon the agreed transfer syntax. The default DICOM transfer syntax uses little endian encoding.

5.8 Pixel Data Encoding

The following three data elements define the pixel structure:

- Bits Allocated (0028, 0100): The size of the pixel cell.
- Bits Stored (0028, 0101): The number of bits used to represent a single pixel.
- High Bit (0028, 0102): Specifies where the high order bit of the bits stored is to be placed with respect to the bits allocated. Figure 5.3 illustrates two examples.

The field of bits representing the value of a pixel is a binary 2's complement integer or an unsigned integer, as specified by the data element "pixel representation". The minimum actual pixel value in the pixel data is specified by "smallest image pixel value" while the maximum value is specified by "largest image pixel value".

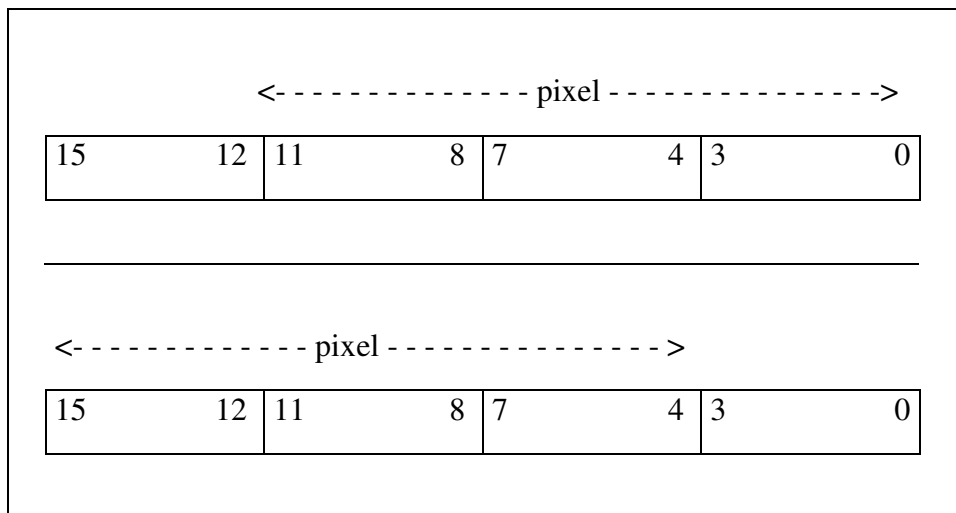


Figure 5.3: Two examples of bit organization with values of bits allocated of 16, bits stored 12, and high bit equal to 11 and 15 respectively.

5.9 Transfer Syntax

The transfer syntax is a set of rules used to avoid ambiguities. It allows communicating applications to negotiate common encoding techniques (e.g. byte ordering, compression, etc.). DICOM defines standard transfer syntaxes and assigns a unique name to each one.

The default transfer syntax is known as "DICOM Implicit VR Little Endian Transfer Syntax" and must be supported by every conformant DICOM implementation.

6 MAMMOGRAPHY

In 1913, Albert Salomon, a German surgeon, was the first to try x-rays on breast tissue extracted during surgery (Gold *et al.* 1990). He used it with the aim of distinguishing cancerous from healthy tissue. After Salomon's experiments, no publications appeared until 1927, when Otto Kleinschmidt, another German surgeon, suggested the use of the technique. The American radiologist Stafford L. Warren documented the use of *in vivo* mammography in the Rochester Memorial Hospital in New York during 1930. One year later, Walter Vogel reported a classification of breast tissues and Paul S. Seabold his investigations on diagnosis of breast cancer by means of mammography.

Jacob Gersohn-Cohen, in the 1950s, suggested the use of collimation and compression. In 1949, the Uruguayan Raul Leborgne set the stage for mammography screening by indicating that microcalcifications could be detected in incipient lesions.

In 1960, Robert L. Egan developed a mammographic technique that used industrial film and was easily reproducible. In 1963, the Cancer Control Program of the U.S. Public Health Service organized a conference, whose results established that Egan's technique could be learnt by other radiologists; that images of acceptable quality could be produced; that through mammography cancerous tissue could be differentiated from healthy tissue; and that mammography could be used to screen asymptomatic women. Between 1963 and 1966, Philip Strax, Louis Venet and Sam Shapiro organized the first screening trial.

In 1971, the first commercial mammography system was available. The technology evolved introducing many technological improvements including the introduction of film digitization and, in the year 1999, the first full-field digital mammography system was introduced in the market.

6.1 Conventional and Digital Mammography

Conventional mammography, also known as screen-film mammography, uses film and faces the problem of archiving. Moreover, during each examination, only four images are obtained and they cannot be evaluated by more than one specialist at the same time in different places. Image quality in copies is rather poor. Frequently, the images are scanned and digitized. However, the digitized images do not provide any new information and images wrongly taken cannot be enhanced (Heywang-Köbrunner 2001).

Full-field digital mammography, briefly digital mammography, uses an electronic detector and overcomes all the disadvantages of the conventional systems. Moreover, digital images do not need to be developed as film, they are directly available and can be seen on a monitor seconds after the take. This allows not only being able to examine more women during the day, but also reduces the stress that the patient experiences while waiting for the

results. Conventional mammography has limited contrast, while digital mammography has a high contrast. Though the human eye perception capabilities for contrast may not profit from this, computer-aided diagnosis does. Computer-aided diagnosis is possible since the existence of digital images. Different programs can access the images and perform semi or full-automated evaluations. Image parts can be depicted where suspicious tissue is highlighted, that the physician may have not discovered from just looking to the image. Digital mammography allows having multiple copies of an image without loose of quality. Moreover, many specialists may evaluate the image at the same time in different places. Contrast and brightness of digital mammograms can be modified on a computer (Heywang-Köbrunner 2001).

6.2 Digital Mammography Systems

The requirements on a mammography system are relatively high in comparison with x-rays imaging methods used for the examinations of other body parts.

The different breast tissues have very small differences with respect to absorption properties. Therefore, low energy x-rays are used in mammography, because they allow to see very small differences in absorption. In the images, it should be possible to see clearly microcalcifications and fibrocystic changes. The use of low energy x-rays requires a higher dose. As the x-rays dose should be maintained as low as possible, to protect the patient, very strict recommendations for the use of mammography have been developed (Aichinger *et al.* 2004).

The most important components of a mammography system are the x-ray tube, the compression plate, the antiscatter grid, the detector, and the post-processing and displaying unit (figure 6.1) (Heywang-Köbrunner 2001).

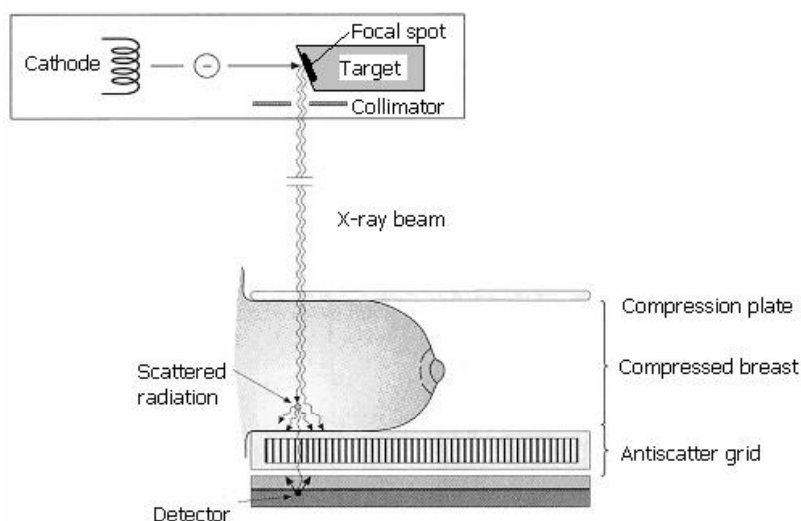


Figure 6.1: Mammographic image technique. Overview of components. Adapted from Heywang-Köbrunner (2001).

In the vacuum tube, there is a cathode to emit electrons and an anode to collect them, establishing a flow of electrical current through the tube. A high voltage electrical current power source is connected across cathode and anode. It allows the voltage to be turned on and off for precise amounts of time and the current flow can be controlled. Electrons focused on the anode collide with other electrons and accelerate them. An amount of the generated energy is emitted or radiated as x-ray photons, perpendicular to the path of the electron current. To achieve high tissue contrast, low energy x-rays are produced using special targets and filters.

Common target/filter combinations are molybdenum/molybdenum, molybdenum/rhodium, rhodium/rhodium, tungsten/molybdenum and tungsten/rhodium. The range of photonic energies emitted by the system can be adjusted by changing the applied voltage (kVp). The number of emitted x-ray photons (dose) can be adjusted by controlling the current flow. Automatic exposure control systems are used to provide the best voltage for individual breast thickness and density; and to ensure that the radiation intensities do not exceed the capacity of the detector. A collimator is used to avoid radiation going beyond the edges of the image receptor.

Breast compression contributes to improve resolution by making tissue near to the image receptor, reduce blurring by immobilizing the tissues, improve contrast by reducing scattering through smaller breast thickness, improve visualization of pathologies that do not deform during compression, and permits a reduction in the dose because the thickness of tissue to be penetrated is reduced.

During the examination, photons are emitted in the x-ray tube, enter the patient and they are absorbed, transmitted or scattered. Photons transmitted without interaction are called primary photons. Scattered photons are secondary photons. The primary photons build the radiographic image but are impaired by the secondary ones. Scattered radiation interferes with image quality. The pernicious effect of the scattered radiation is controlled through compression and collimation. Other technique necessary for scattered radiation reduction are antiscatter grids. They consist of a periodic array of radio-opaque foil strips separated by strips of radiolucent spacing material. The grid is placed between the breast and the image receptor. During exposure, the grid moves perpendicular to the path of the beam and to the orientation of the strips to prevent the strips from appearing on the mammogram as thin lines. Grid efficiency depends upon the ratio of strip height to strip spacing. This ratio is known as grid ratio. A larger grid ratio improves efficiency. Although this increases radiation dose, a significant improvement of image quality is obtained, that justifies using a grid (Heywang-Köbrunner 2001).

Nowadays, three types of digital detection techniques are available: indirect detection, direct detection and direct photon counting (Swedish Radiation Protection Authority 2002). Sensors commonly used in indirect detection systems are photostimulable phosphor, phosphor charge-couple device, and phosphor amorphous silicon. Indirect techniques

convert x-rays to visible light, which is converted into an electric signal, which is then digitized. Direct techniques convert x-rays into an electric signal without the intermediate step via visible light. Direct sensors are based in amorphous selenium. The direct photon counting technique does not integrate energy but directly counts the photons entering the detector and uses a solid-state detector filled with silicon, krypton, gallium arsenic or cadmium zinc tellurium.

Digital mammography allows performing post-processing. Contrast and resolution can be improved. Noise can be reduced. The display unit should be capable of showing four images at a time, have enough grayscale span and spatial resolution.

6.3 Mammograms used for Tests

The digital mammograms used in this project were acquired in the “Institut für Mammadiagnostic” in Esslingen (Germany) on the digital mammography system Giotto IMAGE MD (figure 6.2), which is produced by “Internazionale Medico Scientifica” in Bologna (Italy). The Giotto IMAGE MD uses a direct conversion flat detector with amorphous selenium measuring 18x24 cm. The target/filter combination used to take the images is molybdenum/rhodium.



Figure 6.2: Giotto Mammography System developed and commercialized by Internazionale Medico Scientifica S.r.l. (2006).

The DICOM compliant images are from 59 different patients. The images were anonymized to maintain patient data protection. For each patient there are four images, two of each breast, with the mediolateral-oblique and cranial-caudal views. The resolution of an image is 2016x2816 pixels and the color depth of these images is 13 bits.

Only unprocessed digital mammograms were considered because their pixels are approximately proportional to x-ray beam intensity and no contrast or brightness

enhancement were applied on them. Nevertheless, the methods are for use with any digital mammogram. As a result of the standardization and comparison techniques developed, images with different detector size, target/filter combination, resolution and color depth can be used.

The required parameters for the analysis are obtained from the images' data sets. The exponential law of attenuation needs also the linear attenuation coefficients of glandular and fatty tissues. Tabular empirical data is used from Aichinger *et al.* (2004).

7 COMPUTATIONAL METHODS FOR THE ANALYSIS OF DIGITAL MAMMOGRAMS

The analysis of volumetric breast density means finding a function that maps the pixels' gray levels into the combinations of tissues projected in them. This mapping together with the projected breast area and the compressed breast thickness allows the calculation of the actual volume of the tissues in the breast.

The images contain objects, the pixels, that should be assigned to classes. The feature that characterizes the classes and objects would be the combination of fatty and fibroglandular tissue they represent. This means, for example, that, if the compressed breast thickness were equal to K millimeters, we would have $K+1$ classes. These classes can be expressed as a couple (fat , gla) where fat describes the amount of fatty tissue and gla the amount of fibroglandular tissue behind a pixel and, $fat = 0, 1, 2, \dots K$; $gla = 0, 1, 2, \dots K$; and $fat+gla = K$. Due to this complementary relationship of fat and gla , the classes can simply be described using only the variable gla . Therefore, the problem would mean to map a gray level into an amount of glandular tissue gla .

The image containing the pixels can be represented as a histogram, when the position of the pixels is not relevant. The histogram h plots the number of pixels in the image n_k (vertical axis) with a particular gray level k (horizontal axis):

$$h(k) = n_k \quad (\text{Equation 7.1})$$

The histogram representation is very advantageous when the position of the pixels in the image is not relevant because a calculation on a gray level can be used for all the pixels with that gray level just by multiplying the result by the amount of pixels with that intensity. Otherwise, if the position of the pixels in the image plays a role, it could be represented as a spatial signal: a two-dimensional array F with

$$F = [f(p(x, y))]_{MN} \quad (\text{Equation 7.2})$$

where (x,y) is the spatial two-dimensional coordinate of pixels. $M \times N$ denotes the total amount of pixels in an image. The gray level of a pixel $p(x,y)$ is given by $f(p(x,y))$.

As not all the pixels in the image are objects representing fibroglandular tissue, since some pixels belong to the background or to the pectoral muscle, the image should be segmented and the histogram generated only for the pixels that actually are a projection of glandular and fatty tissue. The pixels in the background could be considered as another variable meaning "no-tissue", but this would only decrease the speed of the classification.

Therefore, if we use the histogram representation to describe the problem it would mean to have a histogram like in figure 7.1 (after pectoral muscle and background segmentation) where some thresholds are marked. The gray level highlighted in red would correspond with the maximum value of I_{gla} , this is a combination of no fat and an amount of fibroglandular tissue equal to the compressed breast thickness. In the same way, the gray levels marked in green mean a maximum amount of fat (I_{fat}) equivalent with the compressed breast tissue. The values between this green threshold and the yellow one (the background) mean fatty tissue but for the border where the breast height is smaller than the compressed breast thickness. The problem would be to find an appropriate function to map the gray values between I_{gla} and I_{fat} into amounts of fibroglandular tissue.

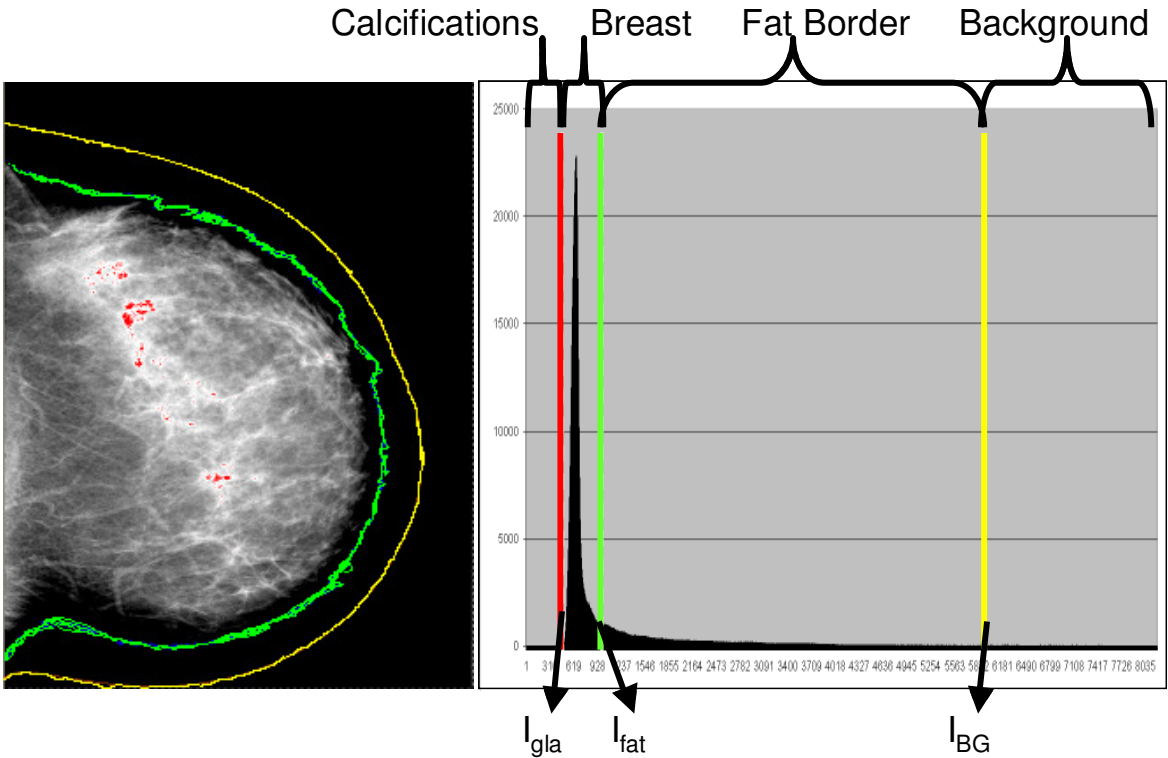


Figure 7.1: A mammogram and its histogram with thresholds: red means pure glandular tissue, green purely fatty tissue, and yellow separates the breast from the background pixels.

All the methods developed and used, their input, output and interactions are shown in figure 7.2.

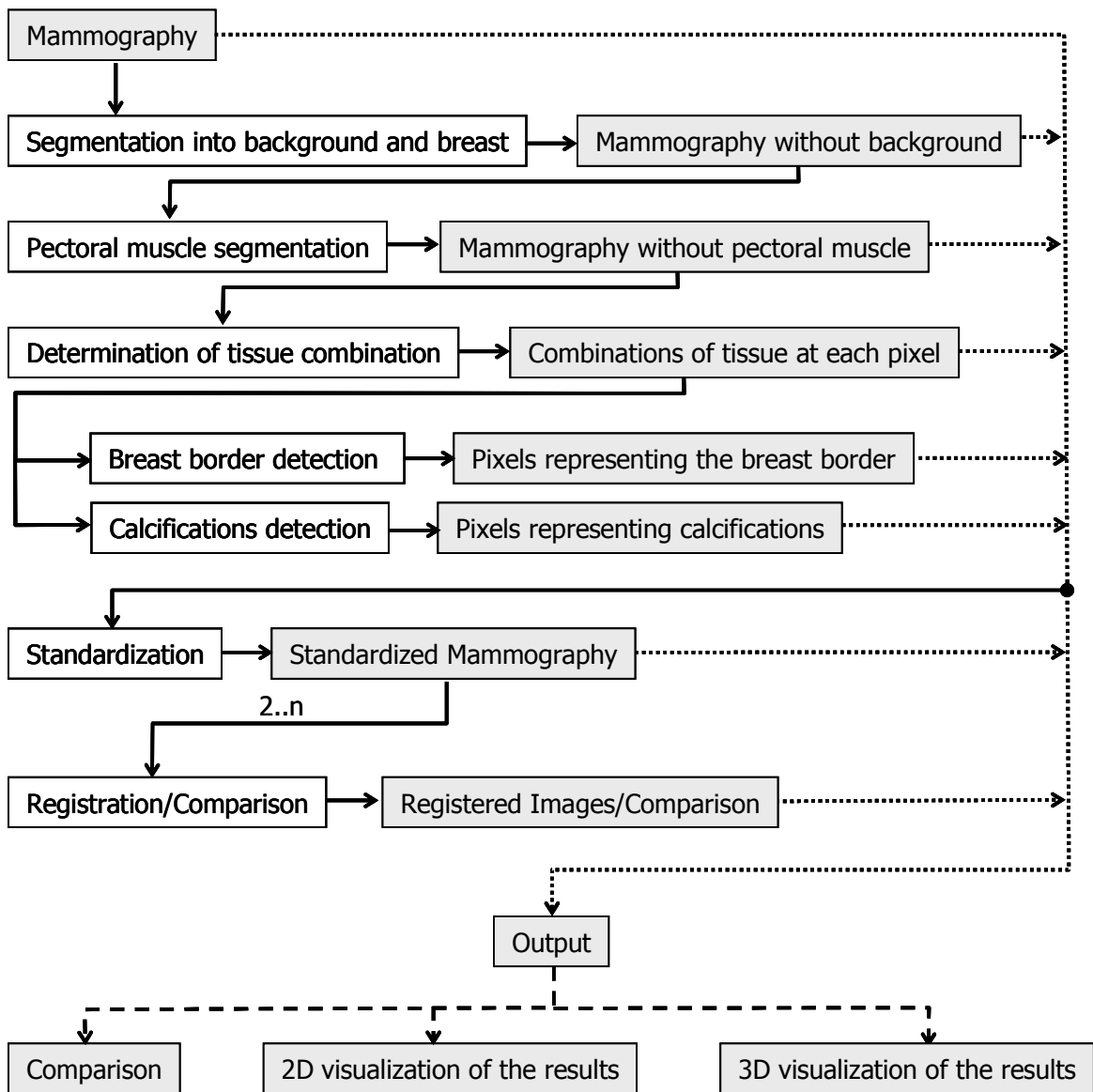


Figure 7.2: The methods developed and their interaction.

7.1 Breast Segmentation

A first step in analyzing the image is to make sure that the measurements are only performed in the region of interest, the breast region, and that the background of the mammogram does not influence the calculations.

In order to accomplish the segmentation of the breast tissues from the background, a thresholding technique is used to find a value, which is the best boundary for the given image.

To find an appropriate threshold, histogram analysis is needed. The thresholding method finds two regions: the breast and the background. Therefore, one value I_{BG} in the range of the histogram that best marks those regions has to be found. Then,

$$\begin{aligned}
&\text{if } h(i) < I_{BG} \text{ and } f(p(x, y)) = i \Rightarrow (x, y) \in \text{Breast} \\
&\text{if } h(i) \geq I_{BG} \text{ and } f(p(x, y)) = i \Rightarrow (x, y) \in \text{Background}
\end{aligned}
\tag{Equation 7.3}$$

for $i = 0, \dots, k-1$ positions in the histogram h and pixels $p(x, y)$ with intensity $f(p(x, y))$.

As we know that, the mammograms are bimodal, meaning that there are two clearly separated areas (breast and background), we choose the threshold I_{BG} at the valley bottom of the histogram.

7.2 Pectoral Muscle Segmentation

The method presented on the next section relies on the assumption that the digital mammogram only shows fatty and fibroglandular tissues. This is the case on images showing the crano-caudal view. In the mammograms showing the mediolateral-oblique view, additionally to the breast (fatty and fibroglandular tissues), the pectoral muscle is shown. When analyzing the images, the algorithm in section 7.3 may find some pixels in the projection of the pectoral muscle as “purely fibroglandular tissue” and produce wrong results. For this reason, the segmentation of the pectoral muscle region in the image is needed.

As the pectoral muscle is identified by its position in the image, it is necessary to use the array representation of the mammogram. Components forming the pectoral muscle are identified based on position, intensity and shape. Concerning the appearance of the pectoral region, we assume that the pectoral muscle is approximately triangular, that it is situated in a corner of the mammogram and that the pectoral muscle region has a higher intensity than the adjacent region. It is further assumed that the file contains additional image information such as view, laterality, window width, window center (this is the normal case in FFDM).

The pectoral muscle segmentation is achieved using edge-based region growing. The seeds are automatically selected in the image left border, where the muscle is situated (s. figure 7.3). This means that all pixels $p(i, 0)$, where $i = 0, 1, 2, \dots, M-1$ and $M = \text{the number of rows in the image}$, are specified as an initial seed of the region PM . This applies for images with laterality equal to “left”; images with laterality equal to “right”, are mirrored.

For the definition of the edge, the image is divided in two regions. One region, F_1 , comprises the first third of the image: all the pixels $p(i, j)$, with $i=0, 1, 2, \dots, M/3; j=0, 1, 2, \dots, N-1$; and $N = \text{the number of columns in the image}$. The other region, F_2 , is the rest of the image. This is done because in the second region F_2 the difference of intensity between the pectoral muscle and the adjacent region is not as high as in the first region F_1 . The edge is defined as

$$E = \{p(x, y) \mid f(p(x, y)) = \frac{ww}{d} + wc\}
\tag{Equation 7.4}$$

where w_w and w_c are the window width and window center of the image and can be found on the DICOM data set. The value of d was empirically found to bring optimal results and defined as 5 for F_1 and as 15 for F_2 .

After having the seeds and the edges that define the border of the pectoral muscle, the region PM has to be extracted from the image and converted in a part of the background. The seeds grow horizontally by iteratively merging adjacent pixels until the muscle edges F_1 or F_2 are met; the pixels inside the breast having the same value as F_2 are never reached (figure 7.4).



Figure 7.3: For the segmentation of the pectoral muscle, the seeds are automatically selected in the image left edge, where the muscle is situated.

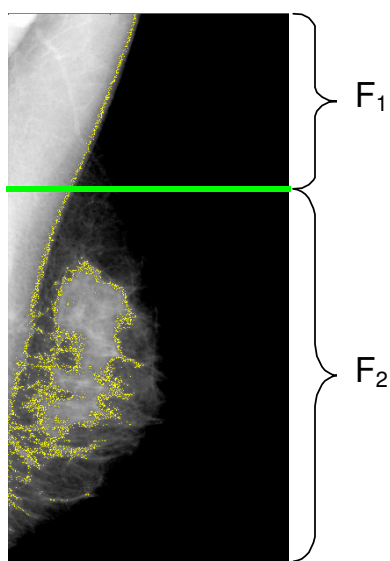


Figure 7.4: The pectoral boundary (in yellow) is detected by a change of high intensity into low intensity. Note that later the seeds will not grow inside the breast.

As we have assumed that the pectoral region has a triangular shape, the curve to be found as the pectoral muscle edge can be thought to be approximately a line going up-down and from right to left. It is actually not a line but the function should globally decrease from the right to the left side, and locally small increasing steps should be allowed.

The seeds situated on the left side of the image grow independently from left to right (figure 7.5). If one of these horizontal regions grows extremely (figure 7.6), its edge is determined by interpolating between the upper and bottom adjacent regions.

If the edges between regions are equal to zero, meaning that they did not grow, the edges in the intermediate regions are also set to zero, meaning that the breast region has been reached. Some regions may not grow enough due to dark pixels in the muscle, which may have the same value as the pectoral edge (figure 7.7). These regions are merged with their upper regions.

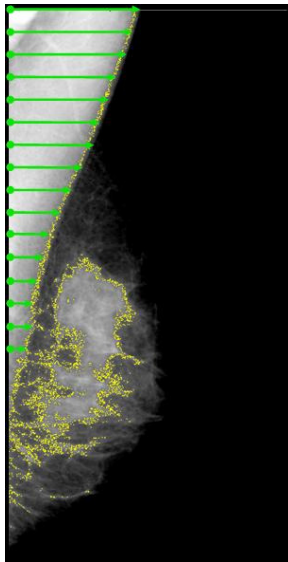


Figure 7.5: The seeds situated on the left side of the image grow independently from left to right until the muscle edge in the image is met.

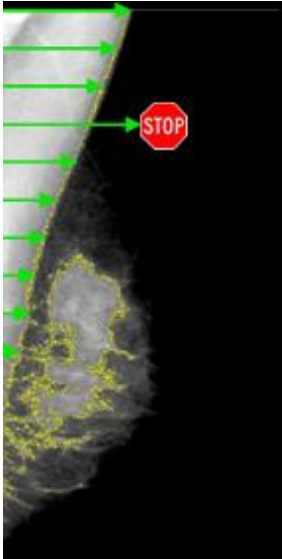


Figure 7.6: If one of these horizontal regions grows extremely, its edge is determined by interpolating between the upper and bottom adjacent regions.

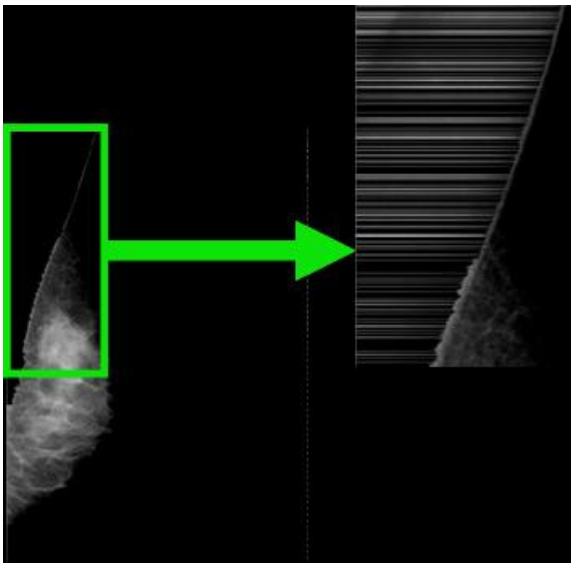


Figure 7.7: For each limit found the region is merged with upper regions, to include intermediate regions that did not grow enough.

7.3 Determination of Breast Composition

In order to analyze digital mammograms and observe breast composition, pixel values have to be interpreted. However, there is not a direct method to obtain the values of the photon energy leaving the breast from the pixels. A method is presented here that transforms pixel values into amounts of fibroglandular tissue.

In this section, an approach is presented on how a pixel gray level is built from the interaction of the x-ray beam with the breast tissues, and how, with this knowledge, the amounts of fibroglandular and fatty tissues in the breast can be calculated.

As seen in Chapter 4, the physical process where photons are absorbed by the breast tissues is described through the “exponential law of attenuation”. This law states that the amount of photons passing the breast is exponentially related to the amount of incident photons. Furthermore, it depends on breast thickness and composition, i.e. on the amount and density of fatty and fibroglandular tissues.

During image acquisition, an x-ray beam with intensity J_0 reaches the compressed breast, which has thickness T , it is attenuated by the different tissues and it reaches the electronic detector with energy J . The exponential law of attenuation can be then expressed as:

$$J = J_0 e^{-\mu T} \quad (\text{Equation 7.5})$$

where μ is the linear attenuation coefficient of the material.

Two kinds of tissue can be distinguished in the breast: fatty and fibroglandular tissue. It is proved that considering only these two components should result in a good approximation when calculating breast composition (Highnam and Brady 1999). Based on this assumption, the exponential law of attenuation can be written as:

$$J = J_0 e^{-\mu_1 T_1} e^{-\mu_2 T_2} \quad (\text{Equation 7.6})$$

where μ_1 is the linear attenuation coefficient of fibroglandular tissue,

μ_2 is the linear attenuation coefficient of fatty tissue,

T_1 is the thickness of fibroglandular tissue and is unknown,

T_2 is the thickness of fatty tissue and is unknown.

The linear attenuation coefficients are empirical data and are available in the literature as tabular data (Aichinger *et al.* 2004). The total compressed breast thickness T is known and it is stored in the image description on data element (0018, 11A0). Additionally, the sum of the thicknesses of the tissues should be equal to the thickness of the compressed breast:

$$T = T_1 + T_2 \quad (\text{Equation 7.7})$$

Based on equations 7.6 and 7.7 a new equation is derived by replacing T_2 by $T - T_1$:

$$J = J_0 e^{-\mu_1 T_1} e^{-\mu_2 (T - T_1)} \quad (\text{Equation 7.8})$$

The determination of breast composition can be seen as the determination of T_1 , the amount of fibroglandular tissue projected in a pixel. The values J_0 and J , the x-ray intensity reached and leaving the compressed breast, are not available in the file. The ratio J/J_0 is reflected in each pixel in the image and it is considered equal to X/X_0 , where X is the value

of the pixel being analyzed, and X_0 represents the pixel value that should be used for “no tissue”. Using this reasoning, only one unknown is left: the amount of glandular tissue in the pixel T_1 ; and equation 7.8 can be written substituting the energies J and J_0 by gray levels X and X_0 :

$$X = X_0 e^{-\mu_1 T_1} e^{-\mu_2 (T - T_1)} \quad (\text{Equation 7.9})$$

The value for X_0 , the gray level representing “no tissue”, could be obtained from the background, but in most images, the background is set to a fixed saturation value that does not correspond with the energy entering the breast. The problem is to find the ratio X/X_0 for each pixel, because there are still more unknowns than equations and, therefore, infinite solutions.

In order to reduce the number of unknowns, a new equation is introduced. In this equation, the pixel value for “purely fat” (the value searched for the threshold I_{fat} in figure 7.1) is used in equation 7.9, this would mean that T_1 is equal to zero and T_2 is equal to T :

$$I_{fat} = X_0 e^{-\mu_2 T} \quad (\text{Equation 7.10})$$

I_{fat} is the value of the pixel being analyzed, when considering that this value means “purely fat”, i.e. the x-ray beam crossed only fatty tissue. As no fibroglandular tissue is present, the variables μ_1 and T_1 disappear and the thickness of fatty tissue is equal to the compressed breast thickness T .

By dividing equation 7.9 through equation 7.10, the term with X_0 cancels:

$$\begin{aligned} \frac{X}{I_{fat}} &= \frac{X_0 e^{-\mu_1 T_1} e^{-\mu_2 (T - T_1)}}{X_0 e^{-\mu_2 T}} \\ \frac{X}{I_{fat}} &= e^{-(\mu_1 - \mu_2) T_1} \end{aligned} \quad (\text{Equation 7.11})$$

It follows that the only unknown is the amount of glandular tissue T_1 :

$$T_1(X) = -\frac{\ln \frac{X}{I_{fat}}}{\mu_1 - \mu_2} \quad (\text{Equation 7.12})$$

The problem has been reduced to the determination of I_{fat} . This operation takes the following steps:

- The argument of the $\ln()$ should be greater than zero, this means that all pixels with gray level $X > 0$ can be analyzed.
- The thickness of glandular tissue at each pixel T_1 should always be greater or equal to zero: $T_1 \geq 0$; $\mu_1 - \mu_2$ is known and always greater than zero, so $-\ln(X/I_{fat}) > \mu_1 - \mu_2$ and

$\ln(X/I_{fat}) < 0$; so $X < I_{fat}$. This means that all pixels representing some fibroglandular tissue have to be smaller than I_{fat} .

- The thickness of glandular tissue at each pixel should always be smaller or equal to the breast thickness: $T_1 \leq T$.
- The value of I_{fat} is first set as the maximum value in the histogram that is smaller than the background threshold I_{BG} .
- For this I_{fat} , and for $T_1 = T$, the value of X should be equal to I_{gla} (the value searched for the threshold I_{gla} in figure 7.1).
- Then all the possible combinations of I_{fat} and I_{gla} are iteratively calculated, reducing each time the value of I_{fat} by one unit.
- We choose the value of I_{fat} to be equal to that where the pair I_{fat} and I_{gla} maximizes the amount of pixels having a gray level between them. Therefore, the pair (I_{fat}, I_{gla}) is optimal when $\sum_{X=I_{gla}}^{I_{fat}} h(X)$, where $h(X)$ is the histogram function (the number of pixels in the image having X as gray level), is a maximum.
- Once the values for I_{fat} and I_{gla} were found, the amount of glandular tissue T_1 can be calculated for each gray level X , with $(I_{gla} < X < I_{fat})$.

After having the value of T_1 for all pixels, the thickness of the compressed breast T and the area of a pixel A_p , which is given in the image data set, the volume of fibroglandular tissue for each gray level (Vol_i) and for the whole breast (Vol_B) can be calculated:

$$Vol_i = A_p * T_1(i) * h(i) \quad \text{(Equation 7.13)}$$

$$Vol_B = \sum_i Vol_i \quad \text{(Equation 7.14)}$$

In the same way, the percentages of fibroglandular tissue at each gray level (Per_i) and for the whole breast (Per_B) can be calculated:

$$Per_i = 100 * T_1(i) / T \quad \text{(Equation 7.15)}$$

$$Per_B = \sum_i Per_i \quad \text{(Equation 7.16)}$$

Values that are smaller than I_{gla} may suggest the presence of calcifications. Values greater than I_{fat} correspond to the breast periphery. These values can be used to segment the image into background, border and breast. Another segmentation options can be achieved by selecting threshold values for different desired combinations of fatty and glandular tissues.

In order to perform the calculations, the file information accompanying the image (DICOM header) has to be previously read. The header's elements used to read and interpret the pixel data are (NEMA 2004d):

- Presentation Intent Type: The value for this tag should be FOR PROCESSING, meaning that no image enhancement was performed on the image after acquisition;
- KVP [Peak KV]: The voltage output of the x-ray generator used, to search for the linear attenuation coefficients in the tables listing them;
- Body Part Thickness: The average thickness in millimeters of the examined breast when compressed (the value of variable T in our algorithm);
- Photometric Interpretation: MONOCHROME1, the minimum pixel value is intended to be displayed as white;
- Bits Allocated: Number of bits allocated for each pixel sample;
- Bits Stored: Number of bits stored for each pixel sample;
- High Bit: Most significant bit for pixel sample data;
- Pixel Representation: Data representation of the pixel samples;
- Pixel Intensity Relationship: The relationship between the pixel sample values and the x-ray beam intensity. This value should be equal to LIN (approximately proportional to x-ray beam).

Further assumptions for this model are: 1) the compressed breast has a constant thickness, 2) the x-ray beam is perpendicular to the breast surface, and 3) the scattered component is equal to zero.

Saskia van Engeland and co-workers (Van Engeland *et al.* 2006) developed independently and parallel to our research a model for estimation of dense tissue volume from FFDMs. Tissue composition at a given pixel is computed after performing breast thickness compensation, using a reference value for fatty tissue. They assigned to this value the maximum pixel value in the breast tissue projection using a large quartile (0.99) of the pixel value histogram. Their model is also based upon the Lambert Law of Absorption. They as well use the division of two equations to reduce the number of variables. To validate the model they used 88 FFDMs and compared the volume estimates with volumes obtained by semi-automatic segmentation of breast magnetic resonance imaging data, which they consider as the gold standard.

Error Estimation: Linear Attenuation Coefficients Dependence

We would like to know how the model for the determination of breast composition depends on external factors. We want to know how sensible equation 7.12 is to changes in the variables μ_1 and μ_2 (the linear attenuation coefficients).

The error ΔT_1 in the estimation of the amount of fibroglandular tissue T_1 for a gray level, due to variability in the linear attenuation coefficient of fibroglandular tissue μ_1 , is given by:

$$\Delta T_1 = T_1(\mu_1 + \Delta\mu_1) - T_1(\mu_1) \quad (\text{Equation 7.17})$$

$$\Delta T_1 = -\frac{\ln \frac{X}{I_{fat}}}{\mu_1 + \Delta\mu_1 - \mu_2} + \frac{\ln \frac{X}{I_{fat}}}{\mu_1 - \mu_2}$$

$$\Delta T_1 = \frac{\ln \frac{X}{I_{fat}} * (\mu_1 + \Delta\mu_1 - \mu_2) - \ln \frac{X}{I_{fat}} * (\mu_1 - \mu_2)}{(\mu_1 - \mu_2)^2 + (\mu_1 - \mu_2) * \Delta\mu_1}$$

$$\Delta T_1 = \frac{\Delta\mu_1 * \ln \frac{X}{I_{fat}}}{(\mu_1 - \mu_2)^2 + (\mu_1 - \mu_2) * \Delta\mu_1} \quad (\text{Equation 7.18})$$

In figure 7.8, this is graphically described. The horizontal axis contains the differences of the linear attenuation coefficients ($\mu_1 - \mu_2$) and the vertical axis the error in density (ΔT_1). For the term $\ln(X/I_{fat})$ we chose typical values for dense tissue, fatty tissue and an intermediate value. These values are respectively -0.75 , -0.01 and -0.33 ; and they are represented by a black, a gray and a dashed line. We chose also an error in the linear attenuation coefficient of fibroglandular tissue, $\Delta\mu_1$, equal to -0.005 (figure 7.8 a) and 0.005 (figure 7.8 b).

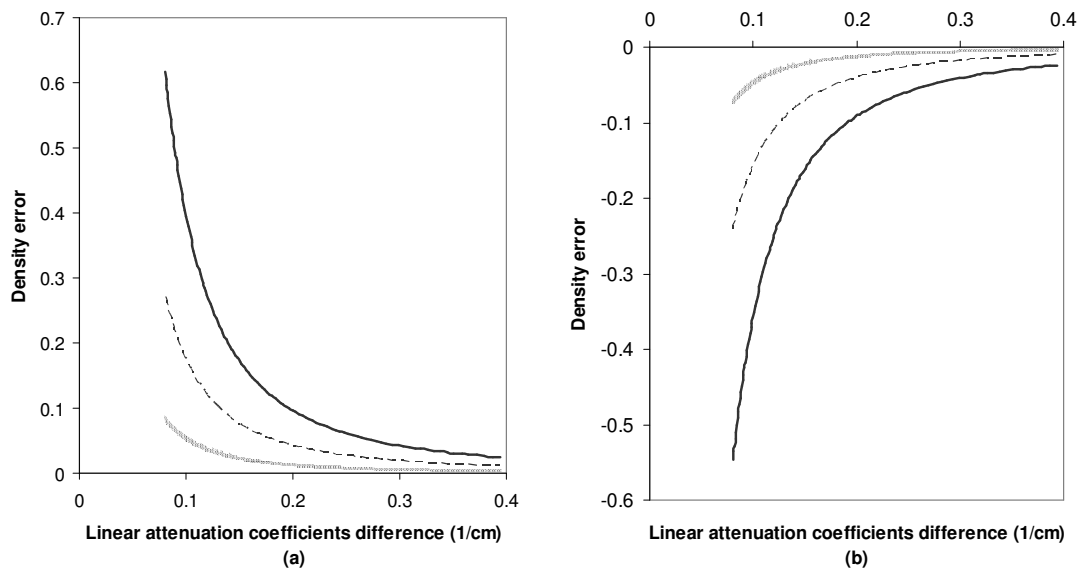


Figure 7.8: Density error as a function of the difference of the linear attenuation coefficients. In diagram (a) $\Delta\mu_1 = -0.005$ and in diagram (b) $\Delta\mu_1 = 0.005$. The value of term $\ln(X/I_{fat})$ is -0.75 , -0.33 and -0.1 for the black, dashed and gray curves, respectively.

The error ΔT_1 in the estimation of the amount of fibroglandular tissue T_1 for a gray level, due to variability in the linear attenuation coefficient of fatty tissue μ_2 , is given by:

$$\Delta T_1 = T_1(\mu_2 + \Delta\mu_2) - T_1(\mu_2) \quad (\text{Equation 7.19})$$

$$\Delta T_1 = \frac{\ln \frac{X}{I_{\text{fat}}}}{\mu_1 - (\mu_2 + \Delta\mu_2)} - \frac{\ln \frac{X}{I_{\text{fat}}}}{\mu_1 - \mu_2}$$

$$\Delta T_1 = \frac{\ln \frac{X}{I_{\text{fat}}} * (\mu_1 - \mu_2) - \ln \frac{X}{I_{\text{fat}}} * (\mu_1 - \mu_2 - \Delta\mu_2)}{(\mu_1 - \mu_2)^2 - (\mu_1 - \mu_2) * \Delta\mu_2}$$

$$\Delta T_1 = \frac{\Delta\mu_2 * \ln \frac{X}{I_{\text{fat}}}}{(\mu_1 - \mu_2) * \Delta\mu_2 - (\mu_1 - \mu_2)^2} \quad (\text{Equation 7.20})$$

A graphical presentation of this equation is shown in figure 7.9. Once again, the horizontal axis contains the differences of the linear attenuation coefficients ($\mu_1 - \mu_2$) and the vertical axis the error in density (ΔT_1). The term $\ln(X/I_{\text{fat}})$ for typical values of dense tissue, fatty tissue and an intermediate value takes respectively -0.75 , -0.01 and -0.33 . They are represented by a black, a gray and a dashed line. The error in the linear attenuation coefficient of fatty tissue, $\Delta\mu_2$, was set -0.005 (figure 7.9 a) and 0.005 (figure 7.9 b).

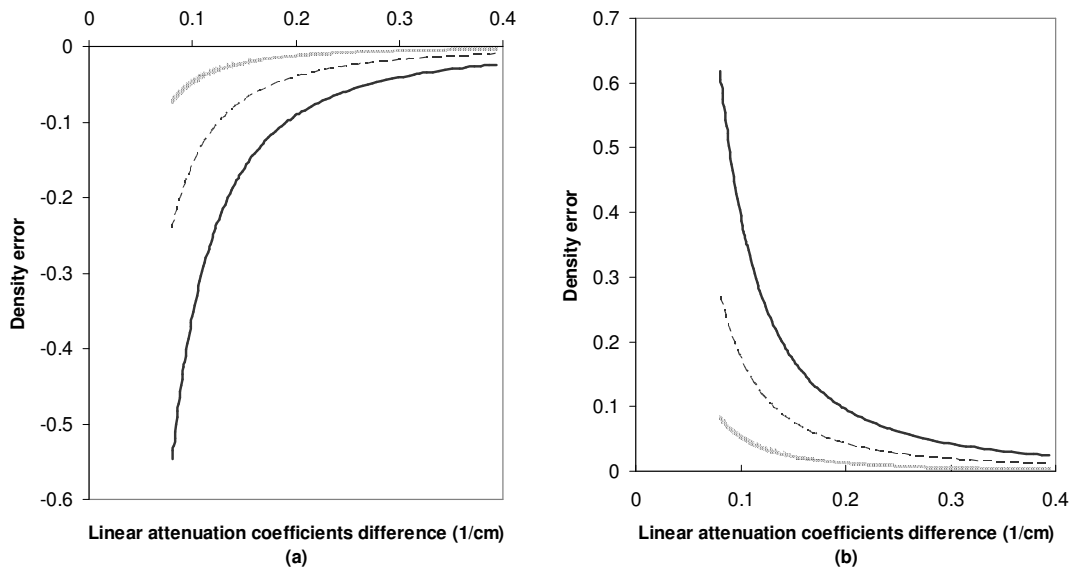


Figure 7.9: Density error as a function of the difference of the linear attenuation coefficients. In diagram (a) $\Delta\mu_2 = -0.005$ and in diagram (b) $\Delta\mu_2 = 0.005$. The value of the term $\ln(X/I_{\text{fat}})$ is -0.75 , -0.33 and -0.01 for the black, dashed and gray curves, respectively.

From figures 7.8 and 7.9, we can deduce that a less accurate estimation of the attenuation coefficients results in a less accurate estimation of the breast density.

We can see that the error in the estimation of the amount of fibroglandular tissue increases with breast density: it is bigger for dense breasts and smaller for fatty breasts.

An error in the estimation of one of the attenuation coefficients of ± 0.005 means for fatty breasts an absolute variation of the density of less than 10% and for dense breasts of less than 60%.

It should be observed that the difference of the linear attenuation coefficients has a big influence in the estimation model. In the error estimations, the inverse of the difference is significant. This explains the decrease in error with an increasing difference of the linear attenuation coefficients.

The difference of the linear attenuation coefficients decreases with increasing photon energy (remember figure 4.1). This means that the best results are obtained with a low energy. Unfortunately, this also means a larger exposure of the patient to the radiation.

All this gives a clear indication on the accuracy with which the linear attenuation coefficients should be estimated to decrease the total variation of the density to satisfactory levels.

7.4 Breast Border Detection

The largest single feature on a mammogram is the skin-air interface or breast border. Extraction of the breast contour is useful for a number of reasons, for instance, for image registration based on the alignment of features. The breast border can be easily found by calculating the value of X_0 , the pixels representing “no tissue”, using equation 6.12.

$$X_0 = \frac{X_{fat}}{e^{-\mu_2 T}} \quad (\text{Equation 7.21})$$

7.5 Detection of Calcifications

Calcifications are small mineral deposits in the breast tissue. To develop the calculation of the amounts of the different tissues in the breast it was assumed that calcification could be ignored. On the one hand, fibroglandular tissue has a higher attenuation coefficient as fatty tissue; on the other hand, calcium has a significantly higher attenuation coefficient than fibroglandular tissue. Sometimes, X_{gla} is not the smallest value appearing in the histogram. Moreover, these values have the meaning that there is some material in the image having a higher density than fibroglandular tissue, i.e. calcification. So, calcifications (X_{cal}) could be found by searching for these values in the histogram:

$$X_{cal} = X_i \quad \text{for all } X_i < X_{gla} \quad (\text{Equation 7.22})$$

7.6 Data Visualization

Standard display techniques are used to show the results using a monitor. The image is a matrix, whose number of rows and columns is given by the data elements (0028, 0010) and (0028, 0011), respectively.

The pixel values are read according to the schema “bits allocated-bits stored-high bit” (see figure 5.3). The pixel gray levels are shown using the RGB system, with the parameters r (red), g (green) and b (blue), in which gray levels can be shown by giving the same value to these three variables.

The amount of gray levels used is given by a power of 2 equal to $2^{\text{Bits Stored}}$ and may differ from the number of gray levels that the display device is capable to show.

The data elements window center (0028, 1050) and window width (0028, 1051) define a transformation between the pixels as they are in the file (real pixel-values) and the pixel values for display. The data element window width is always greater than 1. This value shows the set of pixel values that are displayed. The data element window center is always equal or greater than 1. This value contains the average pixel value in the set defined by windows width. These data elements are used by the algorithm shown in figure 7.10, where x is the input value, y the output value in a set of values ranging from y_{\min} to y_{\max} , c the window center and w the window width.

```
if (x <= c - 0.5 - (w-1)/2) then
  y = ymin
elseif (x > c - 0.5 + (w-1)/2) then
  y = ymax
else
  y = ((x - (c - 0.5)) / (w-1) + 0.5) * (ymax - ymin) + ymin
```

Figure 7.10: Algorithm for the transformation between “real pixels” and “display pixels”.

The brightness and contrast of the image change with these parameters. This can be seen in figure 7.11. The upper side of the figure shows the same image with different values of window center and window width. The x axis in the function, in the down side of the figure, is the set of values of the input. The y axis is the set of values of the output. When window width is set to smaller values, the contrast is higher. When window center is set to smaller values, the brightness is higher.

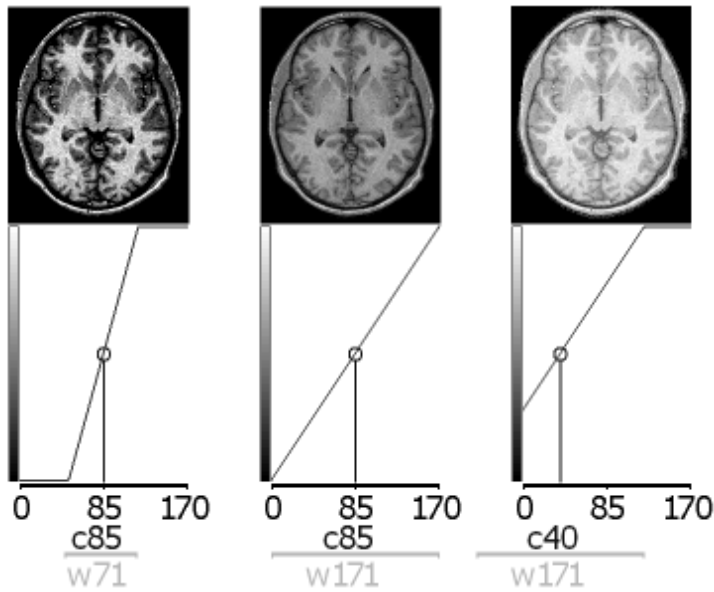


Figure 7.11: Effect of changes of window center and window width (Rorden 2006).

The results of the calculations can be seen as tissue combinations by setting thresholds. Some examples are shown in table 7.1.

Table 7.1: Examples of the thresholds used to show the tissues combinations.

PIXEL	(r, g, b)	Result
$(\text{pixel} > X_0+a)$ or $(\text{pixel} = \text{Background})$	(0, 0, 0)	Background in black
$(\text{pixel} \leq X_0+a)$ and $(\text{pixel} > X_0-a)$	(255, 255, 0)	Border in yellow
$(\text{pixel} > X_{\text{fat}})$ && $(\text{pixel} < X_0)$	(0, 0, 255)	100% fat in the outer part of the breast in blue
$(\text{pixel} = X_{\text{fat}})$	(0, 0, 255)	100% fat in blue
$(\text{pixel} \geq \text{Gla}20)$ and $(\text{pixel} < X_{\text{fat}})$	(0, 190, 60)	20-1% glandular tissue in green
$(\text{pixel} \geq \text{Gla}40)$ and $(\text{pixel} < \text{Gla}20)$	(255, 255, 0)	40-21% glandular tissue in yellow
$(\text{pixel} \geq \text{Gla}60)$ and $(\text{pixel} < \text{Gla}40)$	(255, 190, 0)	60-41% glandular tissue in orange
$(\text{pixel} \geq \text{Gla}80)$ and $(\text{pixel} < \text{Gla}60)$	(233, 150, 122)	80-61% glandular tissue in dark pink
$(\text{pixel} \geq X_{\text{gla}})$ and $(\text{pixel} < \text{Gla}80)$	(255, 0, 0)	100-80% glandular tissue in red
$(\text{pixel} < X_{\text{gla}})$	(255, 0, 0)	Calcifications in red

3D Data Visualization

Height fields are used to visualize data that consists of a two-dimensional regular mesh and if there exists a value in each point of the mesh. The pixels of a standardized digital

mammogram can be considered as such a mesh. In every position of the standardized image a value for the thickness of glandular tissue is given. These values are presented as peaks of the height field above the corresponding position in the mammogram. The structure of a field shows local trends and, by rotating the view, it is possible to inspect the data from different angles.

An alternative method to display height fields is contouring. The marching squares algorithm is applied in order to achieve this kind of visualization.

If the radiologist wants to get a general overview of the complete distribution of the glandular tissue in the breast, a height field may not be the best choice because it contains many local maxima. Therefore, it is necessary to interpolate the height field. The resulting surface is presented either as a Bézier surface or as a NURBS surface. In both cases, the global trends are easier to locate because the surfaces are smoother than a height field.

A schematic view of the implementation of the three-dimensional visualization of the data is presented in figure 7.12.

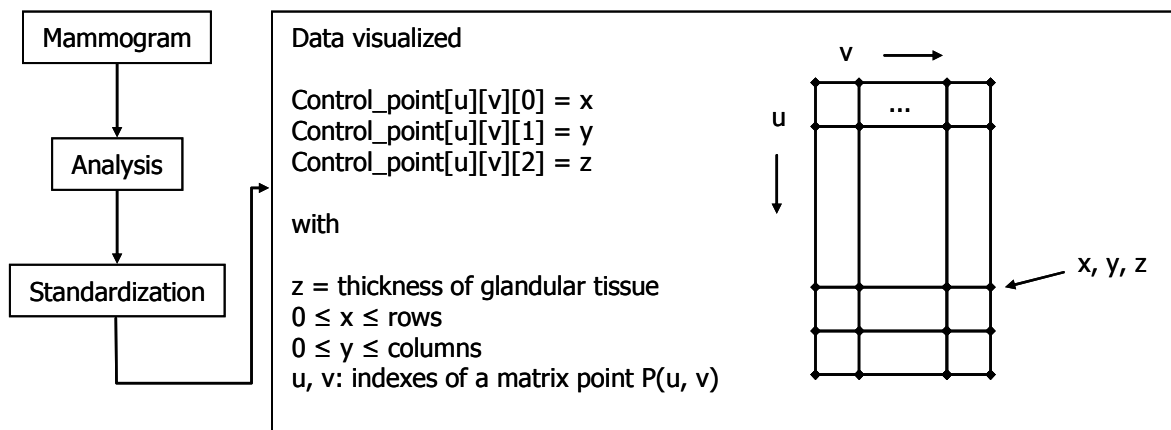


Figure 7.12: A schematic view of the mammogram visualization as surface.

7.7 Digital Mammogram Standardization

In order to compare mammograms and to determine whether they are similar or divergent, a reference point, against which the images could be evaluated, has to be defined. As the standardization is based on a new concept, there is no defined general point of reference.

The calculation of the amount of glandular tissue for each pixel results in comparable values: it produces a matrix of millimeters of glandular tissue.

The gray levels of the transformed image would then range from zero to a maximum value of glandular tissue. This maximum is defined as 80.0 millimeters, because the attenuation coefficient information is available for compressed breast thicknesses smaller or equal to this value. Only rare cases would present a mammogram with breast thickness greater than

eight centimeters. An extrapolation of the coefficients of attenuation is then possible, but the error may be very large.

Once the images are converted into matrices of millimeters of glandular tissue, they have to be scaled. An image size of 1024x1024 was selected for the standardized images because it represents a good trade-off between speed and accuracy for image registration. The scaling factor is selected as the ratio between the rows of the image and 1024 (the rows of the scaled image). The scaling procedure is explained in more detail on section 7.8.

Showing the images to the user in 800 different gray levels would not let him or her profit from the image standardization, since no good contrast would be possible. For this reason, the images are then presented in colors.

A scale ranging from red to yellow was chosen, going through magenta, blue, cyan and green (figure 7.13). The mapping of the amounts of glandular tissue to this color scale may differ according to the type of comparison to be performed. The comparison may be intrasubject, using as reference point a former image of the patient; intersubject, with some image of other patient; or atlas, when the image was obtained based on information of many subjects.



Figure 7.13: The color scale used to show the standardized mammograms.

Therefore, the standard images can be colored in two different ways: one for intrasubject comparisons and one for intersubject/atlas comparisons. This is done in order to better profit from the color scale when performing intrasubject comparison of mammograms with small compressed breast thickness values.

To map from the amount of millimeters in a pixel to a color in the scale, the variable *max_value* is defined as the maximum value in the two images (80.0 mm in the case of intersubject/atlas comparison) that would correspond to the color red. The minimum value is 0.0 mm and it corresponds to yellow in the color scale. The amount of glandular tissue corresponding to the other colors is defined by the variable $z = \text{max_value}/5$. This value is added to yellow (*min_value*) to get green (*int1*), and then to the value of green to get cyan (*int2*), and again to cyan to get blue (*int3*) and finally to blue to get magenta (*int4*). Between each of these intermediate colors, there is only a difference of 255 in one of the variables *r*, *g*, or *b*. In order to get the *rgb* value between the intermediate values, a variable *x* is defined with $x = 255/z$ and is then multiplied by the difference of the upper value in the subinterval and the amount of glandular tissue. This process is illustrated in figures 7.14. in addition, 7.15.


```

read mm; //amount of glandular tissue in the pixel
z=max_value/5;
x=255/z;
//red
if (mm>=max_value) → r=255; g=0; b=0;
//red to magenta (increase blue)
if (mm<max_value) and (mm>=int4) → r=255; g=0; b=x*(max_value-mm);
//magenta to blue (decrease red)
if (mm<int4) and (mm>=int3) → r=x*(mm-int3); g=0; b=255;
//blue to cyan (increase green)
if (mm<int3) and (mm>=int2) → r=0; g=x*(int3-mm); b=255;
//cyan to green (decrease blue)
if (mm<int2) and (mm>=int1) → r=0; g=255; b=(mm-int1);
//green to yellow (increase red)
if (mm<int1) and (mm>=0) → r=x*(int1-mm); g=0; b=0;

```

Figure 7.14: Mapping of the amount of glandular tissue in millimeters into a color in the color scale.

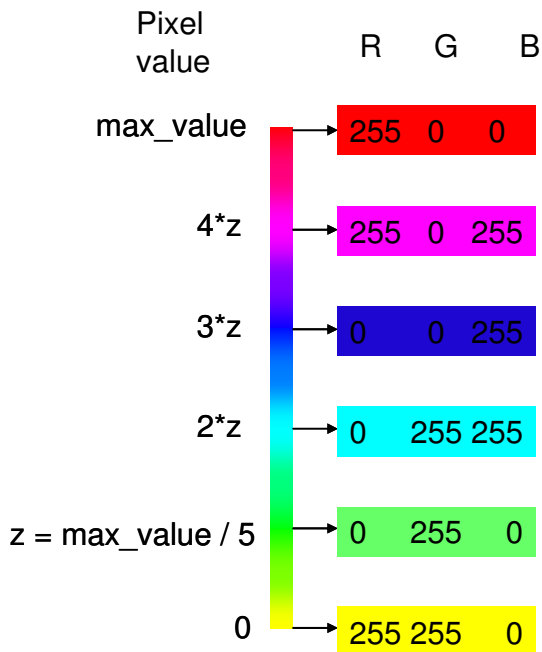


Figure 7.15: The color scale and the correspondence of color and pixel value.

7.8 Registration and Comparison of Mammograms

Radiologists need to search for asymmetries in the views of left and right breasts and to compare mammograms of the same breast, shifted in time, to find abnormalities. The comparison between images of the same breast, acquired at different points in time, is called temporal analysis. Bilateral analysis works with two images acquired at the same time, one of each breast. This difficult evaluation may be impaired by different factors such as variations in positioning and compression.

It is important to clear that the word compression, taken in an engineering sense, is misleading as the breast tissues do not compress but deform and displace with no loss of volume. This is important because an unchanged volume does not imply a change in density, and thus the linear attenuation coefficients of the tissues remain constant. During the examination, compression is essential because it reduces the radiation dose and improves contrast and resolution. The degree of breast compression varies from examination to examination and, hence, it is no standard value (figure 7.16).

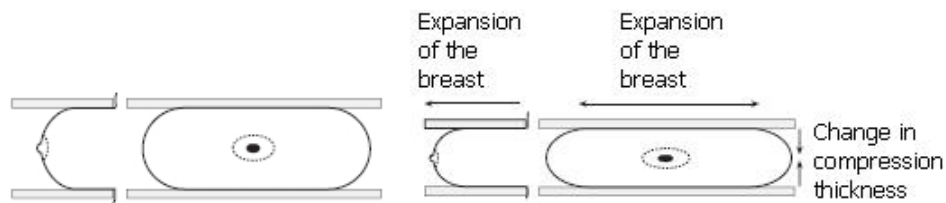


Figure 7.16: The magnitude of breast compression may change between examinations (Wirth 2000).

Compression causes global differences as well as local movements among the tissues according to the densities of abnormalities. Different tissues move relatively differently. Consequently, the thickness of the breast varies due to the amount of pressure applied, according to the size of the breast, and the composition and compressibility of the breast tissues. The way in which a breast is compressed depends on the composition of the breast, and the woman's response to compression. Increased compression causes a change in compression thickness and an expansion in the size of the breast.

Differences in the position angles and translational differences may appear between the mammograms to be compared. A correct breast positioning is very important. Ideally, the breast should be symmetrically distributed (figure 7.17a). Inappropriate positioning may cause the breast to roll. Consequently, the nipple may appear just partially or not at all and the breast non-symmetrically distributed about the nipple (figure 7.17b). Other deformations may occur such as translational changes or rotational changes due to differences in the position angle (figure 7.18).

The variations due to positioning and compression can be though suppressed through registration. Registration consists in aligning the images in a manner that corresponding features can be compared and integrated. Registration is subsequently the determination of a transform, which optimally matches the two images. During the registration process, a target image is mapped onto a reference image. After registration, the mammograms may be subtracted to see the differences between the registered images.

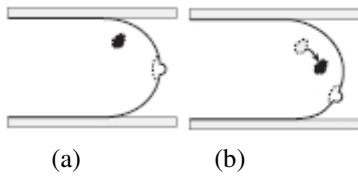


Figure 7.17: (a) When the breast is properly positioned, it should be symmetrically distributed among the nipple. (b) Inappropriate positioning may cause the breast to roll (Wirth 2000).

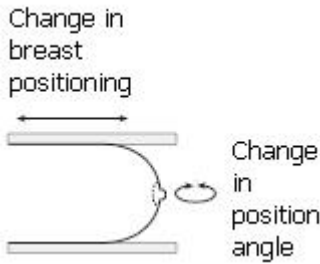


Figure 7.18: Translational and rotational changes occur due to differences in positioning (Wirth 2000).

To achieve the image matching, mutual information based registration (Pluim *et al.* 2003) is applied, which is a method based on the images entropies. Entropy is a quantity describing uncertainty from information theory. Hartley proposed a measurement for information of a message.

For a message of n symbols, with s different possibilities for each symbol, there are s^n possible messages (ignoring semantic). However, Hartley wanted a measure (H) that increases linearly with message length. Therefore, he proposed that, given messages of length n_1 and n_2 from s_1 and s_2 number of symbols, if the number of possible messages is equal, then the amount of information per message is also equal. He defined a measure of information that depends on the number of possible messages:

$$H = n \log s = \log s^n \quad (\text{Equation 7.23})$$

When the quantity of possible messages is bigger, the amount of information from a message is also bigger. With only one message possible, there is no gain of information from it ($\log 1 = 0$). On the other hand, this measure can be considered as a measure of uncertainty. When there are more messages that could be received, there is more uncertainty about which message will be received. If there is only one message, there is no uncertainty.

This measure takes for granted that all symbols may occur with the same probability. Shannon suggested a measure including the probability of occurrence of the different symbols. Given events p_1, \dots, p_m , the Shannon entropy is defined as

$$H = \sum_i p_i \log \frac{1}{p_i} = -\sum_i p_i \log p_i \quad (\text{Equation 7.24})$$

Hartley's entropy can be derived from Shannon's entropy, for the assumption that all messages are equally likely to occur

$$H = -\sum \frac{1}{s^n} \log \frac{1}{s^n} = \sum \frac{1}{s^n} \log s^n = \log s^n \quad (\text{Equation 7.25})$$

The expression $\log (1/p_i)$ means that the amount of information obtained from a message with probability p_i is inversely related to the probability of occurrence of the message. The more extraordinary a message, the more meaning is assigned to occurrence of the message. The information per message is weighted by the probability of occurrence. The entropy H is the average amount of information that could be obtained from a particular set of messages. Shannon's measure relies on the number of possible messages and on the probability of occurrence of each message.

Shannon's entropy can be calculated for an image, if the distribution of gray values of the image is considered. A probability distribution of gray values can be computed through the addition of the number of times each gray value occurs in the image and dividing those numbers by the total amount of occurrences. By minimizing the joint entropies of the images, they could be registered

$$-\sum_{i,j} p(i, j) \log p(i, j) \quad (\text{Equation 7.26})$$

A better measure for image registration is mutual information. For two images A and B , mutual information I is defined as

$$I(A, B) = H(B) - H(B|A) \quad (\text{Equation 7.27})$$

where $H(B)$ is the Shannon's entropy of image B . $H(B|A)$ denotes the conditional entropy, which is based on the conditional probabilities $p(b|a)$, the chance of gray value b on image B given that the corresponding pixel in A has gray value a . Mutual information is the amount by which the uncertainty about B decreases when A is given. Since A and B can be interchanged, $I(A, B)$ is also the amount of information B contains about A . For this reason, it is mutual information. The registration of the images equals to maximizing mutual information. The images should be aligned in a way that the amount of information they contain about each other is maximal.

Mutual information can also be defined considering joint entropies

$$I(A, B) = H(A) + H(B) - H(A, B) \quad (\text{Equation 7.28})$$

The expression $-H(A, B)$ means that the minimization of the joint entropy contributes to the maximization of mutual information.

Another definition of mutual information is related to the Kullback-Leibler distance, a measure of the distance between two distributions:

$$\sum_i p(i) \log \frac{p(i)}{q(i)} \quad (\text{Equation 7.29})$$

for two distributions q and p . Corresponding to the Kullback-Leibler measure, the mutual information of images A and B is defined as

$$I(A,B) = \sum_{a,b} p(a,b) \log \frac{p(a,b)}{p(a)p(b)} \quad (\text{Equation 7.30})$$

It measures the distance between the joint distribution of the images' gray values $p(a,b)$ and the joint distribution in case of independence of the images, $p(a)p(b)$.

Studholme *et al.* (1999) presented a normalized measure of mutual information:

$$\text{NMI}(A,B) = \frac{H(A) + H(B)}{H(A,B)} \quad (\text{Equation 7.31})$$

For the implementation, the joint probabilities distribution of intensities in two images has to be computed. This is performed by computing a joint histogram of intensities. Each entry $h(a,b)$ in the histogram denotes the number of times intensity a in one image coincides with b in the other image. Dividing the entries by the total number of entries yields a probability distribution. The probability distributions of each image, the marginal probabilities of each image separately, are found by summing over the rows, respectively columns, of the histogram.

The application of the transformation T to the target image will obligatorily change the joint probability function $p(a,b)$. Mutual information is then calculated once for each transformation T , until registration is achieved. The registration criterion states that if the images are geometrically aligned, the value of I is maximum. Therefore, we denote $I(A,B,T)$ and present the registration criterion by the expression

$$I(A,B,T)_{\max} = I(A,B,T^*) \quad (\text{Equation 7.32})$$

where T^* is the optimal registration transformation.

There are different options for the transformation. A combination of three different transformations can be chosen: translations, rotations and scaling. The translations should compensate for changes in positioning, the rotations for changes in position angle and the scaling would compensate for changes in compression.

The geometric transformations are defined as a map $S: R^2 \rightarrow R^2$, where each point (x, y) in R^2 is assigned a new location $(x', y') = S(x, y)$. Using matrix notation, the transformations are expressed as:

$$\text{Translation} \quad \begin{pmatrix} x' \\ y' \\ 1 \end{pmatrix} = \begin{pmatrix} 1 & 0 & t_x \\ 0 & 1 & t_y \\ 0 & 0 & 1 \end{pmatrix} \begin{pmatrix} x \\ y \\ 1 \end{pmatrix} \quad (\text{Equation 7.33})$$

$$\text{Rotation} \quad \begin{pmatrix} x' \\ y' \\ 1 \end{pmatrix} = \begin{pmatrix} \cos \theta & -\sin \theta & 0 \\ \sin \theta & \cos \theta & 0 \\ 0 & 0 & 1 \end{pmatrix} \begin{pmatrix} x \\ y \\ 1 \end{pmatrix} \quad (\text{Equation 7.34})$$

$$\text{Scale} \quad \begin{pmatrix} x' \\ y' \\ 1 \end{pmatrix} = \begin{pmatrix} s_x & 0 & 0 \\ 0 & s_y & 0 \\ 0 & 0 & 1 \end{pmatrix} \begin{pmatrix} x \\ y \\ 1 \end{pmatrix} \quad (\text{Equation 7.35})$$

In order to find an appropriate transformation, we first perform an scaling, so that both images have the same value for “compressed breast thickness”. Additionally to the change of size, the total amount of glandular tissue in the target image must remain constant. The scaling factors s_x and s_y for standardization, which are equal, are obtained by dividing the image number of rows by the standard image number of rows. For registration, these scaling factors are calculated by dividing the number of pixels in the images to be compared. When scaling, the number of pixels changes, but the amount of glandular tissue remains constant by an increase or decrease of the pixels values.

The step of scaling may result in a decrease of mutual information. However, if the breast size did not changed drastically, the volume should be approximately equal for both images, and therefore the breast area, if the breast thicknesses are set to the same value.

After scaling a combination of rotations and translations that maximizes mutual information should be found. This is an optimization problem that can be solved using an optimization algorithm to choose the combination of movements (left, up, rotate right,...) that maximizes the mutual information of the images.

For the implementation in our software prototype, we chose to limit the optimization to three steps:

- After scaling, translations to the left and to the right are evaluated and the best of them is applied to the floating image;
- After applying the former transformation, a similar decision is made in regard of moving the floating image up or down;
- The last decision is to choose a movement of rotation with a positive or negative angle.

Each of the former steps can be evaluated for a number of iterations.

The comparison of the mammograms is presented as a numerical relationship of the amounts of tissues and it is visualized through the extraction of the registered images.

Figure 7.19 illustrates the registration process.

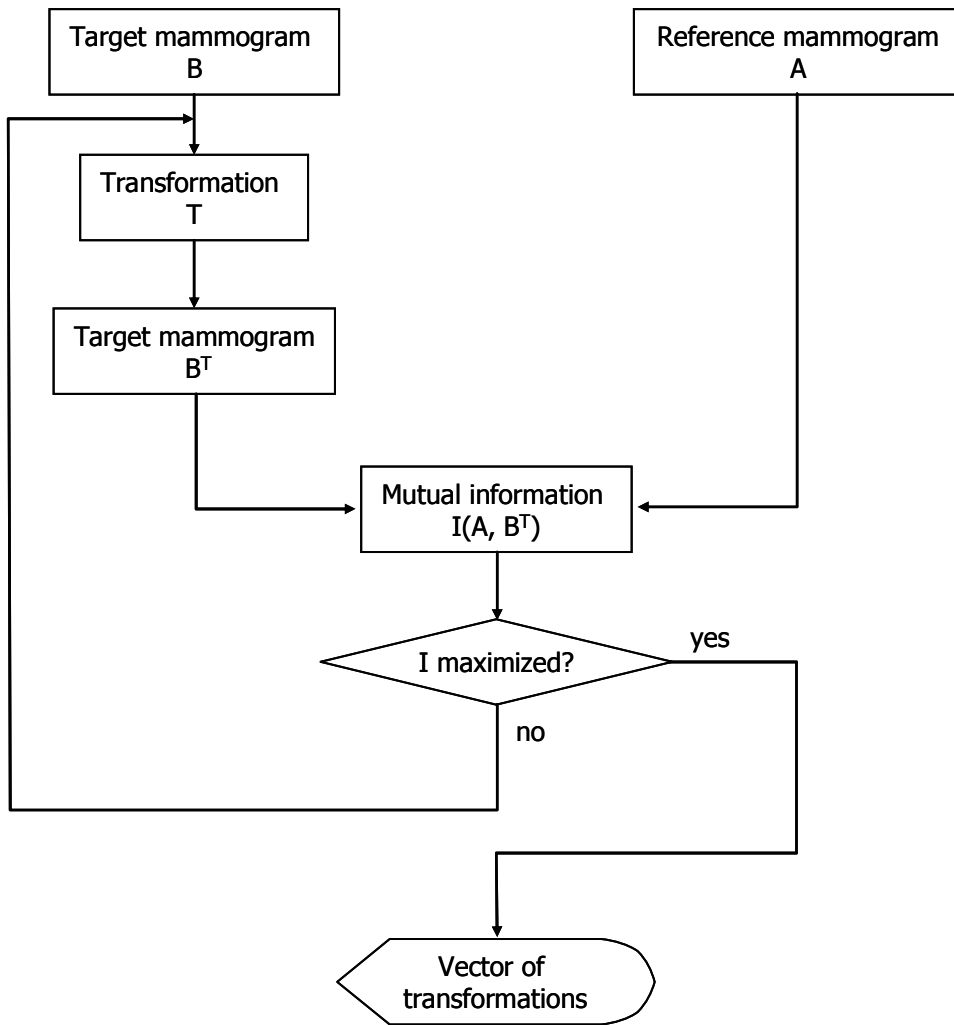


Figure 7.19: The process of maximizing mutual information.

8 SOFTWARE ARCHITECTURE

8.1 System View

The software should be integrated into a digital mammography environment. Such an environment has a basic configuration with an acquisition device, storage and an image processing and reading station. Advanced environments include also many stations connected through a network for distant evaluation of the mammograms (figure 8.1).

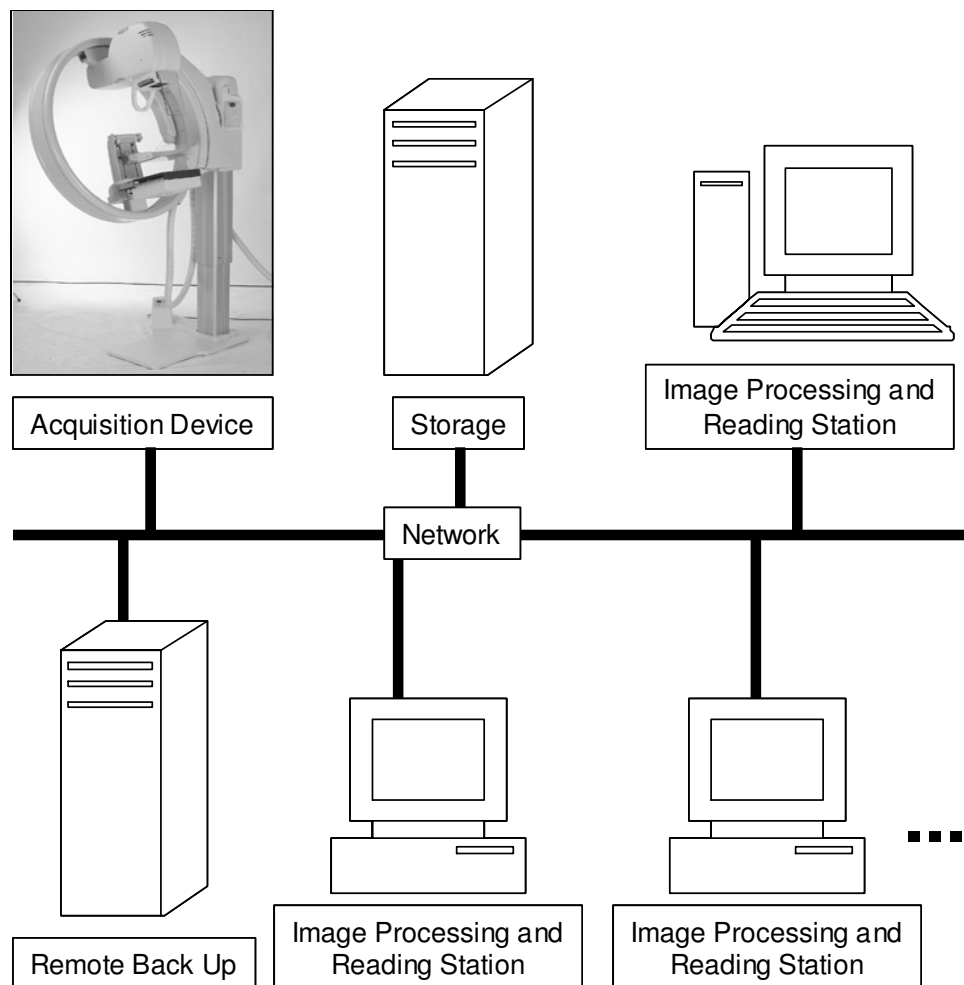


Figure 8.1: Structure of a digital mammography environment.

For the implementation of the methods developed we chose to assign the software to the image processing and reading station. Another option can be to integrate parts of the algorithms to the hardware in the acquisition device.

8.2 Requirements

The minimal functional requirements for this software prototype are as follows:

- The application must be built around a graphical user interface.
- The application should be able to read mammograms in the DICOM file format.
- The application should be able to display mammograms in the DICOM file format.
- The application should be able to display the mammograms DICOM header metainformation used.
- The application should allow zooming in and out the image.
- The application should allow adjusting the contrast and brightness of the image.
- The application should perform the segmentation of the mammograms into breast, background and pectoral muscle.
- The application should be able to open the MS Excel files containing the linear attenuation coefficients and find the appropriate coefficients for the image being analyzed.
- The application should calculate the volumetric breast density.
- The application should present the results of the calculations as a text.
- The application should store the image path together with the results of the analysis.
- The application should show and hide the different views of the mammogram (standard and percentages of fibroglandular tissue).
- The application should generate and show the histogram of the mammograms.
- The application should be able to register two mammograms.
- The application should generate a difference image as a result of the registration process.
- The application should be able to model the amount of glandular tissue as height fields, contours, Bézier surface and NURBS.
- The application should enable the user to move, rotate and translate the surfaces generated.
- The code of the application should be easily extensible.

8.3 Conceptual Modular View

The system consists of four modules (figure 8.2): DICOM Reader, 2D Viewer, 3D Viewer and Image Analyzer. This last module consists of four submodules: Segmentation, Evaluation, Standardization and Registration.

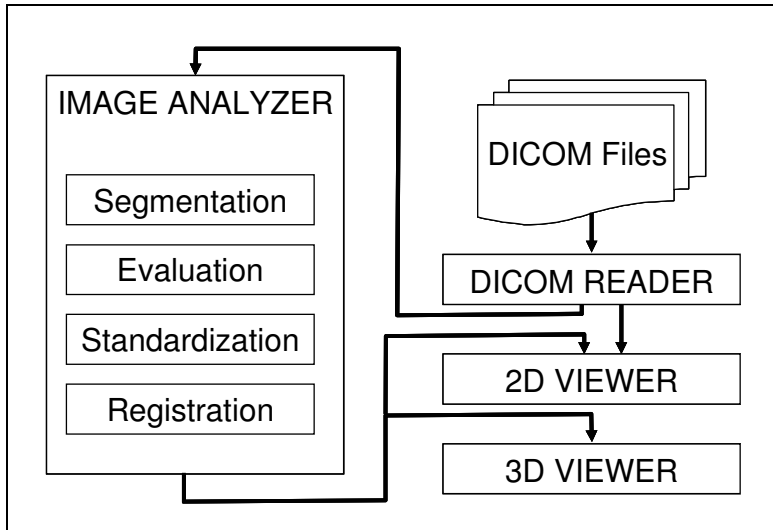


Figure 8.2: The DICOM Reader loads the mammograms and gives them to be evaluated to the Image Analyzer and to be shown to the 2D Viewer. The Image Analyzer performs the main operations and delivers the results to the 2D and 3D Viewers.

The DICOM Reader loads the mammograms. As described before, the DICOM files consist of a Header and a Data Set, where the image is encapsulated together with some parameters. From the Data Set, the DICOM Reader gets the Data Elements that are later used by the other modules. These parameters are the following:

- Modality: this parameter describes the image acquisition technique used to examine the patient; for mammography it should be MG. The system checks this value to make sure that the file being opened is actually a mammogram.
- Presentation Intent Type: this parameter specifies whether the image is raw or for display, in our case it should have the value FOR PROCESSING, indicating that it is a raw unprocessed file. If it is not a raw image, it can be shown but not analyzed, since it means that the pixels intensities are not linearly related to the photons energies.
- Peak Kilo Voltage: this value indicates the voltage output of the x-ray generator used and it is used to search for the appropriate linear attenuation coefficients.
- Body Part Thickness: this variable gives the thickness in millimeters of the examined compressed breast. It is used by the analyzer to calculate the volumetric breast density.

- View Position: this parameter could take the value CC for cranio-caudal or MLO for mediolateral-oblique. The MLO mammograms are later processed to segment the pectoral muscle.
- Image Laterality: refers to the examined breast L stands for “left” and R for “right”. In the case of mammograms with view position MLO and laterality of R, they are mirrored before performing the pectoral muscle subtraction.
- Photometric Interpretation: this value indicates the intended interpretation of the pixel data. MONOCHROME1 (the expected value for raw images) means that the minimum pixel value is intended to be displayed as white.
- Rows and Columns: these parameters specify respectively the number of rows and columns in the image and they are used to generate the matrix of pixels containing the image.
- Bits Allocated, Bits Stored and High Bit: these values describe the pixels. They are used to read the pixel data. This data is divided into pixels samples with “bits allocated” bits. Bits Stored indicates the number of bits used in each sample, and the value of high bit gives the most significant bit in a pixel sample.
- Window Center and Window Width: these two parameters specify a linear conversion from stored pixel values. Values “below” the window are displayed as the minimum output value and input values “above” the window are displayed as the maximum output value. These values are used to adjust the contrast and brightness of the images.
- Pixel Data: this element contains the image as a sequence of pixel samples.

All these parameters are stored in a DICOM object, which can be used by the other modules. This module is also responsible for the generation of the histogram.

The Image Analyzer receives the DICOM objects and processes them. The first two operations that this module performs are the segmentation of the background and in the MLO images the extraction of the pectoral muscle.

After having segmented the images, the values of the linear attenuation coefficients are searched and used to evaluate the images in the submodule Evaluation. This submodule generates text files where the results of the analysis are stored. Moreover, this submodule creates a matrix of volumetric breast density by assigning to pixels in the original image a cell in the matrix with the correspondent amount of glandular tissue. The matrix is later given to the other modules for standardization and visualization.

The submodule Standardization scales the matrix of glandular amounts and assigns a color to each value according to the color scale.

The last submodule, Registration, performs the comparison of mammograms when two images are loaded. It takes the standardized images and aligns them according to the

algorithm for mutual information based registration. It gives, additionally the transformations performed and generates a third image, a difference image of the mammograms compared and give the three images to the 2D Viewer.

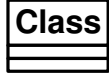
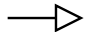

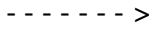
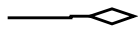
The 2D Viewer makes the results visible. It can show the original images, the standardized values and the distribution of glandular tissue as percentages of the compressed breast density. This module enables the user also to zoom in and out the image and to change the contrast and brightness. It also can reset all the operations performed by the user to set the image back to the defaults values.

The 3D Viewer is a module to generate the modeling of the matrix of glandular tissue as height fields, contours, Bézier surface and NURBS surface. It shows these different views and allows the user to move, rotate and zoom in and out of the visualized objects.

8.4 Structural Design

Class hierarchy and relationships between classes are shown in figure 8.3., which was drawn using UML notation (the elements used and their meaning are summarized in table 8.1). We present the most relevant classes used in the implementation, together with their relationships to the conceptual modular view of the software.

Table 8.1: Summary of UML notation for class diagrams.

Element	Meaning
	Class
	Inheritance
	Association
	Dependency
	Aggregation

The class CObject is a basic class for many MFC¹-Classes. The classes CImgEvalApp and CImgEvalDoc are used by all the modules described in the conceptual view. The document class CImgEvalDoc contains all the data that the modules share. It encapsulates important elements such as the image and the results of the evaluation. It inherits from the class CDocument, which is a child of the class CCmdTarget.

In the application class CImgEvalApp, the main interface window is defined together with the communication with the operating system. This class inherits from CWinApp, which itself is a child of CWinThread, which is a child of CCmdTarget.

The modules Image Analyzer, 2D Viewer and 3D Viewer have their frames and windows. The class CWnd is the basic class for all the window classes. The classes CMainFrame, CViewerFrame and CSurfaceFrame define the characteristics of the frames of Image Analyzer, 2D Viewer and 3D Viewer, respectively. These three classes are child classes from the abstract class CFrameWnd. The windows they contain are defined in the classes CImgEvalView, CDICOMView and CSurfaceView, which inherit their properties and methods from the class CView.

The class CDlgInfo contains information about the software version and the class CHelpDialog shows the program's help. Both are derived from CDialog, which itself is a child of CWnd. Other classes derived from CDialog are CHistogram and CBrightCont and they are used by the 2D Viewer to show the histogram of an image and to adjust the brightness and contrast. The class CDICOMToolbar describes the properties of the toolbar used by the 2D Viewer and it is derived from CDialogBar, which is a child of CControlBar. The toolbar contains an slider element that is described in the class CDICOMSlider that is derived from CSliderControl.

All subclasses of COleDispatchDriver are used by the Image Analyzer to perform the evaluation of the volumetric breast density. COleDispatchDriver implements the client of the automation of MS Office. Its subclasses make it possible to use the functionality of MS Excel. For example, the classes CCharts and CChart contain functions to manipulate diagrams. With the help of the classes CWorkbook, CWorkbooks, CWorksheet and CWorksheets, the desired sheet in a book can be accessed. The class CRange, which, to keep the diagram simple, is not depicted in figure 8.3, to access a cell in a worksheet. All these mentioned children of COleDispatchDriver are associated to the class CAutomation, which reads all the parameters needed from the MS Excel documents. CAutomation is a part of the class CEvaluation, which reads the image and performs the calculations of density. The class CDataElmDescription is used to translate the data elements in the image header and their values into text.

¹ MFC: Microsoft Foundation Class Library

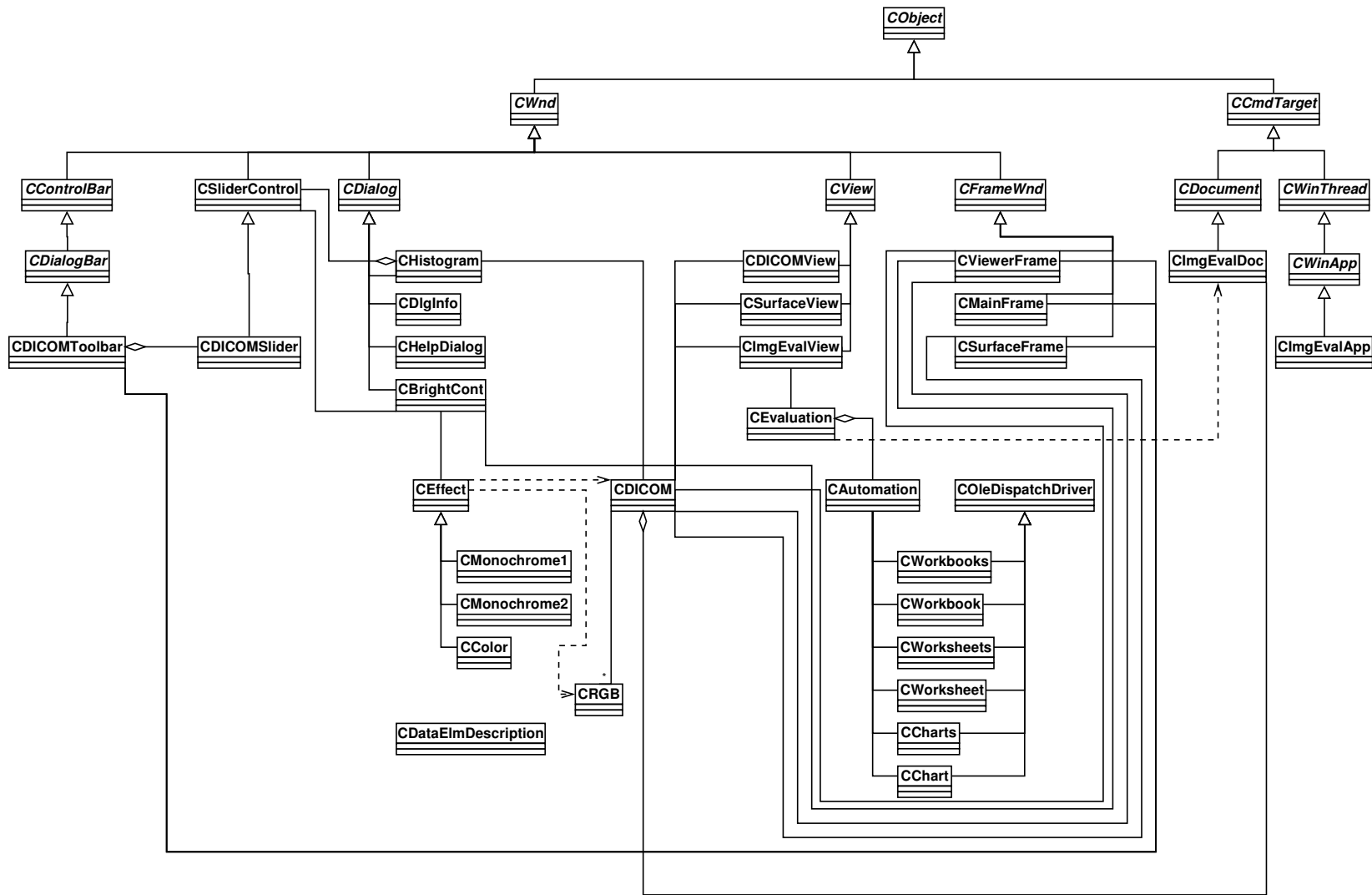


Figure 8.3: Class hierarchy and relationships.

The class CDICOM encapsulates all the image information and it includes the document object of type CImgEvalDoc. It also contains the pixel matrix that has elements of type CRGB. The images are shown through CDICOM. CRGB describes the component red, green and blue of a pixel. The class CEffect and their subclasses CMonochrome1, CMonochrome2 and CColor, are used by the 2D Viewer. They correspond to the different presentation modes in which an image can be shown.

For the implementation of the 3D Viewer, the classes CSurfaceFrame and CSurfaceView are used. The last one implements OpenGL. It defines the render context, the initialization of OpenGL, the control points, the different graphic objects and transformation, as well as the methods that enable the processing of different mouse events. CSurfaceFrame defines the window frame in which the different 3D elements are shown.

8.5 Behavioral Design

Sequence diagrams are shown for the main data flows. We made use of the UML notation. The elements used and their meaning are summarized in table 8.2.

Table 8.2: Summary of UML notation for sequence diagrams.

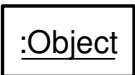

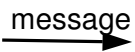
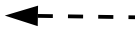
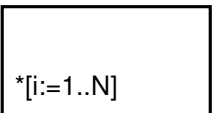
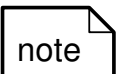
Element	Meaning
	Object
	Lifeline and focus of control
	Message / Call
	Return
	Iteration
	Note

Figure 8.4 shows the sequence used to read the photon energy. This parameter is needed to read the appropriate linear attenuation coefficients. Photon energies for different target/filter combinations, x-ray tube voltage and breast thicknesses are stored in the file MD_Tabs_SB_File. A CAutomation object opens MS Excel and works with it. The first step is to tell to a CWorkbooks object to open the requested file. Afterwards, the CAutomation object searches with the help of a CWorkbook object the pages in the file. Subsequently, the required page is searched according to the target/filter combination using get_items() on a CWorksheets object. Thereafter, the photon energy is obtained using the x-ray tube voltage and breast thickness specified in the DICOM data elements.

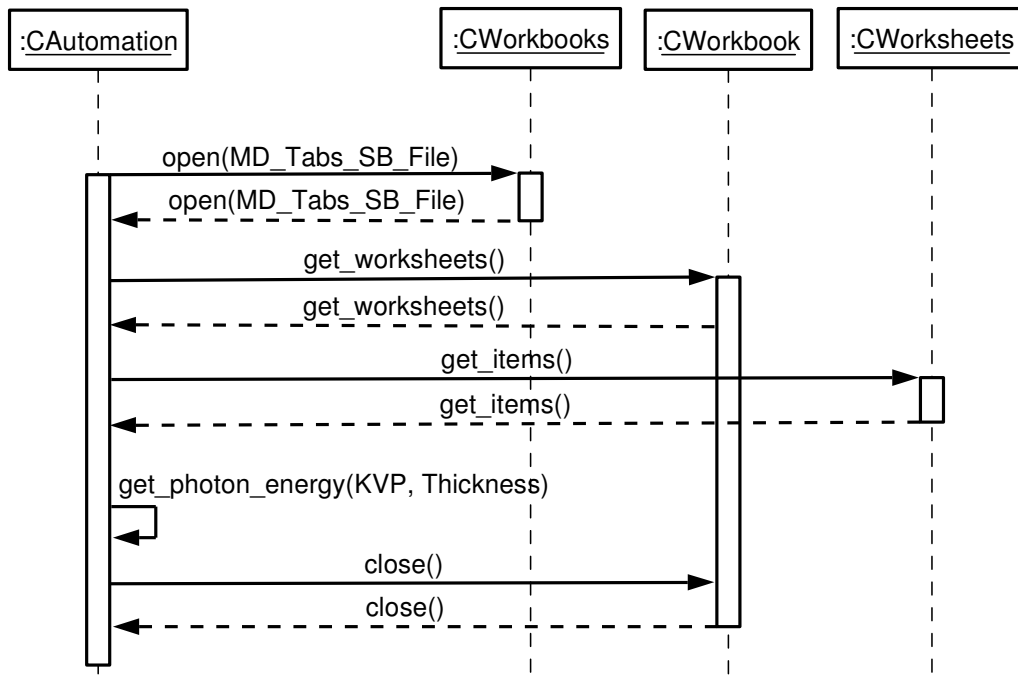


Figure 8.4: Sequence to read photon energy.

Using the photon energy, the CAutomation object can then search the linear attenuation coefficients corresponding to the mammogram. Figure 8.5 shows the sequence used to perform this operation. Mass attenuation coefficients and material densities are stored in the file MYR_50_1_File. Using these two parameters, the linear attenuation coefficients can be calculated. The process is the same as before: a CAutomation object opens MS Excel and works with it. Using a CWorkbooks object, the file is opened. A CWorkbook object searches the pages and the required page is obtained through a CWorksheets object. The object CWorksheet and CRange are used to obtain the content. When the cells in the file were found, the values can be read.

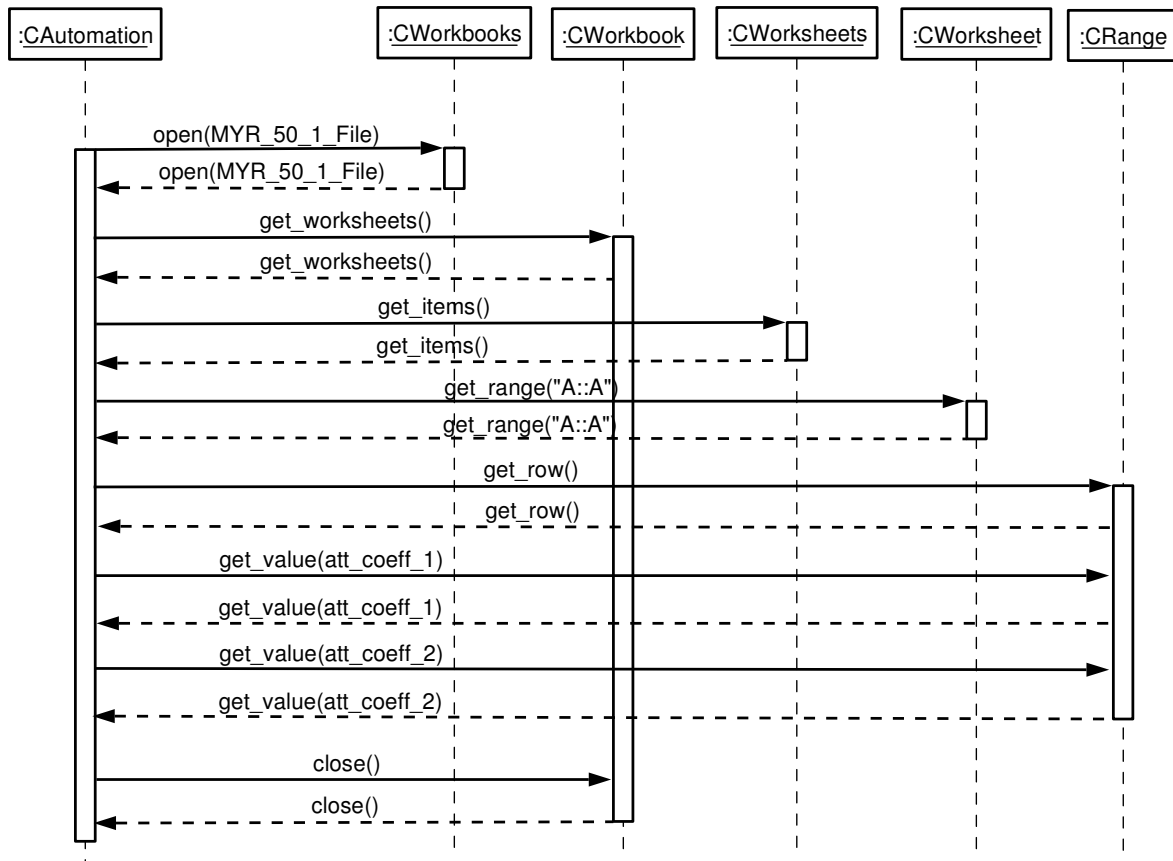


Figure 8.5: Sequence to read the linear attenuation coefficients.

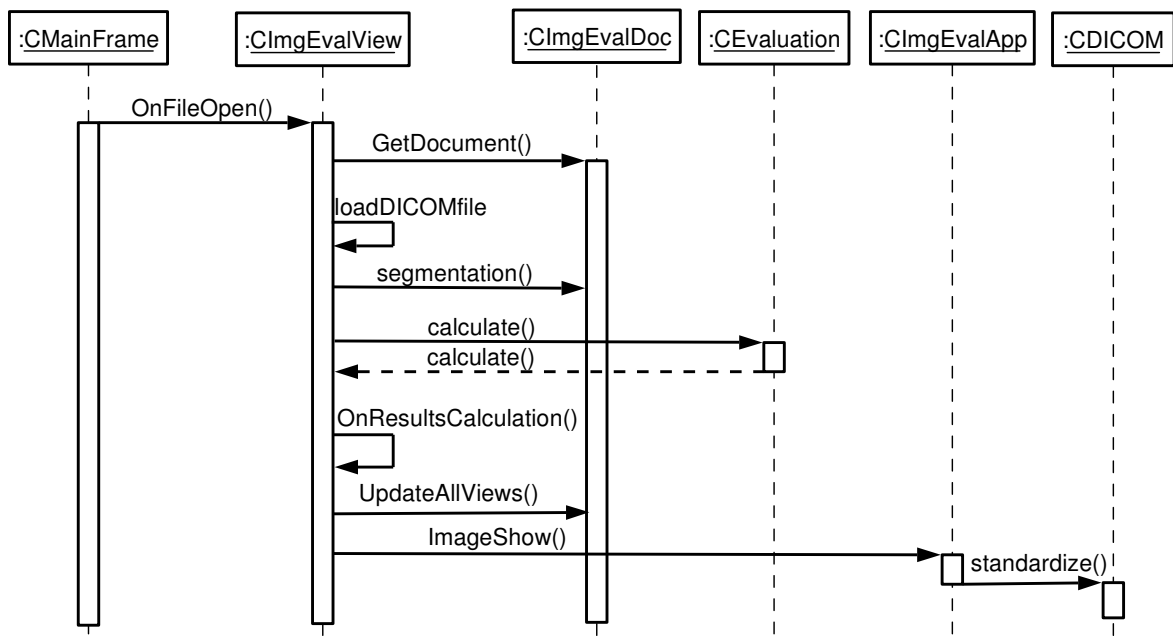


Figure 8.6: Sequence to treat one image by opening it, loading the DICOM data elements, segmenting the breast region, calculating the volumetric breast density, showing the image and setting it into the standard format.

The main sequence (figure 8.6) is started by the user from a menu using the Open option. This event triggers the operation OnFileOpen() on a CImgEvalView object. A new CImgEvalDoc is created and the file can be loaded. After loading the image, it is segmented and the volumetric breast density is calculated by a CEvaluation object. Then the results can be updated and the application can show the image. The results are sent to a CDICOM object to be processed and standardized.

The CImgEvalView object opens the file using the loadDICOMfile function, which is described in more detail in figure 8.7. Using a CFile object, the file is opened and iteratively, the elements can be read. The first elements are 128 zeros, which are followed by the string DICM. Then, the data elements are read one by one until the end of the file. Finally, the file is closed.

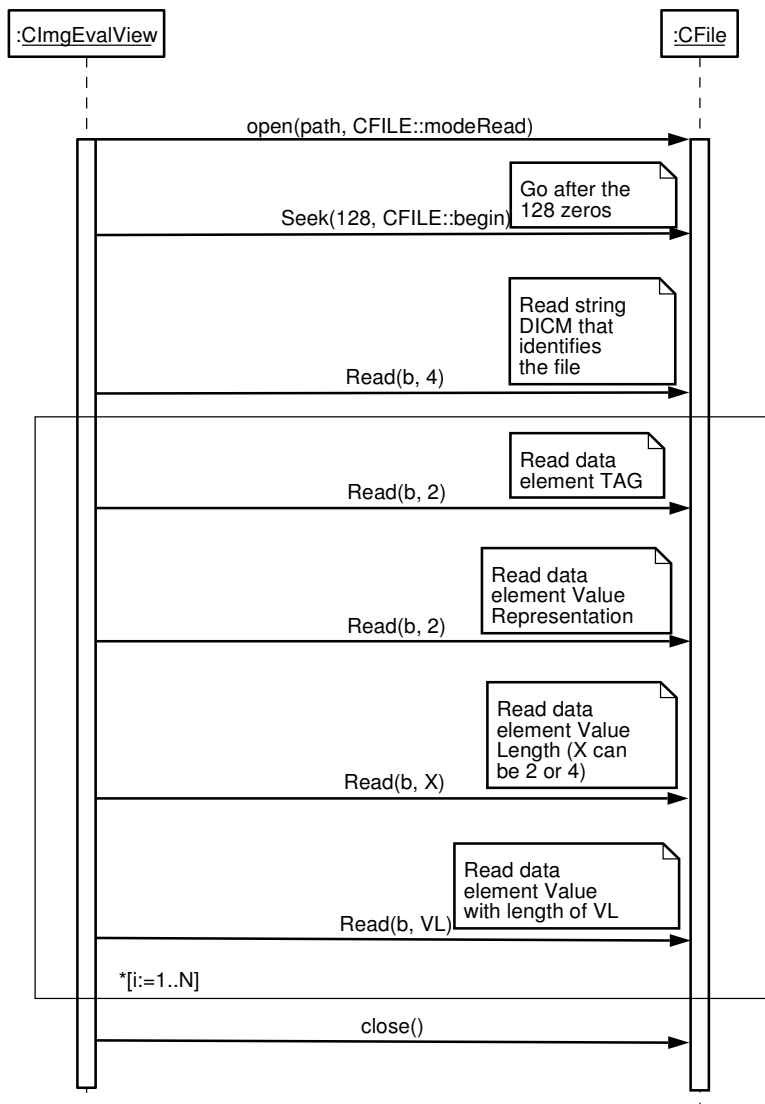


Figure 8.7: Sequence to load the DICOM header and data elements.

To display the image, the application creates the frames needed and loads the image onto them. A CDICOM object translates the pixel gray levels, which are integer values into RGB pixels and the window is updated.

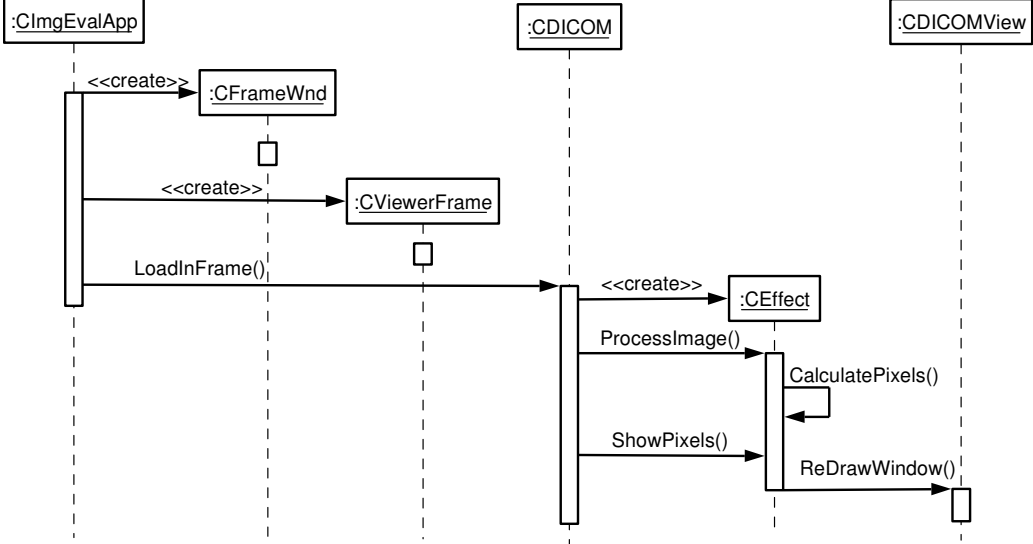


Figure 8.8: Sequence to display the image.

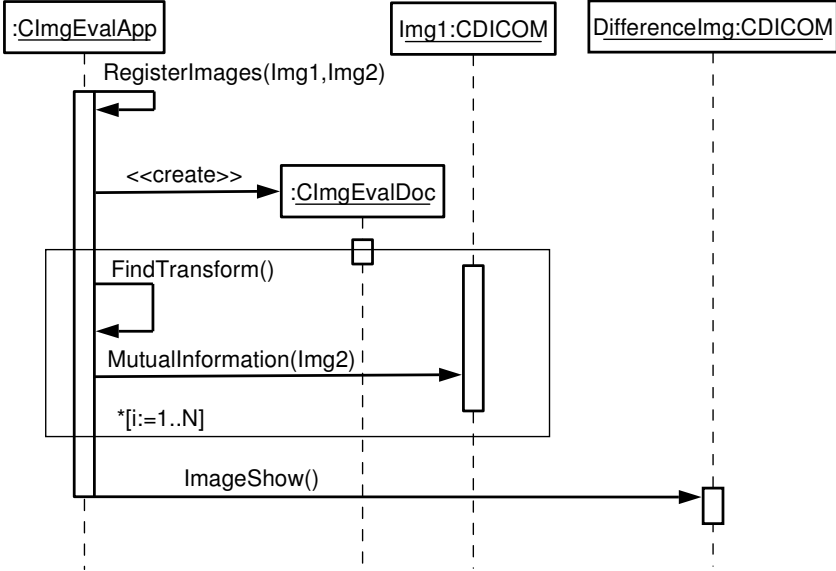


Figure 8.9: Sequence to create the difference image.

The application triggers the process of registration when two images were opened to be compared. To begin the process, a new object is created to store the difference image. Then, the two images are registered and the difference image is send to the display.

8.6 User Interface

The user interface consists in a set of windows, that were developed to be easily and intuitively understood by the user.

Main Window

This window contains three menus: File, Results and Help (figure 8.10).

The menu File has three items:

- Open to open one image, analyze it and show it. It triggers the Open window (figure 8.11),
- Open to compare to do the same with a second image and compare it with the first one,
- Exit to quit the application.

The menu Results contains seven items:

- Comparison to show the last comparison performed,
- Header data to display the DICOM file header data,
- Histogram opens a new window showing the image histogram,
- Calculation shows the result of the volumetric breast density calculation,
- Short overview displays a list summarizing the results of all the images analyzed,
- Complete overview shows the same data as Calculation for all the images,
- Reset all results erases the files containing the results.

The menu Help contains two items:

- Program help shows instructions on how to use the software,
- About ImgEval displays information on the software version.



Figure 8.10: Main program window.

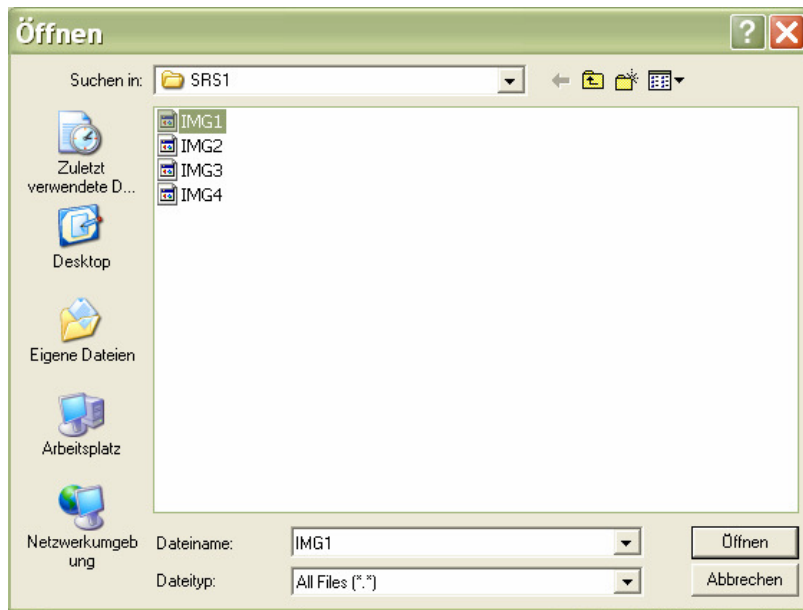


Figure 8.11: Open Window.

Viewer Window

This window shows an image using different options. It contains five menus: File, View, Edit, Segmentation, and Help (figure 8.12).

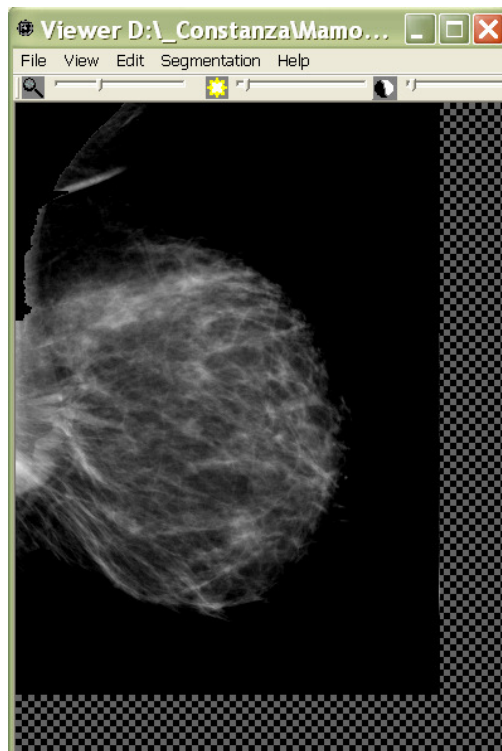


Figure 8.12: Viewer Window.

The menu **File** has one item: **Close** to close the window.

The menu **View** has three items:

- **Toolbar** to open the toolbar if it has been closed,
- **Histogram** to show the image's histogram,
- **3D** that triggers a 3D viewer window.

The menu **Edit** has two items:

- **Zoom**, which allows zooming the image in three levels: 25%, 50% and 100%,
- **Brightness/Contrast** opens the Brightness/Contrast window,

The menu **Segmentation** has three items:

- **Standard** is used to show the standardized image,
- **Percentages** to highlight different breast density regions,
- **Hide** to return to the original image shown in gray levels.

The menu **Help** shows instructions on how to use the different menus in the Viewer.

Brightness/Contrast Window

This window allows the user to change the brightness and contrast of the image shown in the Viewer window (figure 8.12). It has a ComboBox to choose the pixel interpretation (Monochrome1, Monochrome2 or Color). It contains two Slider Controls to change brightness and contrast and a Check Box Control to let the user see the changes before accepting them.



Figure 8.13: Brightness/Contrast Window.

3D Viewer Window

This window shows the different options of the three-dimensional presentation of the volumetric breast density (figure 8.13). It contains two menus: Edit and View.

The menu **Edit** has six items, four of which are used to select the kind of transformation the user wants to apply to the image (**Move**, **Rotate**, **Resize** and **Zoom**). Another item allows resetting the transformations made (**Reset**) and the last item is used to close the window.

The menu **View** has four items to select the kind of presentation wished: height fields, surface (Bézier/NURBS), contour plot and to show the parts segmented during image analysis.

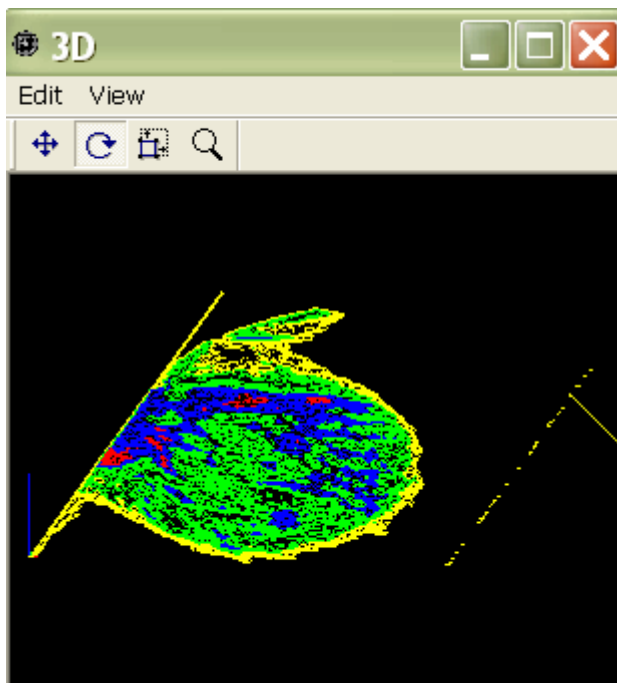


Figure 8.14: 3D Viewer Window.

9 RESULTS

The method for the analysis of breast composition transforms pixel values in amounts of glandular tissue. For tests we used images from 59 patients from one examination. The most of these 59 patients had four mammograms taken: two of each breast (one CC and one MLO image per breast).

The results are presented as a comparison of the calculations of the volume of fibroglandular tissue in CC and MLO mammograms of the same breast, which should be equal (figure 9.1).

Each point in the diagram represents the amount of fibroglandular tissue. In the X axe, the results for the MLO views are presented and on the Y axe for the CC views. Ideally, the values for the MLO and CC views of each patient should meet in the diagonal line, meaning that they are equal. This is because these two views are a projection of the same breast and at the same time.

In figure 9.2, the same results are shown for images where no pectoral muscle segmentation was performed; and it can be seen how important this pre-processing step is for the calculations.

The results are also shown as a comparison of the volume of fibroglandular tissue in CC and MLO mammograms of the right and left breasts, because they are very similar, and asymmetries between right and left breasts should be considered as a warning signal.

In figures 9.3 and 9.4, the results are presented for breasts with no significant asymmetries, to show the correctness of the calculations. Once again, each point in the graphic represents the amount of fibroglandular tissue. In the X axe, the results for the left breast are shown, on the Y axe for the right breast. Figure 9.3 shows this for the MLO views and figure 9.4 for the CC views. Here, the values for the left and right breasts should meet in the diagonal line, meaning that they are very similar.

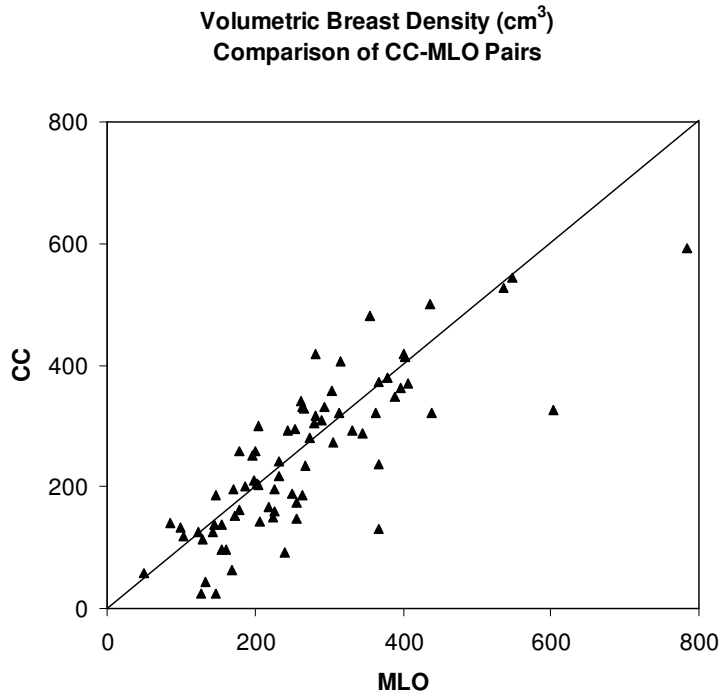


Figure 9.1: Volumes of glandular tissue [cm³]. Comparison of the CC/MLO pairs, with pectoral muscle segmentation.

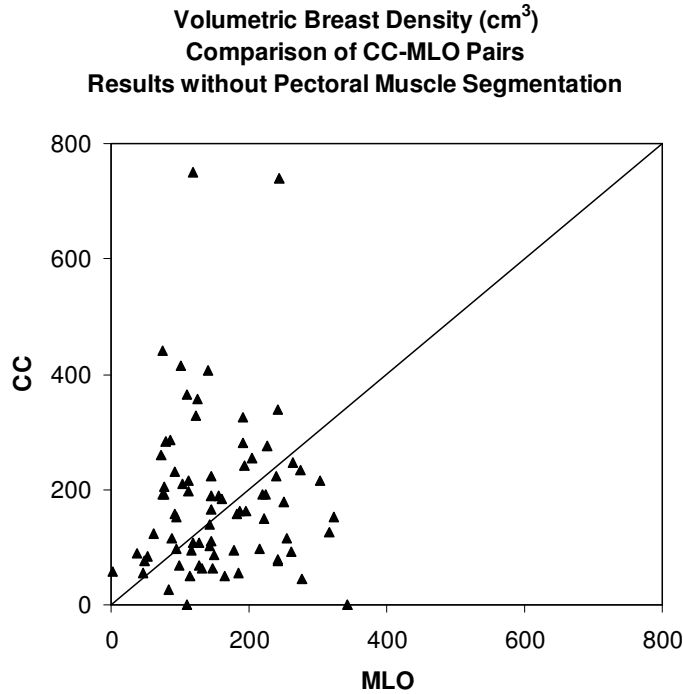


Figure 9.2: Volumes of glandular tissue [cm³]. Comparison of the CC/MLO pairs, without pectoral muscle segmentation.

**Volumetric Breast Density (cm³)
Comparison of CC-Left/CC-Right Pairs**

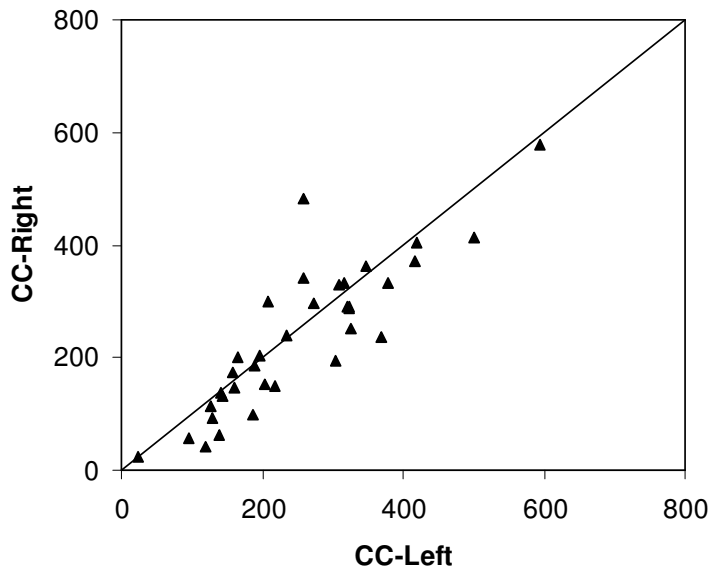


Figure 9.3: Volumes of glandular tissue [cm³]. Comparison of the CC-Left/CC-Right pairs.

**Volumetric Breast Density (cm³)
Comparison of MLO-Left/MLO-Right Pairs**

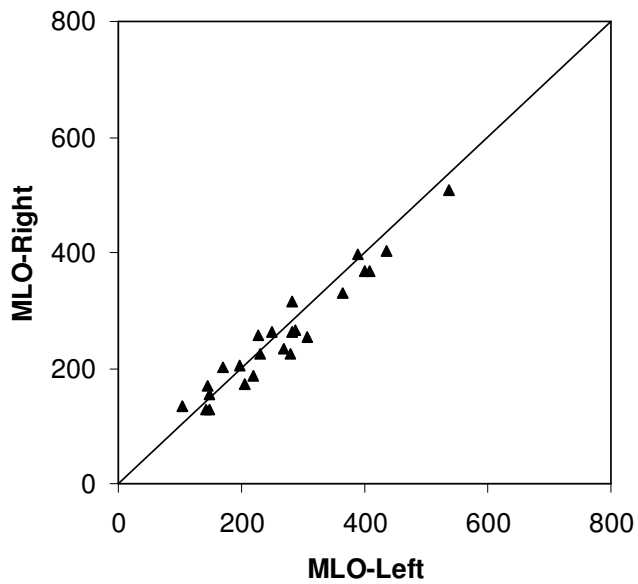


Figure 9.4: Volumes of glandular tissue [cm³]. Comparison of the MLO-Left/MLO-Right pairs.

When information is graphically shown, it is possible in many cases to obtain a more efficient analysis of the data. This is also valid for medical data. By means of visualization, data obtained through medical examination can be decomposed and presented for different intentions like diagnosis, therapy and post-operative attention.

In this project, visualization is needed to show the results of the methods as well. The following information is graphically presented in the developed software prototype:

- The mammograms as they are;
- The segmentation of the pectoral muscle in MLO views;
- The distribution of fibroglandular tissue in 2D and 3D presentations;
- The breast border;
- Calcifications, when present;
- The registered images and the result of extracting two registered images.

In the next pages, some examples of the graphical results are illustrated. In figure 9.5 four examples of the results of the pectoral muscle segmentation are shown.

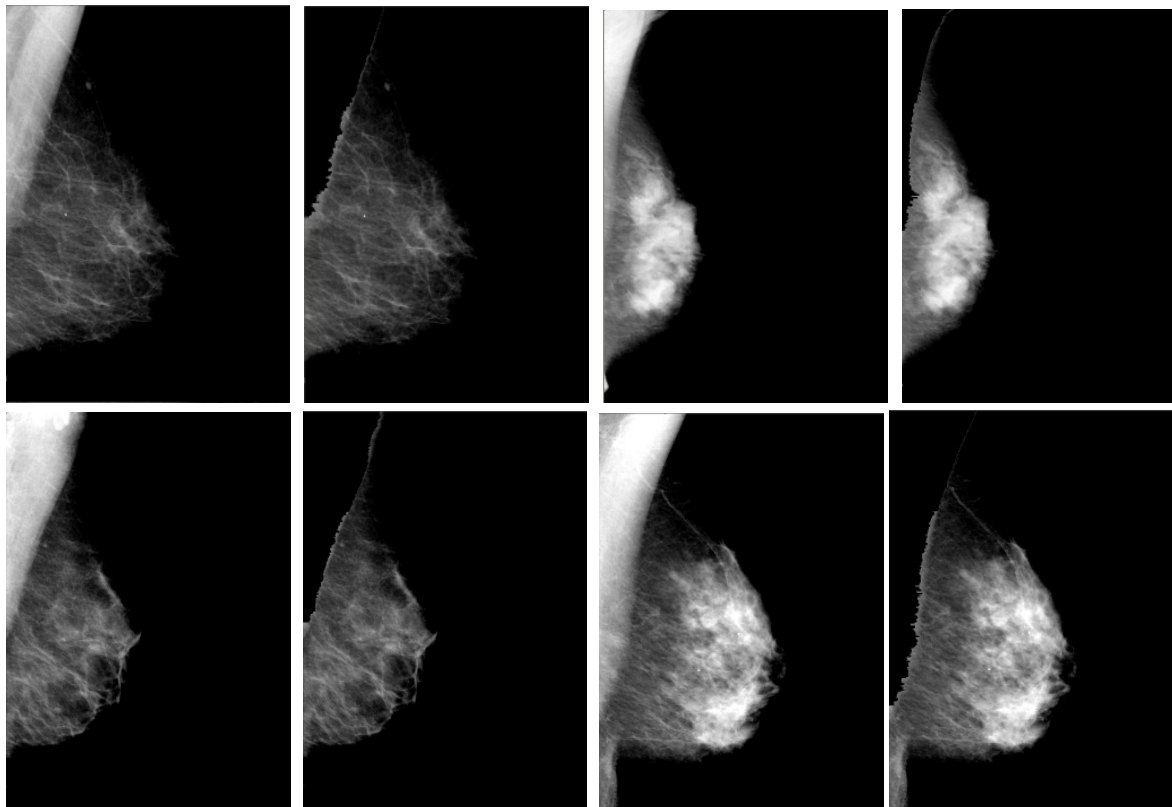


Figure 9.5: Examples for the pectoral muscle segmentation for four patients showing the original mammogram and the mammogram obtained after the pectoral muscle subtraction.

We would also like to show an example of undersegmentation due to very small differences in intensity between muscle and breast tissue, which could be interactively changed, by reducing the value of the edge (figure 9.6).



Figure 9.6: An example showing undersegmentation. This is caused due to weak differences of intensity between the pectoral muscle and the breast tissue.

Figures 9.7-9.9 show, respectively, images corresponding to a total amount of glandular tissue equal to 54, 40 and 18%. The outer red line corresponds to the border, the blue line in the middle presents the pixels corresponding to I_{fat} , the pixels between these two lines are considered are “purely fatty tissue”. The red area inside of the breast represents values where the amount of glandular tissue is equal or greater to 100%, which may suggest the presence of microcalcifications. In each histogram, the values for “purely glandular” (I_{gla}) and “purely fat” (I_{fat}) are shown with red and blue lines. The orange line corresponds to the value of the pixels in the breast border.

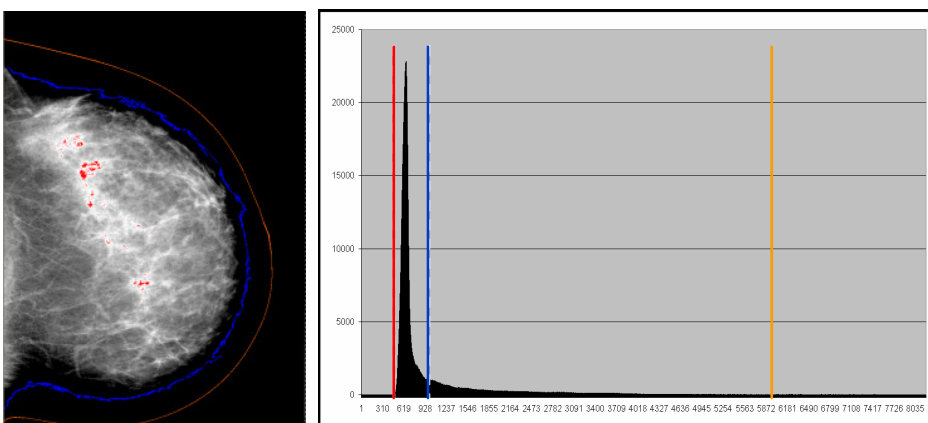


Figure 9.7: Image segmentation and histogram for a fraction of dense tissue of 54%.

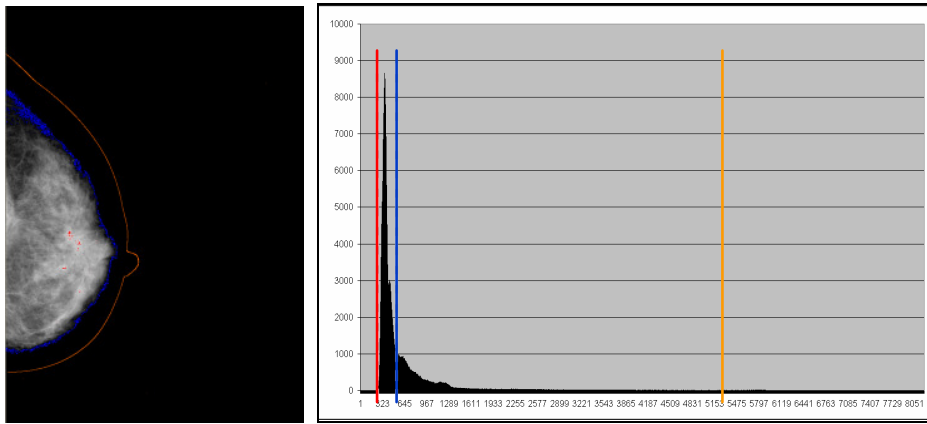


Figure 9.8: Image segmentation and histogram for a fraction of dense tissue of 40%.

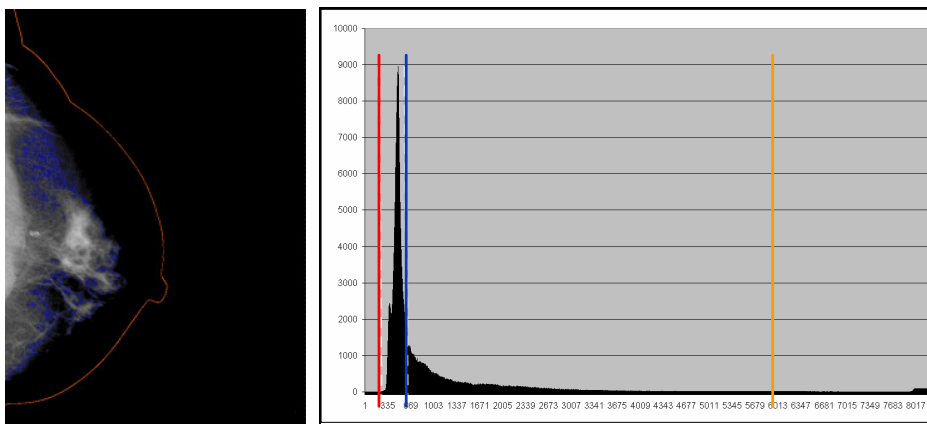


Figure 9.9: Image segmentation and histogram for a fraction of dense tissue of 18%.

Figure 9.10 illustrates how different percentages of glandular tissue in a mammogram are shown using different colors.

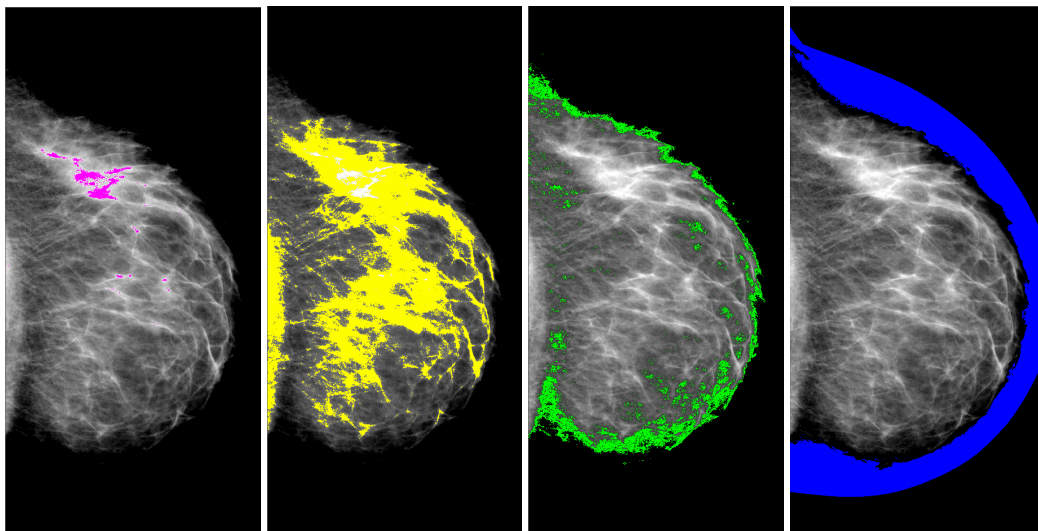


Figure 9.10: Segmentation of the mammogram according to percentages of glandular tissue: 70% (magenta), 50% (yellow), 25% (green) and 0% (blue).

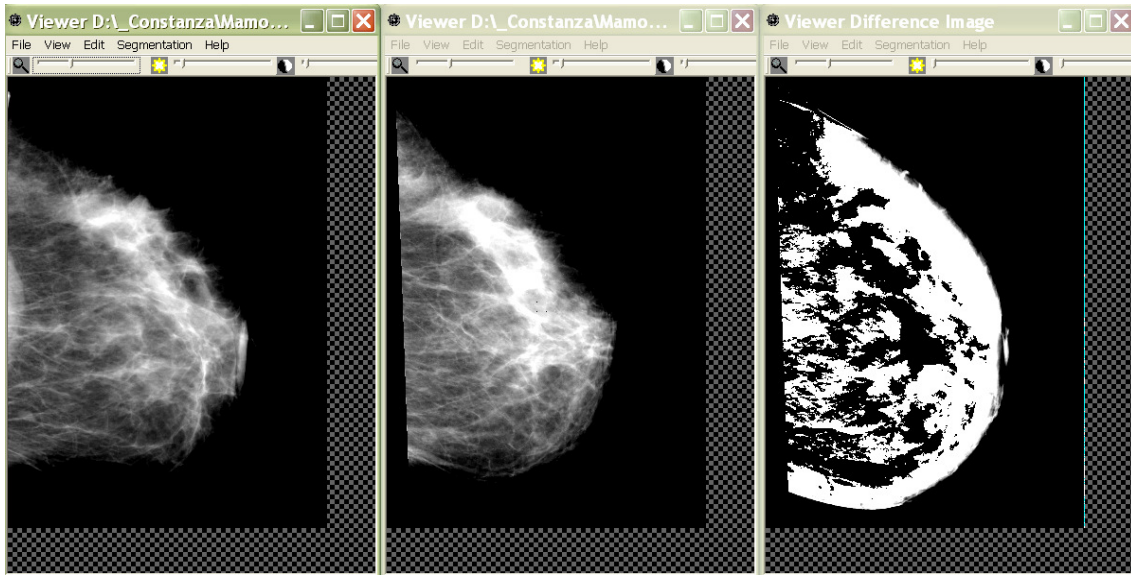


Figure 9.11: Two mammograms (left, center) and the result of their registration (right).

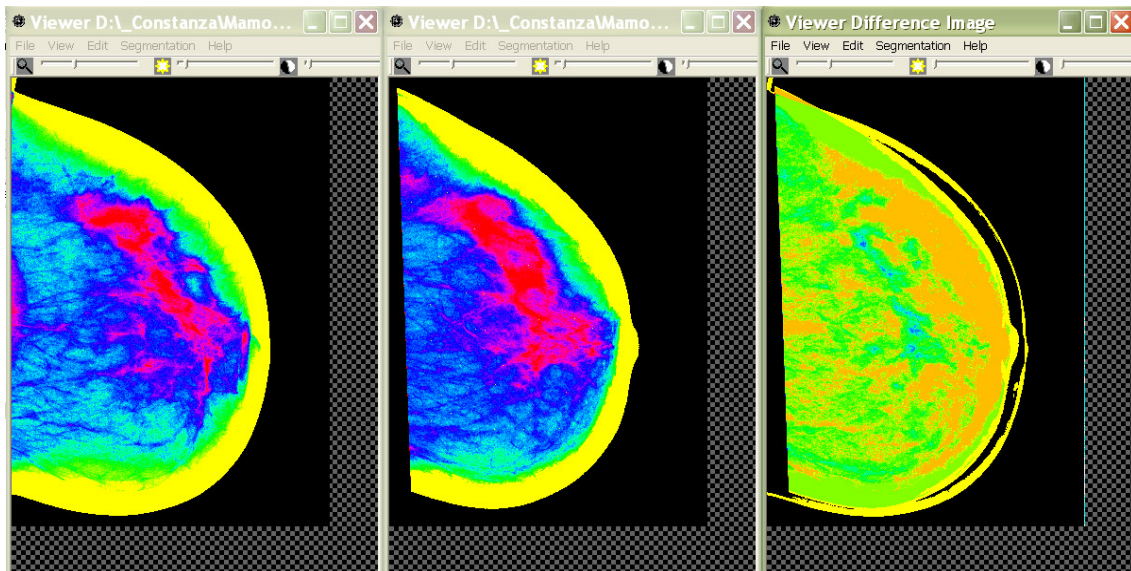


Figure 9.12: Two standardized mammograms (left, center) and the standardized result of their registration (right).

Figure 9.11 shows two mammograms to be compared and the result of their registration. Figure 9.12 illustrates the same case showing the standardization using the color scale. The mammograms on the right are the result of the registration and extraction of the two other ones. If the two compared mammograms were the same, the result of their registration would be completely yellow.

These results are also accompanied with numerical information such as volumes of the different tissues and their differences.

Figures 9.13-9.16 show the three-dimensional views respectively as height fields, contours, NURBS and Bézier surfaces. These are different options that were developed to see how

the amount of glandular tissue, as a characteristic third dimension, can be modeled. Which of these four options is the best, should be decided by the user. However, from a first sight into these examples it is clear that color can be used as an important tool to have a clearer view of the distribution of the height of glandular tissue.

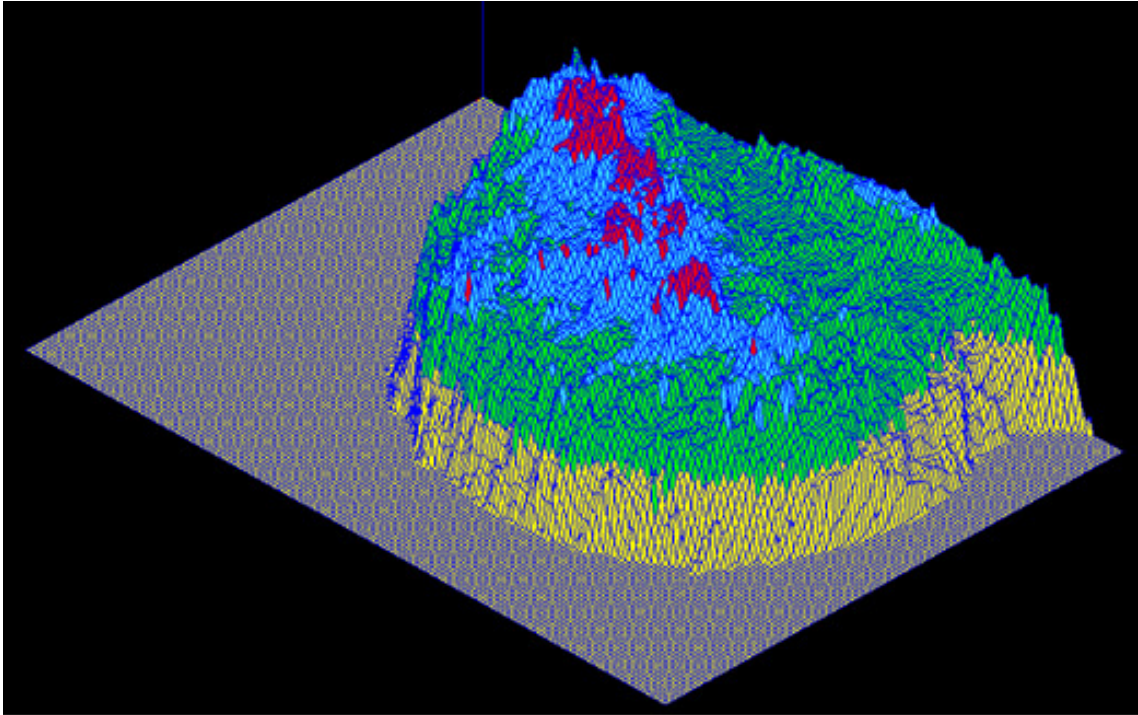


Figure 9.13: View as height fields.

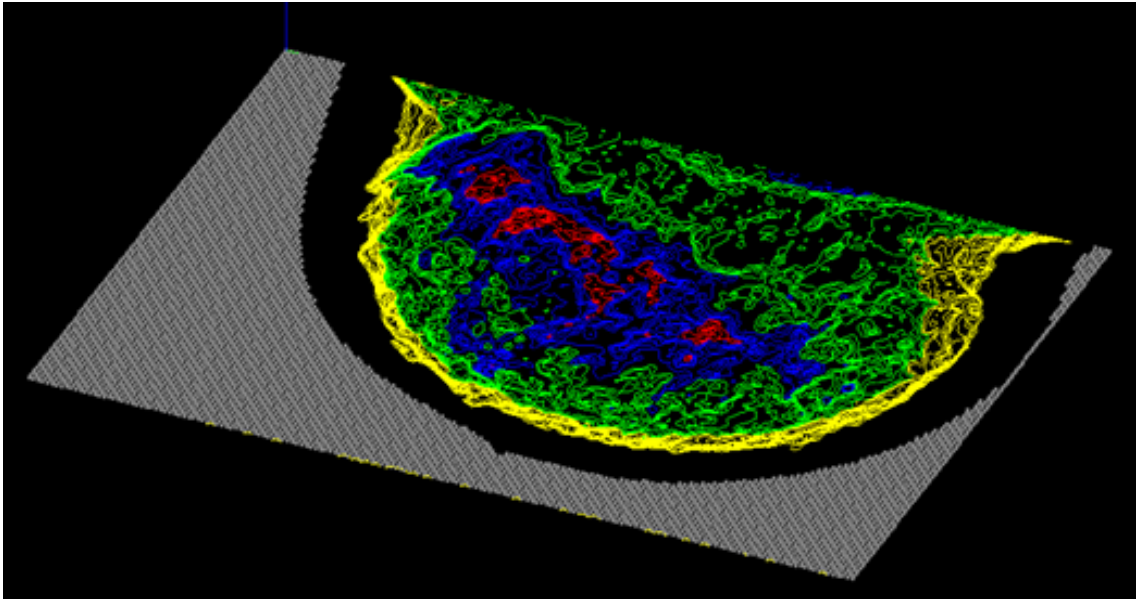


Figure 9.14: View as contours.

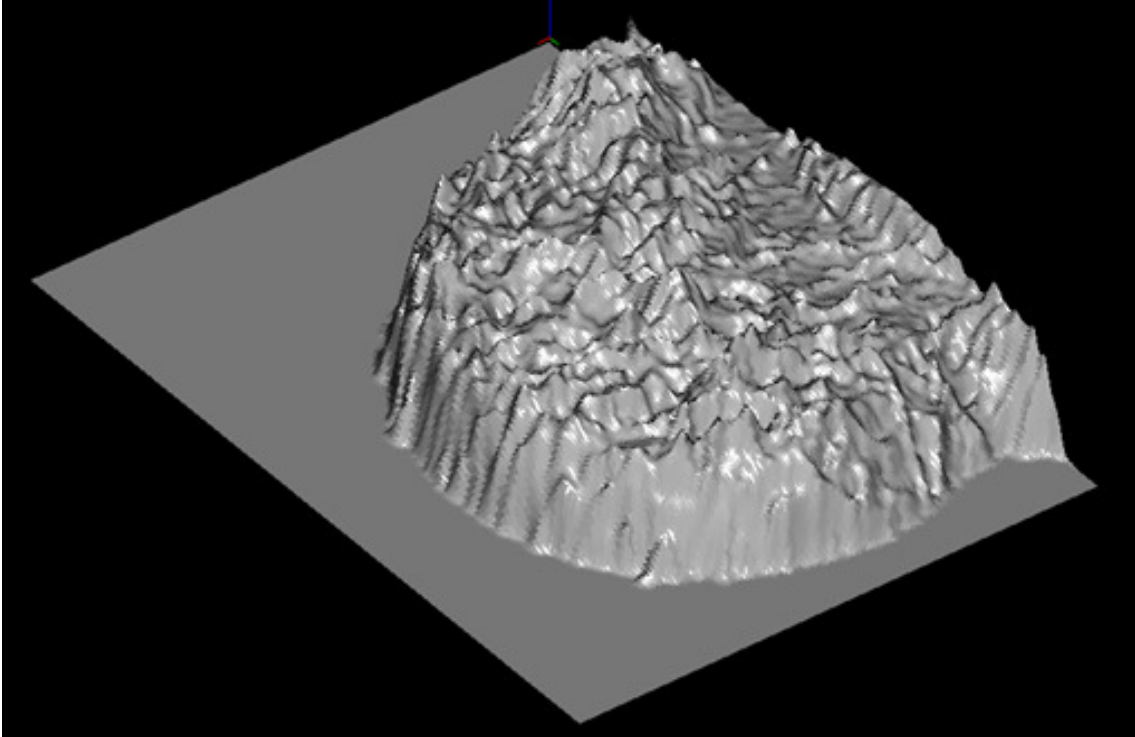


Figure 9.15: View as NURBS surface.

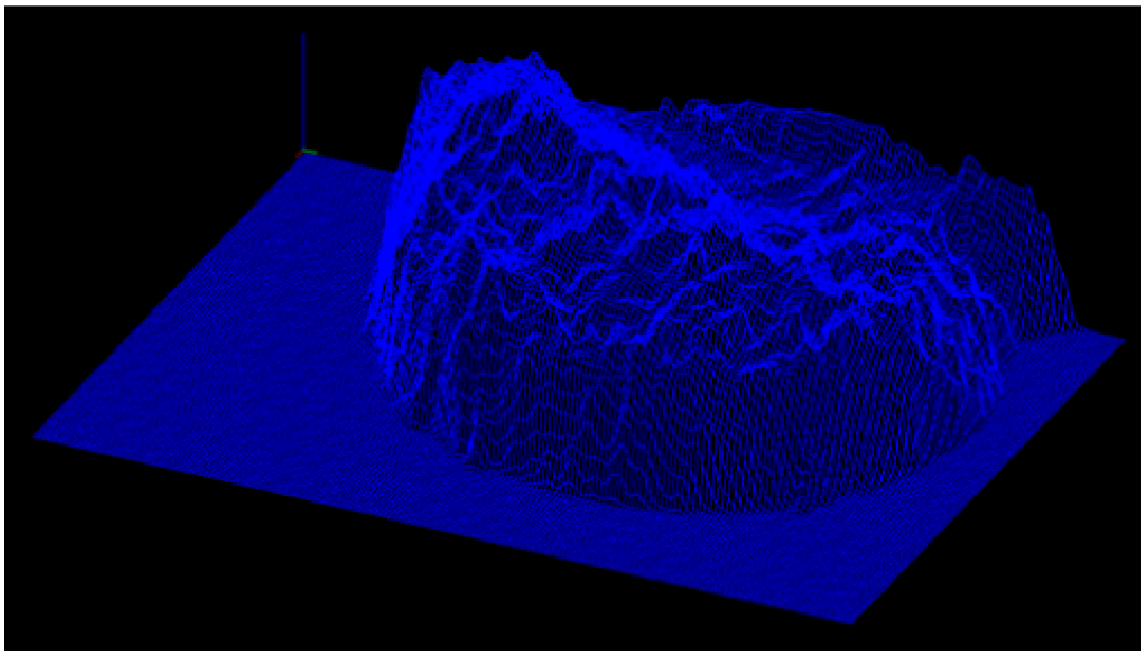


Figure 9.16: View as Bézier surface.

10 CONCLUSIONS

Together with the increasing importance of medical imaging in clinical practice, the need for medical image analysis to extract objective, quantitative information from medical images has grown considerably. In this work, we presented computer-based image analysis methods and their application in digital mammograms, together with a software prototype that implements them to probe their practical use.

The most significant result of our research is a new method for the measurement of volumetric breast density from full-field digital mammograms, which adds a qualitative third dimension to the images. This method considers the gray levels as a three-dimensional object, by adding information about the amount of the tissues projected on it. This could not be done by a radiologist because of the limitations of human perception. Moreover, manual visual analysis is highly subjective because it relies on the observer's perception. This results in intra- and interobserver variability in the measurements. Automated analysis is a way to overcome this problem. Through the interpretation of gray levels in digital mammograms as amounts of glandular tissue, the radiologist is provided not only with the percentage of glandular tissue in the whole breast but she has the possibility to determine the quantity of this tissue at an arbitrary location of the image. The method allows performing estimations of breast composition and additionally provides interesting thresholds to segment the image. We have also seen that a less accurate estimation of attenuation coefficients results in a less accurate estimation of breast density, and, that the error in the estimation of the amount of fibroglandular tissue increases with breast density. It was shown that the difference of the linear attenuation coefficients has a big influence in the estimation model, and, that the error decreases with an increasing difference of the linear attenuation coefficients.

As a result of the measurement of volumetric breast density, a way to show the mammograms in a standardized form was obtained. The presentation of the digital mammograms as standardized images, based on the amounts of fibroglandular tissue, with fixed size and pixel value for a determined quantity of tissue is the basis for the comparison of the images, independently of acquisition parameters, detector size and image resolution, contrast and brightness. We want to remark here that there is not only one standard. The color scale can be configured to vary the point against which the images should be compared and so we can obtain a standardized image with respect to a patient or to many patients.

The standardized images can then be compared. An essential prerequisite for the analysis of multitemporal images is that they should be aligned. This requires a geometric operation, which is called image registration. This was achieved through the maximization of mutual information, which assumes that the statistical dependency between the

intensities of corresponding pixels in the images or the information that one image contains about the other is maximal at registration. Since this approach does not rely on the absolute value of the intensities but on their co-occurrences, and because no limiting assumptions are imposed on the photometric relationship between both images, maximization of mutual information is a powerful method that has been applied successfully to a wide range of different applications of image registration. The comparison of mammograms provides a numerical relationship of the amounts of tissues and it is visualized through the extraction of the registered images. It is possible to follow the evolution of the patient by temporal comparison of her mammograms and a bilateral comparison of the left and right mammograms taken on the same study.

Besides these main solutions, we presented methods that are needed as complementary tasks. The images needed to be segmented before any analysis could be performed. We segmented the images into breast and background using thresholding. Afterwards, the pectoral muscle is extracted. The correct determination of breast composition relies on the accuracy of these pre-processing methods that segment the image into background, pectoral muscle and breast. The segmentation of the pectoral muscle is achieved using a new algorithm. This step in the analysis of the images is very important because the pixels in the pectoral muscle may be interpreted as “pure glandular tissue”, which would lead to wrong results in the estimation of the breast composition. The method is based on region growing, edge detection and upon typical characteristics of MLO mammograms. The method overcomes the limitation of the straight-line hypothesis imposed by former methods and works without user interaction. These segmentation approaches have the advantage that they are simple to understand and to implement. We saw also in our experiments, that when the assumptions we made about the pectoral muscle region are not fulfilled, the algorithm could result in undersegmentation. One improvement could be implemented in the software that allows the user to accept or reject a segmentation. If the segmentation is rejected the user could modify the value of the pectoral muscle edge, or another method could be used to obtain a new segmentation of the pectoral muscle. In the 120 test images we used, only one undersegmentation occurred.

The method used for pixel interpretation can be used not only in the estimation of breast composition, but it also resulted to be successful for the detection of the breast border, a feature that may be used, for instance, for image registration. Additionally, the pixels signifying a tissue densest as glandular tissue, may suggest the presence of calcifications.

All the results can be seen in the two-dimensional presentations through the coloring of the different features, i.e. breast border, pectoral muscle, percentages and amounts of tissues. Additionally, a visualization approach was presented that adds a new dimension to the two-dimensional mammograms through the modeling of the amount of glandular tissue present in the breast based on the glandular tissue calculation algorithm. The developed tool has the ability to present the amount of the glandular tissue in the interior of the breast as a

height field, change the colormap, create contours and translate, scale and rotate the data. This kind of presentation of the breast structure may help the radiologist when assessing a mammogram giving an enhanced perspective of the situation. These are different options that were developed to see how the amount of glandular tissue, as a characteristic third dimension, can be modeled. Which of these four options is the best, should be decided by the user. However, from a first sight into the examples it is clear that color can be used as an important tool to have a better view of the distribution of the height of glandular tissue.

All these features were implemented in a software prototype. The programs were run in a standard PC (2.66 GHz, 1 GB RAM) and they performed in an acceptable time. The registration of the images runs in a less optimal time because it uses semi-exhaustive optimization.

The application of the developed methods is the identification of women with a higher breast cancer risk, as this risk could be derived from changes in the volumetric breast density. If a woman with a higher breast cancer risk is identified, more examinations could be recommended. In addition, patients suffering of cancer could be healed faster through an early detection. This may imply higher screening costs, but also lower follow-up costs due to less surgeries, chemotherapy, radiotherapy, rehabilitations and follow-up examinations.

This project presented not only new methods; also, *old* methods were optimized for their application in digital mammograms. All the work is based on computer science methods related to image analysis and pattern recognition, and could be used in other areas involving x-rays images such as in the quality control of car parts and their materials.

While the advantages of the mammogram analysis approach presented here are evident by the results, several interesting questions remain to be investigated. Further work may include a reconstruction of the breast volume using the CC and MLO views, using a two-view registration based on the distribution of the tissues. In the segmentation of the pectoral muscle the option of accepting or rejecting it could be added. Moreover, the fatty breast border was assumed to have the complete compressed breast thickness. Our model could be extended to consider this feature as having a decreasing height as it approaches the edge of the breast. Furthermore, experiments could be run that model the x-ray angle or the scattered component. For the registration of the mammograms, different optimization methods could be tested to find the optimal transformation.

REFERENCES

- ABDEL-MOTTALEB, M. AND CARMAN, C., 1996. Locating the boundary between breast skin edge and the background in digitized mammograms. *In: K. DOI, ed. Digital mammography '96: proceedings of the 3rd international workshop on digital mammography, 9-12 June 1996 Chicago, USA.* Amsterdam: Elsevier, 467-470.
- ABRAMOWSKI, S. AND MÜLLER, H., 1991. *Geometrisches Modellieren.* Mannheim: BI-Wissenschafts-Verlag.
- AICHINGER, H., DIERKER, J. AND JOITE-BARFUSS, S., 2004. *Radiation exposure and image quality in x-ray diagnostic radiology. Physical principles and clinical applications.* Springer.
- AMERICAN COLLEGE OF RADIOLOGY, 2003. *Breast imaging reporting and data system (BI-RADS).* 4th ed. Reston, VA: American College of Radiology.
- ANGEL, E., 2003. *Interactive computer graphics: a top-down approach with OpenGL.* Boston, MA: Addison-Wesley.
- BERTZ, J., HENTSCHEL, S., HUNSDÖRFER, G., KAATSCH, P., KATALINIC, A., LEHNERT, M., SCHÖN, D., STEGMAIER, C. AND ZIEGLER, H., 2004. *Krebs in Deutschland. 4. überarbeitete, aktualisierte Ausgabe.* Saarbrücken: Arbeitsgemeinschaft Bevölkerungsbezogener Krebsregister in Deutschland und das RKI.
- BERTZ, J., GIERSIEPEN, K., HABERLAND, J., HENTSCHEL, S., KAATSCH, P., KATALINIC, A., STABENOW, R., STEGMAIER, C. AND ZIEGLER, H., 2006. *Krebs in Deutschland. 5. überarbeitete, aktualisierte Ausgabe.* Saarbrücken: Gesellschaft der epidemiologischen Krebsregister in Deutschland e.V. und das RKI.
- BICK, U. AND GIGER, M., 1995. Automated segmentation of digitized mammograms. *Academic radiology*, 2(1), 1-9.
- BLEND, R., RIDEOUT, D.F., KAIZER, L., SHANNON, P., TUDOR-ROBERTS, B. AND BOYD, N.F., 1995. Parenchymal patterns of the breast defined by real time ultrasound. *European journal of cancer prevention*, 4(4), 293-298.
- BOYD, N.F., BYNG, J.W., JONG, R.A., FISHELL, E.K., LITTLE, L.E., MILLER, A.B., LOCKWOOD, G.A., TRITCHLER, D.L. AND YAFFE, M.J., 1995. Quantitative classification of mammographic densities and breast cancer risk: results from the Canadian national breast screening study. *Journal of the national cancer institute*, 87(9), 670-675.
- BRZAKOVIC, D., VUJOVIC, N. AND NESKOVIC, M., 1994b. Early detection of cancerous changes by mammogram comparison. *In: A.K. Katsaggelos, ed. Proc. SPIE vol. 2308, visual communications and image processing '94, 29 September 1994 Chicago, USA.* Bellingham: The International Society for Optical Engineering, 1520-1531.

- BRZAKOVIC, D., VUJOVIC, N., NESKOVIC, M., BRZAKOVIC, P. AND FOGARTY, K., 1994a. Mammogram analysis by comparison with previous screenings. In: A.G. GALE, ed. *Digital mammography: proceedings of the 2nd international workshop on digital mammography, 10-12 July 1994 York, England*. Amsterdam: Elsevier, 131-139.
- BYNG, J. AND BOYD, N., 1996. Automated analysis of mammographic densities. *Physics in medicine and biology*, 41(5), 909-923.
- BYNG, J.W., YAFFE, M.J., JONG, R.A., SHUMAK, R.S., LOCKWOOD, G.A., TRITCHLER, D.L. AND BOYD, N.F., 1998. Analysis of mammographic density and breast cancer risk for digitized mammograms. *Radiographics*, 18(6), 1587-1598.
- CHANDRASEKHAR, R. AND ATTIKIIOUZEL, Y., 1996. Gross segmentation of mammograms using a polynomial model. *IEEE medicine and biological society*, 3, 1056-1058.
- CLARK, J.W., 1991. Neural network modelling. *Physics in medicine and biology*, 36(10), 1259-317.
- DAVENPORT, J.W., BEZDEK, J.C. AND HATHAWAY, R.J., 1988. Parameter estimation for finite mixture distributions. *Computers & mathematics with applications*, 15(10), 810-28.
- DEAN, D., AND MIN, K.J., 2003. Deformable templates for preoperative computer-aided design and fabrication of large cranial implants. *International congress series*, 1256, 710-715.
- DEUTSCHE BUNDESTAG, 2006. *Drucksache 16/2237: Antwort der Bundesregierung auf die Kleine Anfrage der Abgeordneten Ina Lenke, Daniel Bahr (Münster), Heinz Lanfermann, weiterer Abgeordneter und der Fraktion der FPD. Drucksache 16/2102* [online]. Available from: <http://dip.bundestag.de/btd/16/022/1602237.pdf> [Accessed 17 July 2006].
- DÖSSEL, O., 2000. *Bildgebende Verfahren in der Medizin*. Heidelberg: Springer.
- DUNCAN, J.S. AND AYACHE, N., 2000. Medical image analysis: progress over two decades and the challenges ahead. *IEEE transactions on pattern analysis and machine intelligence*, 22(1), 85-106.
- ECKERT, R., NEYHART, J.T., BURD, L., POLIKAR, R., MANDAYAM, S.A., AND TSENG, M., 2003. Neural and decision theoretic approaches for the automated segmentation of radiodense tissue in digitized mammograms. *Review of qualitative nondestructive evaluation*, 22, 1735-1742.
- ENCARNAÇÃO, J.L., LINDNER, R., AND SCHLECHTENDAHL, E.G., 1990. *Computer aided design. software and devices for medical applications*. Springer.
- ENCARNAÇÃO, J.L., ed., 2006. *Medical technology: software and devices for medical applications*. Darmstadt: INI-GraphicsNet.

- EUFINGER, H., SAYLOR, B., 2001. Computer assisted prefabrication of individual craniofacial implants. *Assoc. Oper. Room Nurs.*,74, 648-654.
- FREEDMAN, M., SAN MARTIN, J., O'GORMAN, J., ECKERT, S., LIPPMAN, M.E., LO, S.C.B., WALLS, E.L. AND ZENGET, J., 2001. Digitized mammography: a clinical trial of postmenopausal women randomly assigned to receive raloxifene, estrogen or placebo. *Journal of the national cancer institute*, 93(1), 51-56.
- GARBETT, I., 2004. *Light attenuation and exponential laws* [online]. Available from: <http://plus.maths.org/issue13/index.html> [Accessed 28 March 2007].
- GIGER, M.L., LU, P., HUO, Z., BICK, U., VYBORNY, C.J., SCHMIDT, R.A., ZHANG, W., METZ, C.E., WOLVERTON, D., NISHIKAWA, R.M., ZOURAS, W. AND DOI, K., 1994. CAD in digital mammography: computerized detection and classification of masses. In: A.G. GALE, ed. *Digital mammography: proceedings of the 2nd international workshop on digital mammography, 10-12 July 1994 York, England*. Amsterdam: Elsevier, 281- 287.
- GOLD, R.H., BASSETT, L.W. AND WIDOFF, B.E., 1990. Highlights of the history of mammography. *Radiographics*, 10, 1111-1131.
- GONZALEZ, R.C. AND WOODS, R.E., 1992. *Digital image processing*. Reading, MA: Addison-Wesley.
- GOODSITT, M.M. AND CHAN, H., 1998. Classification of compressed breast shapes for the design of equalization filters in x-ray mammography. *Medical physics*, 25(6), 937-948.
- GRAHAM, S.J., BRONSKILL, M.J., BYNG, J.W., YAFFE, M.J. AND BOYD, N.F. 1996. Quantitative correlation of breast tissue parameters using magnetic resonance and x-ray mammography. *British journal of cancer*, 73(2), 162-168.
- GULIATO, D., RANGAYYAN, R.M., CARNIELL, M.A., ZUFFO, J.A. AND DESAUTELS, J.E.L., 1998. Segmentation of breast tumors in mammograms by fuzzy region growing. In: *Proceedings of the 20th annual international conference of the IEEE engineering in medicine and biology society, 29 October- 1 November Hong Kong*. Los Alamitos: IEEE Computer Society, 1002-1005.
- HADJIISKI, L., CHAN, H., SAHINER, B., PETRICK, N. AND HELVIE, M.A., 2001. Automated registration of breast lesions in temporal pairs of mammograms for interval change analysis-local affine transformation for improved localization. *Medical physics*, 28(6), 1070-1079.
- HARALICK, R.M. AND SHAPIRO, L.G., 1985. Image segmentation techniques. *Computer vision, graphics, and image processing*, 29(1), 100-132.
- HARVEY, J.A. AND BOVBJERG, V.E., 2004. Quantitative assessment of mammographic breast density: relationship with breast cancer risk. *Radiology*, 230, 29-41.
- HASSANIEN, A.E. AND ALI, J.M., 2004. Digital mammogram segmentation algorithm using pulse coupled neural networks. In: *Proceedings of the third international*

- conference on image and graphics, 18-20 December 2004 Hong Kong*. Los Alamitos: IEEE Computer society, 92-95.
- HEYWANG-KÖBRUNNER, S.H., DERSHAW, D.D. AND SCHREER, S., 2001. *Diagnostic breast imaging*. New York: Thieme.
- HIGHNAM, R. AND BRADY, M., 1999. *Mammographic image analysis*. Dordrecht: Kluwer Academic.
- HIGHNAM, R., JEFFREYS, M., McCORMACK, V., DAVEY SMITH, G. AND BRADY, M., 2007. Comparing measurements of breast density. *Physics in Medicine and Biology*, 52, 5881-5895.
- HOESCHEN, C., 2006. Spagat zwischen heilen und schaden: Strahlenanwendungen in der Medizin. *Mensch+Umwelt Spezial*, 18, 16-22.
- HOYER, A. AND SPIESBERG, W., 1979. Computerized mammogram processing. *Philips technical review*, 38, 347-355.
- HUBBELL, J.H. AND SELTZER, S.M., 2004. *Tables of x-ray mass attenuation coefficients and mass energy-absorption coefficients (version 1.4)* [online]. National Institute of Standards and Technology, Gaithersburg, MD 2004. Available from: <http://physics.nist.gov/xaamdi> [Accessed 28 March 2007].
- IMAGINIS CORPORATION, 2006. *Mammography* [online]. Available from: <http://imagnis.com/breasthealth/mammography.asp> [Accessed 28 March 2007].
- INTERNAZIONALE MEDICO SCIENTIFICA S.R.L., 2006. Available from: <http://imsitaly.com> [Accessed 28 March 2007].
- JONG, R.A., 2005. Surveillance of high risk women. In: *Summary proceedings: 29th annual symposium of the American society of breast disease. 14-16 April 2005 Las Vegas, USA*. Las Vegas: American Society of Breast Disease, 1-5.
- KARSSEMEIJER, N. AND TE BRAKE, G., 1998. Combining single view features and asymmetry for detection of mass lesions. In: N. KARSSEMEIJER, M. THIJSSSEN, J. HENDRIKS AND L. VAN ERNING, eds. *Digital mammography: proceedings of the 4th international workshop on digital mammography. 7-10 June 1998 Nijmegen, The Netherlands*. Dordrecht: Kluwer Academic, 95-102.
- KARSSEMEIJER, N., 1998. Automated classification of parenchymal patterns in mammograms. *Physics in medicine and biology*, 43(2), 365-378.
- KATO, I., BEINART, C., BLEICH, A., SU, S., KIM, M. AND TONIOLO, P.G., 1995. A nested case-control study of mammographic patterns, breast volume, and breast cancer. *Cancer causes control*, 6(5), 431-438.
- KOK-WILES, S.L., BRADY, M. AND HIGHNAM, R., 1998. Comparing mammogram pairs for the detection of lesions. In: N. KARSSEMEIJER, M. THIJSSSEN, J. HENDRIKS AND L. VAN ERNING, eds. *Digital mammography: proceedings of the 4th international workshop on digital mammography. 7-10 June 1998 Nijmegen, The Netherlands*. Dordrecht: Kluwer Academic, 103-110.

- KOLB, T., LICHY, J. AND NEWHOUSE, J., 2002. Comparison of the performance of screening mammography, physical examination, and breast US and evaluation of factors that influence them: an analysis of 27825 patient evaluations. *Radiology*, 225, 165-175.
- KOSTELEC, P.J., WEAVER, J.B. AND HEALY, D.M. JR., 1998. Multiresolution elastic image registration. *Medical physics*, 25(9), 1593-1604.
- LAMPASONA, C., 2006. Erzeugung eines dreidimensionalen Modells der weiblichen Brust aus zweidimensionalen Röntgenbildern. In: K. HAASIS, A. HEINZL AND D. KLUMPP, eds. *Aktuelle Trends in der Softwareforschung - Tagungsband zum do it.software-forschungstag, 13 July Mannheim, Germany*. Heidelberg: dpunkt.verlag, 143-150.
- LAMPASONA, C., 2007. Digitale Mammographie in 3D - erste Schritte zu einer verbesserten Früherkennung. *Best Practice Onkologie*, 2(6), 64.
- LAMPASONA, C. AND ROLLER, D., 2008. A region growing-based method for pectoral muscle segmentation in digital mammograms. In: R. SABLATNY AND O. SCHERZER, eds. *Proceedings of the fifth IASTED international conference on signal processing, pattern recognition and applications, 13-15 February 2008 Innsbruck, Austria*. Anaheim/Calgary/Zurich: Acta Press, 140-144.
- LAU, T. AND BISCHOFF, W., 1991. Automated detection of breast tumors using the asymmetry approach. *Computers and biomedical research*, 24(3), 273-295.
- LEE, N.A., RUSINEK, H., WEINREB, J., CHANDRA, R., TOTH, H., SINGER, C. AND NEWSTEAD, G., 1997. Fatty and fibroglandular tissue volumes in the breast of woman 20-83 years old: comparison of x-ray mammography and computer-assisted MR imaging. *American journal of roentgenology*, 168(2), 501-506.
- LEHMANN, T., HIETNER, J. AND HANDELS, H., 2002. Medizinische Bildverarbeitung. In: T.M. LEHMANN, ed. *Handbuch der Medizinischen Informatik*. Vienna: Hanser, 339-414.
- LI, H.D., KALLERGI, M., CLARKE, P., JAIN, V.K. AND CLARK, R.A., 1995. Markov random field for tumor detection in digital mammography. *IEEE transactions on medical imaging*, 14(3), 565-576.
- MA, F., BAJGER, M. AND BOTTEMA, M.J., 2005. Extracting the pectoral muscle in screening mammograms using a graph pyramid. In: B.C. LOVELL AND A.J. MAEDER, eds. *Proc. of the APRS workshop on digital image computing, 21 February 2005 Southbank, Australia*. St Lucia, QLD 4072 Australia: The University of Queensland, 27-32.
- MAINTZ, J.B.A. AND VIERGEVER, M.A., 1998. A survey of medical image registration. *Medical image analysis*, 2(1), 1-36.
- MARTI, R., ZWIGGELAAR, R. AND RUBIN, C., 2001. Automatic registration of mammograms based on linear structures. In: *Lecture notes in computer science - proceedings of the 17th international conference information processing in medical imaging, 18-22 June 2001 Davis, CA, USA*. Berlin: Springer, 162-168.

- MASEK, M. AND ATTIKIOUZEL Y., 2000. Skin air interface extraction from mammograms using an automatic local thresholding algorithm. *In: J. JAN, J. KOZUMPLÍK, I. PROVAZNÍK AND Z. SZABÓ, eds. Proceedings of 15th biennial international conference BIOSIGNAL 2000, 21-23 June 2000 Brno, Czech Republic.* Brno: VUTIUM, 204-206.
- MCGARRY, G. AND DERICHE, M., 2000. Mammographic image segmentation using a tissue-mixture model and Markov random fields. *In: Proceedings of the 2000 international conference on image processing, 10-13 September 2000 Vancouver.* IEEE Computer Society, 3, 416-419.
- MÉNDEZ, A. AND TAHOSES, P., 1996. Automatic detection of breast border and nipple in digital mammograms. *Computer methods and programs in biomedicine*, 49(3), 253-262.
- MÉNDEZ, A.J., TAHOSES, P.G., LADO, M.J., SOUTO, M. AND VIDAL, J.J., 1998. Computer-aided diagnosis: automatic detection of malignant masses in digitized mammograms. *Med Phys*, 25(6), 957-964.
- MÉNDEZ, A.J., TAHOSES, P.G., LADO, M.J., SOUTO, M., AND VIDAL, J.J., 1996. Computer-aided diagnosis: detection of masses on digital mammograms. *In: B.G. MERTZIOS, P. LIATSIS, eds. Proceedings of the third international workshop on image and signal processing on the theme of advances in computational intelligence. 4-7 November 1996 Manchester, England.* Elsevier, 465-468.
- NATIONAL CANCER INSTITUTE, 2006. *Dictionary of cancer terms* [online]. Available from: <http://www.cancer.gov/dictionary> [Accessed 28 March 2007].
- NEMA, 2004a. *Digital imaging and communications in medicine (DICOM) Part 1: Introduction and overview.* Rosslyn VA: National Electrical Manufacturers Association.
- NEMA, 2004b. *Digital imaging and communications in medicine (DICOM) Part 5: Data structure and encoding.* Rosslyn VA: National Electrical Manufacturers Association.
- NEMA, 2004c. *Digital imaging and communications in medicine (DICOM) Part 6: Data dictionary.* Rosslyn VA: National Electrical Manufacturers Association.
- NEMA, 2004d. *Digital imaging and communications in medicine (DICOM) Part 10: Media storage and file format for data interchange.* Rosslyn VA: National Electrical Manufacturers Association.
- NISHIKAWA, R.H., GIGER, M.L., DOI, K., VYBORNÝ, C.J., SCHMIDT, R.A., METZ, C.E., WU, C.Y., YIN, F.F., JIANG, Y., HUO, Z., LU, P., ZHANG, W., EMA, E., BICK, U., PAPAIOANNOU, J. AND NAGEL, R.H., 1993. Computer-aided detection and diagnosis of masses and clustered microcalcifications from digital mammograms. *In: R.S. ACHARYA AND D.B. GOLDFOF, eds. Proc. SPIE vol. 1905, Biomedical Image Processing and Biomedical Visualization, 1-4 February 1993 San Jose, CA, USA.* Bellingham: The International Society for Optical Engineering, 422-432.
- ORLAMÜNDER, D. AND MASCOLUS, W., 2004. *Computergrafik und OpenGL: eine systematische Einführung.* Munich: Hanser 2004.

- PAL, N.R. AND PAL, S.K., 1993. A review on image segmentation techniques. *Pattern recognition*, 26(9), 1277-1294.
- PHAM, D.L. AND PRINCE, J.L., 1999. An adaptive fuzzy c-means algorithm for image segmentation in the presence of intensity inhomogeneities. *Pattern recognition letters*, 20, 57-68.
- PHAM, D.L., XU, C. AND PRINCE, J.L., 2000. Current methods in medical image segmentation. *Annual review of biomedical engineering*, 2, 315-337.
- PLUIM, J.P.W., MAINTZ, J.B.A. AND VIERGEVER, A.M., 2003. Mutual-information-based registration of medical images: a survey. *IEEE transactions on medical imaging*, 22(8), 986-1004.
- RABA, D., OLIVER, A., MARTÍ, J., PERACAULA, M. AND ESPUNYA, J., 2005. Breast segmentation with pectoral muscle suppression on digital mammograms. In: J.S. MARQUES, N. PÉREZ DE LA BLANCA AND P. PINA, eds. *Pattern recognition and image analysis: proceedings of the second iberian conference, IbPRIA 2005, part II, 7-9 June 2005 Estoril, Portugal*. Springer, 471-478
- RAJAPAKSE, J.C., GIEDD, J.N. AND RAPOPORT, J.L., 1997. Statistical approach to segmentation of single-channel cerebral MR images *IEEE transactions on medical imaging*, 16(2), 176-86.
- REEM DIAGNOSTIC, 2006. *What is mammography?* [online]. Available from: <http://reemdiagnostic.4t.com> [Accessed 28 March 2007].
- RICHARD, F. AND COHEN, L., 2002. A new image registration technique with free boundary constraints: Application to mammography. In: A. HEYDEN, G. SPARR, M. NIELSEN AND P. JOHANSEN, eds. *Proceedings 7th european conference on computer vision - ECCV 2002, part IV, 28-31 May 2002 Copenhagen, Denmark*. Springer, 531-545.
- RICHARD, F. AND COHEN, L., 2003. Non-rigid image registration with free boundary constraints: application to mammography. *Journal of computer vision and image understanding*, 89(2-3), 166-196.
- RICKARD, H., TOURASSI, G. AND ELMAGHRABY, A. 2003. Self-organizing maps for masking mammography images. In: *Proceedings of the 25th annual international conference of the IEEE engineering in medicine and biology society, 17-21 September 2003 Cancun, Mexico*. IEEE, 302-305.
- ROBB, R.A., 2000. Three-dimensional visualization in medicine and biology. In: I.N. Bankman, ed. *Handbook of medical imaging and analysis*. San Diego: Academic Press, 685-712.
- ROLLER, D., 1995. *CAD - Effiziente Anpassungs- und Variantenkonstruktion*. Heidelberg: Springer.
- ROLLER, D. AND LAMPASONA, C., 2006. A method for interpreting pixel grey levels in digital mammography. In: A. CAMPILHO, M. KAMEL, eds. *Proceedings of the third international conference on image analysis and recognition, lecture notes in*

computer science 4142, part II, 18-20 September Póvoa de Varzim, Portugal. Berlin/Heidelberg: Springer, 580-588.

RORDEN, C., 2006. *The DICOM standard* [online]. Available from: <http://www.sph.sc.edu/comd/rorden/dicom.html> [Accessed 28 March 2007].

SAFTLAS, A.F., HOOVER, R.N., BRINTON, L.A., SZKLO, M., OLSON, D.R., SALANE, M. AND WOLFE, J.N., 1991. Mammographic densities and risk of breast cancer. *Cancer*, 67(11), 2833-2838.

SAHA, P. AND UDUPA, J., 2001. Breast tissue density quantification via digitized mammograms. *IEEE transactions on medical imaging*, 20, 792-803.

SAHOO, P.K., SOLTANI, S. AND WONG, A.K.C., 1988. A survey of thresholding techniques. *Computer vision, graphics, and image processing*, 41(2), 223-60.

SALLAM, M. AND BOWYER, K., 1994. Registering time sequences of mammograms using a two-dimensional image unwarping technique. In: A.G. GALE, ed. *Digital mammography: proceedings of the 2nd international workshop on digital mammography, 10-12 July 1994 York, England*. Amsterdam: Elsevier, 121-130.

SALLAM, M. AND BOWYER, K., 1996. Detecting abnormal densities in mammograms by comparison to previous screenings. In: K. DOI, ed. *Digital mammography '96: proceedings of the 3rd international workshop on digital mammography, 9-12 June 1996 Chicago, USA*. Amsterdam: Elsevier, 417-420.

SALLAM, M., 1997. *Image unwarping and difference analysis: a technique for detecting abnormalities in mammograms*. Thesis (PhD). University of South Florida.

SALLAM, M., HUBIAK, G., BOWYER, K. AND CLARKE, L., 1992. Screening mammogram images for abnormalities developing over time. In: *Conference record of the 1992 IEEE nuclear science symposium and medical imaging conference, 25-31 October 1992 Orlando, FL, USA*. IEEE Nuclear & Plasma Science Society, 2, 1270-1272.

SEMMLow, J. AND SHADAGOPAPPAN, A., 1980. A fully automated system for screening xeromammograms. *Computer and biomedical research*, 13(4), 350-362.

SHEPHERD, J.A., HERVE, L., LANDAU, J., FAN, B., KERLIKOWSKI, K. AND CUMMINGS, S.R., 2005. Novel use of single x-ray absorptimetry for measuring breast density. *Technology in cancer research and treatment*, 4(2), 173-182.

SHEPHERD, J.A., KERLIKOWSKI, K.M., SMITH-BINDMAN, R., GENANT, H.K. AND CUMMINGS, S.R., 2002. Measurements of breast density with dual x-ray absorptimetry: feasibility. *Radiology*, 223, 554-557.

SHESHADRI, H.S. AND KANDASWAMY. A, 2005a Detection of breast cancer tumor based on morphological watershed algorithm. *ICGST international journal on graphics, vision and image processing*, 5(5), 17-21.

SHESHADRI, H.S. AND KANDASWAMY. A, 2005b. Mammogram image analysis using recursive watershed algorithm. In: Y.I. SHOKIN AND O.I. POTATURKIN,

eds. *Proceedings of the ACIT - signal and image processing 2005, 20-24 June 2005 Novosibirsk, Russia*. Calgary: ACTA Press, Track: 490-049.

SIVARAMAKRISHNA, R. 1998. Breast image registration using a textural transformation. *Medical physics*, 25(11), 2249.

SIVARAMAKRISHNA, R. AND GORDON, R., 1995. Mammographic image registration using a pinning function with elastic stretching. In: *Proceedings of the first regional conference., IEEE engineering in medicine and biology society, 1995 and 14th conference of the biomedical engineering society of India. an international meeting, 15-18 February 1995 New Delhi, India*. IEEE, 2, 1.65-1.66.

SIVARAMAKRISHNA, R. AND GORDON, R., 1998. The starbyte algorithm for registration of noisy breast images. In: *IEEE Canadian conference on electrical and computer engineering, 1998, 24-28 May 1998 Waterloo, Canada*. IEEE, 2, 673-676.

SIVARAMAKRISHNA, R., OBUCHOWSKI, N.A., CHILCOTE, W.A. AND POWELL, K.A., 2001. Automatic segmentation of mammographic density. *Academic radiology*, 8(3), 250-256.

STAMATAKIS, E. AND CAIRNS, A., 1994. A novel approach to aligning mammograms. In: A.G. GALE, ed. *Digital mammography: proceedings of the 2nd international workshop on digital mammography, 10-12 July 1994 York, England*. Amsterdam: Elsevier, 255-264.

STUDHOLME, C., HILL, D.L.G. AND HAWKES, D.J., 1999. An overlap invariant entropy measure of 3D medical image alignment. *Pattern recognition*, 32(1), 71-89.

SUCKLING, J., DANCE, D.R., MOSKOVIC, E., LEWIS, D.J. AND BLACKER, S.G., 1995. Segmentation of mammograms using multiple linked self-organizing neural networks. *Medical physics*, 22(2), 145-152.

SUETENS, P., 2002. *Fundamentals of medical imaging*. Cambridge: Cambridge University.

SWEDISH RADIATION PROTECTION AUTHORITY, 2002. *Mammography - recent technical developments and their clinical potential*. Stockholm: Swedish radiation protection authority, 2002: 08.

TOLEDO SANTOS, V., SCHIABEL, H., GÓES, C.E. AND BENATTI, R.H., 2002. A segmentation technique to detect masses in dense breast digitized mammograms. *Journal of digital imaging*, 15(1), 210-213.

URSIN, G., PARISKY, Y.R., PIKE, M.C. AND SPICER, D.V., 2001. Mammographic density changes during the menstrual cycle. *Cancer epidemiology, biomarkers and prevention*, 10, 141-142.

VALVERDE, F.L., GUIL, N. AND MUNZ, J., 2004. Segmentation of vessels from mammograms using a deformable model. *Computer methods and programs in biomedicine*, 73(3), 233-247.

- VAN ENGELAND, S., SNOEREN, P.R., HUISMAN, H., BOETES, C. AND KARSSEMEIJER, N., 2006. Volumetric breast density estimation from full-field digital mammograms. *IEEE transactions on medical imaging*, 25(3), 273-282.
- VICECONTI, M., 2001. HIDE: a new hybrid environment for the design of custom-made hip prostheses. *Methods programs biomed.*, 64, 137-144.
- VON MINCKWITZ, G. AND LOIBL, S., 2001. *Gynäkologie und Geburtshilfe*. Stuttgart: Thieme.
- VUJOVIC, N., BAKIC, P. AND BRZAKOVIC, D., 1996. Detection of potentially cancerous signs by mammogram follow-up. In: K. DOI, ed. *Digital mammography '96: proceedings of the 3rd international workshop on digital mammography, 9-12 June 1996 Chicago, USA*. Amsterdam: Elsevier, 421-424.
- WELLS, W.M., GRIMSON, W.E.L., KIKINS, R. AND JOLESZ, F.A., 1996. Adaptive segmentation of MRI data. *IEEE transactions on medical imaging*, 15(4), 429-42.
- WIRTH, M., LYON, J. AND NIKITENKO, D., 2004. A fuzzy approach to segmenting the breast region in mammograms. In: *Processing NAFIPS '04. IEEE annual meeting of the fuzzy information, 27-30 June 2004 Banff, AB, Canada*. IEEE, 1, 474-479.
- WIRTH, M.A., 2000. A nonrigid approach to medical image registration: matching images of the breast. Thesis (PhD). RMIT University.
- WIRTH, M.A., NARHAN, J. AND GRAY, D., 2002. Nonrigid mammogram registration using mutual information. In: M. SONKA AND J.M. FITZPATRICK, eds. *Medical imaging 2002: image processing, 25 February 2002 San Diego, CA, USA*. Bellingham: The International Society for Optical Engineering, 562-573.
- WOLFE, J.N., 1976. Breast patterns as an index of risk for developing breast cancer. *American journal of roentgenology*, 126(6), 1130-1137.
- WOLFE, J.N., SAFTLAS, A.F. AND SALANE, M., 1987. Mammographic parenchymal patterns and quantitative evaluation of mammographic densities: a case-control study. *American journal of roentgenology*, 148(3), 1087-1092.
- YIN, F.F., GIGER, M.L., DOI, K., METZ, C.E., VYBORNY, C.J. AND SCHMIDT, R.A., 1991. Computerized detection of masses in digital mammograms: analysis of bilateral subtraction images. *Medical physics*, 18(5), 955-963.
- YIN, F.F., GIGER, M.L., DOI, K., VYBORNY, C.J., AND SCHMIDT, R.A., 1994. Computerized detection of masses in digital mammograms: automated alignment of breast images and its effect on bilateral-subtraction technique. *Medical physics*, 21(3), 445-452.
- YIN, F.F., GIGER, M.L., VYBORNY, C.J., DOI, K. AND SCHMIDT, R.A., 1993. Comparison of bilateral-subtraction and single-image processing techniques in the computerized detection of mammographic masses. *Investigative radiology*, 28(6), 473-481.
- ZADEH, L.A., 1965. Fuzzy sets. *Information and control*, 8, 338-53.

- ZHENG, B., QIAN, W. AND CLARKE, L.P., 1996. Digital mammography: mixed feature neural network with spectral entropy decision for detection of microcalcifications. *IEEE transactions on medical imaging*, 15(5), 589-597.
- ZHOU, C., CHAN, H.P., PETRICK, N., HELVIE, M.A., GOODSITT, M.M., SAHINER, B. AND HADJIISKI, L.M., 2001. Computerized image analysis: estimation of breast density on mammograms. *Medical physics*, 28(6), 1056-1069.
- ZOURAS, W.K., GIGER, M.L., LU, P., WOLVERTON, D.E., VYBORNY, C.J. AND DOI, K., 1996. Investigation of a temporal subtraction scheme for computerized detection of breast masses in mammograms. In: K. DOI, ed. *Digital mammography '96: proceedings of the 3rd international workshop on digital mammography, 9-12 June 1996 Chicago, USA*. Amsterdam: Elsevier, 411-415.